5 RESEARCH ACTIVITIES

5.1 NUCLEAR PHYSICS

N. Madhavan

In the past year, the dome structure with 50 neutron detectors and target chamber were commissioned in National Array of Neutron Detectors (NAND), isomer decay measurements were initiated at the focal plane of gas-filled mode of HYbrid Recoil mass Analyzer (HYRA) and a newly designed setup for g-factor measurement using transient field technique was tested in the Gamma Detector Array (GDA) beam-line.

Operation of full superconducting LINAC enabled researchers to carry out nuclear reactions to populate heavy compound nuclei with more symmetric projectile-target combinations. Nuclear reaction experiments focused mainly on studying the effect of shell closure (in target or compound nucleus (CN)) on the survival of heavy CN against fusion-fission and quasi-fission. The evaporation residue (ER) excitation function measurements and ER-tagged gamma-multiplicity measurements were carried out in HYRA, using the gas-filled mode, the latter in conjunction with TIFR spin spectrometer. The fission fragment mass distributions and neutron multiplicity had earlier been measured, for some of these systems, using the previous neutron detector facility at IUAC.

Gamma multiplicity measurements in asymmetric and symmetric reactions populating the same CN, ^{80}Sr* were carried out using HIRA coupled with 14 BGO detectors. This was to confirm an earlier experimental result which indicated that, in the symmetric case, higher l-value partial waves failed to form equilibrated CN. Giant Dipole Resonance (GDR) decay measurements from hot, rotating ^{144}Sm nucleus, with spin selection, were extended to higher energies (temperature). Measurements to extract g-factor of isomeric states in barium isotopes have yielded good results. The g-factors of $9/2^-$ and $23/2^+$ isomeric states in ^{129}Ba have been extracted relative to the known g-factor of 10^+ isomeric state in ^{132}Ba.

Long-lived isomers in ^{193,195}Bi and ^{188}Tl were probed using a Clover germanium detector placed at the focal plane of gas-filled mode of HYRA. Signals from the four crystals of the Clover detector, processed separately, helped in gamma-gamma coincidences with large solid angle. A transition, initially thought to be prompt (and above the isomeric state), was clearly detected at the focal plane and there are indications for the existence of two isomeric states in ^{195}Bi. The dominant gamma-rays detected by the Clover crystals from ^{188}Hg (formed by the decay of ^{188}Tl), independently confirmed the effective transportation of ^{188}Tl isomers to the focal plane.

IUAC is getting ready to host FUSION14 international conference during February 24-28, 2014 with a satellite school on "Nuclear reactions around the Coulomb barrier" on February 21-22, 2014. INGA detectors are expected to be shipped this year to IUAC and VECC to have parallel campaigns with HYRA-INGA facility and alpha-induced reactions, respectively. It is heartening to share the success of some of the nuclear physics students winning accolades based on the work carried out at IUAC: best thesis award (Abhishek Yadav, Aligarh Muslim University), best poster award (Jasmeet Kaur, Panjab University) - both in DAE Nuclear Physics Symposium and one of the five best posters award in ICRTNP-2012 (Vijay Raj Sharma, Aligarh Muslim University).

5.1.1 Fission cross section measurements for ^{16,18}O+^{194,198}Pt Systems

Rohit Sandal[1], B.R. Behera[1], V. Singh[1], M. Kaur[1], S. Mandal[2], S. Kalkal[2], D. Siwal[2], S. Goyal[2], E. Prasad[3], P. Sugathan[4], A. Jhingan[4] and A. Saxena[5]

[1]Department of Physics, Panjab University, Chandigarh 160014, India
[2]Department of Physics and Astrophysics, University of Delhi, Delhi 110007, India
[3]Department of physics, Centeral University of Kerala, Kasaragod 671328, India

[4]Inter University Accelerator Centre, Aruna Asaf Ali Marg, New Delhi 110067, India
[5]Nuclear Physics Division, Bhabha Atomic Research Centre, Mumbai 400085, India

The study of heavy-ion induced fission fragment angular distributions is a rich source of information. These reactions are sensitive to the entrance channel of the interacting heavy ions forming the compound nucleus, and also to the other aspects of the intermediate composite system, as it equilibrates in energy, mass, angular momentum and shape degrees of freedom .The measured fission anisotropies depend on the entrance channel, the deformation and the spin of the target, the mass of the projectile, the bombarding energy with respect to the fusion barrier and the fission dynamics (fission delay)[1,2]. Also fission fragment angular distribution is a sensitive probe to investigate the contribution from non-compound nucleus fission. Investigation of the contribution from non-compound nucleus fission for systems with low Z_PZ_T (Z_P and Z_T are the atomic number of projectile and target, respectively) has been an active area of study in the recent past. Along with these studies it is important to study the isotopic effects on the fission cross section. In this study, fission cross section has been measured by populating the compound nuclei ^{210,212,214,216}Rn (fissility = 0.735, 0.732, 0.729, 0.726, respectively) having same Z(proton number) and different N(neutron number).

The fission dynamics as a function of '(N-Z)/A' and N/Z, the effect of the neutron excess from the reaction system chosen and the contribution coming from near scission configuration is not yet studied systematically[3] . This experiment has been done to study the effect of N/Z on fission dynamics and dissipative dynamics. We report here the results of fission cross section measurements for ^{16,18}O+^{194,198}Pt reactions at different sets of excitation energies which populate the compound nuclei with same Z (Z=86, Rn) but different value of N (i.e different N/Z and (N-Z)/A. This is a part of our programme to study the effect of N/Z in the neutron multiplicity measurements.

The experiment was carried out at GPSC at IUAC Pelletron accelerator, Delhi, using ^{16,18}O DC beam of energies in the range of 85-107 MeV. Self-supporting target of ^{194}Pt having a thickness around 1.7 mg/cm^2 and ^{198}Pt having thickness 2.15 mg/cm^2 were used for the measurement of the angular distribution of fission fragments. The targets were mounted at the center of 1.5 m diameter general purpose scattering chamber. Either of the fission fragments was detected in the angular range of 54° to 168° in the laboratory frame using two Si-detector telescopes (T1,T2) and three ΔE-E gas-surface barrier hybrid detectors (T1,T2,T3) [4]. The thickness of the SSBD detectors was about 300 ⌠m. The E detectors were backed by 10 ⌠m thick E (SSBD) detectors. The thickness of the E detectors in ⊗E-E gas-surface barrier hybrid detectors was 100 ⌠m. The distance of the telescopes (SSBD) from the target were about 13.3 cm and the distance for ⊗ E-E gas-surface barrier hybrid detectors T3, T4 and T5 were 28.7,27.6 and 28.5 cm, respectively. Each detector had an angular coverage of about ±1°. The detector was operated at 100 mbar gas pressure which corresponds to an equivalent silicon thickness of 2.5 ⌠m [4]. Two monitor si-detectors (M1,M2) with 1 mm collimator were kept at 10° with respect to the beam at a distance of about 70 cm from the target to monitor the Rutherford scattering and to monitor beam incidence. The data of the Rutherford scattering was used for the normalization to obtain the absolute fission cross sections. The relative solid angles of the telescopes were taken into account by measuring the data at overlapping angles.

The measured fission fragment angular distributions were transformed from laboratory to centre-of-mass frame using Viola systematics for symmetric fission [5]. Energy loss corrections of the beam in the half target thickness were applied before the conversion to centre-of-mass. Rutherford scattering events in the monitor detectors were used for the normalization to obtain the absolute fission cross sections. The differential fission cross section W(ℓ) was calculated using the expression

$$W(\theta) \propto \frac{d\sigma_{fis}}{d\Omega} = \frac{1}{2}\frac{Y_{fis}}{Y_{mon}}\left(\frac{d\sigma}{d\Omega_{mon}}\right)_R \frac{\Omega_{mon}}{\Omega_{fis}}$$

where Y_{fis} and Y_{mon} are the yields recorded by the fission detector and monitor (Rutherford) detector, respectively. ^$_{\phi 1\sigma}$ $\alpha\nu\delta$ ^$_{mon}$ are the solid angles subtended by the fission detector and monitor detector, respectively. $(d\int/d\hat{})_R$ is the differential Rutherford cross section in the laboratory system.The angular distributions were fitted to the sum of even Legendre polynomials up to order four to extract the fission fragment angular distribution. The experimental fission cross sections are in agreement with the fissility of the concerned compound nuclei; populated ^{210}Rn (fissility = 0.735) shows largest fission cross section and ^{216}Rn (fissility = 0.726) shows the least value of fission cross section among all the CN populated. The fission fragment angular distributions at different beam energies for ^{18}O + ^{198}Pt reaction is shown in the Fig.1.

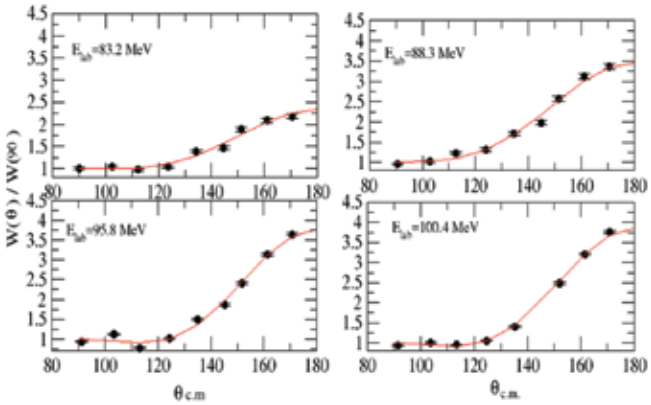

Fig. 1 : Fission fragment angular distributions at different beam energies for ^{18}O + ^{198}Pt. Red lines are the fits using Legendre polynomial.

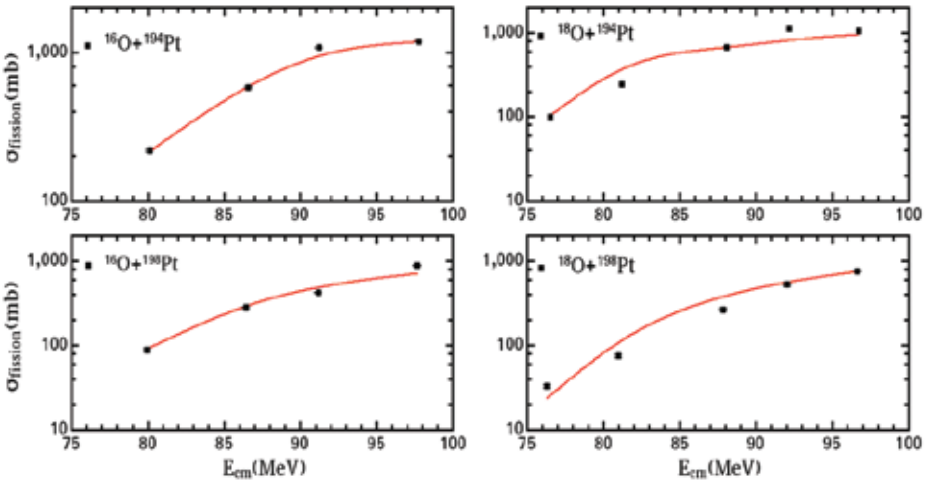

Fig. 2 : Experimental fission cross section for ^{16,18}O+^{194,198}Pt reactions. Red lines are the calculated values from PACE2 code.

The variation of fission cross section obtained experimentally are in agreement with fissility values of the compound nuclei. The experimentally extracted fission cross sections are shown in Fig. 2. Fission cross sections for ^{16}O+^{194}Pt at lower energies are consistent with the data already published [6]. Also it is clear for the Fig. 2 that the fission cross section decreases with the increases of the N/Z value of the compound nuclei.

References

[1] S. Kailas, Phys. Rep. 284 (1997) 381.
[2] J.P. Lestone et. al., J. Phys. G 23 (1997) 1349.
[3] Rohit Sandal et. al., Proc. DAE Symp. Nucl. Phys 53 (2008) 369.
[4] A. Jhingan et. al., Proc. DAE Symp. Nucl. Phys. 56 (2011) 1040.
[5] V.E. Viola, K. Kwiatkowski and M. Walker, Phys. Rev. C 31 (1985) 1550.
[6] E. Prasad et al., Nucl. Phys. A 882 (2012) 62.

5.1.2 Evaporation Residue excitation function measurements for the ^{16,18}O+^{194,198}Pt reactions

Rohit Sandal[1], B.R. Behera[1], N. Madhavan[2], S. Nath[2], J. Gehlot[2], A. Jhingan[2], K.S. Golda[2], H. Singh[4], V. Singh[1], A. Kumar[1], M. Kaur[1], G. Kaur[1], P. Sharma[1], S. Mandal[3], S. Verma[3], E. Prasad[5], K.M. Varier[6], A.M. Vinodkumar[7] and A. Saxena[8]

[1]Department of Physics, Panjab University, Chandigarh 160014, India
[2]Inter University Accelerator Centre, Aruna Asaf Ali Marg, New Delhi 110067, India
[3]Department of Physics and Astrophysics, University of Delhi, Delhi 110007, India
[4]Department of Physics, Kurukshetra University, Kurukshetra 136119, India
[5]Department of Physics, School of Mathematical and Physical Sciences, Central University of Kerala, Kasaragod 671328, India
[6]Department of Physics, Kerala University, Kariavattom Campus, Trivandrum 695581, India
[7]Department of physics,University of Calicut, Calicut 673635, India
[8]Nuclear Physics Division, Bhabha Atomic Research Centre, Mumbai 400085, India

The process of heavy-ion collision has shown unexpected facets that have been uncovered by the considerable amount of work (both experimentally and theoretically), accumulated during the last decade in fusion-fission dynamics. Differences found in the fusion excitation functions as the number of neutrons or protons changes suggest that the structure of the colliding nuclei plays an important role in this kind of reaction [1]. It is also found that fusion-fission reaction dynamics is very much sensitive to the entrance channel parameters. Measurement of evaporation residue (ER) cross section can reveal information about the pre-saddle dissipation. It is also pointed out that ER cross section is a more sensitive probe [2] for understanding nuclear friction. In this report we present the experimental techniques and methods of analysis for extracting the values of the ER cross section for the $^{16,18}O+^{194,198}Pt$ reactions, at different set of excitation energies. These reactions populate the compound nuclei with same Z (Z=86, Rn) but with different values of N (i.e different N/Z and (N-Z)/A). This is a part of our programme to study the effect of N/Z on neutron multiplicity to understand the dissipative effects in fusion-fission dynamics [3].

The experiment was performed at the 15 UD Pelletron accelerator facility of the IUAC, New Delhi. Pulsed $^{16,18}O$ beams with a pulse separation of 4 μs were used in the experiment to bombard isotopically enriched ^{194}Pt and ^{198}Pt targets of thicknesses 260 μg/cm^2 and 170 μg/cm^2 each on 10 μg/cm^2 thick carbon backing, respectively. ER excitation function measurements were performed at laboratory beam energies (after correcting for the loss in the pressure window foil, made of 660 μg/cm^2 carbon, and half thickness of the targets) of 78.0 to 105.6 MeV of ^{16}O and 77.8 to 105.4 MeV of ^{18}O. Along with these measurements, ER excitation function was also measured at few energy points for $^{16}O+^{194}Pt$ reaction, for which data were already published [4]. The heavy ERs produced in the reaction were separated from the intense beam background by the gas-filled separator HYRA [5]. Elastically scattered oxygen ions were detected in two silicon surface barrier detectors placed at ±22.7° with respect to the beam direction. The helium gas pressure in the HYRA was set at 0.15 Torr and the required HYRA magnetic field values were calculated using a simulation program. Low-energy ERs reaching the focal plane were detected using a MWPC. At each energy point, magnetic field values were also optimized by maximizing the ER yield at the focal plane, keeping the pressure fixed at 0.15 Torr. To get the time-of-flight signal, the start was taken from the focal plane MWPC anode and stop signal was taken from the RF used for beam pulsing. The logical 'OR' signal of two monitor detectors and MWPC anode was the master strobe for the data acquisition system.

The total ER cross section was calculated using the following expression

$$\sigma_{ER} = \frac{Y_{ER}}{Y_{Mon}} \left(\frac{d\sigma}{d\Omega} \right)_R \Omega_{Mon} \frac{1}{\varepsilon_{HYRA}}$$

where σ_{ER} is the ER cross section in mb, Y_{ER} is the ER yield at the focal plane, Y_{mon} is the yield in the monitor detector, ε_{HYRA} is the HYRA transmission efficiency, and Ω_{mon} is the solid angle subtended by the monitor detector. $(d\sigma/d\Omega)_R$ is the differential Rutherford cross section in the laboratory system. We followed the method outlined in Ref. [4] to get the transmission efficiency of the HYRA for the given reactions. ER angular distributions

for the reactions $^{16,18}O+^{198}Pt$ along with the $^{16}O+^{194}Pt$ (at 96 MeV beam energy) were simulated using the Monte Carlo code TERS [6]. The statistical model code PACE3 [7] was used to check major decay channels for all the reactions. The angular distributions were simulated (for 10000 events) for individual evaporation channels and those were combined to obtain the total ER angular distribution, taking proper weightage from PACE3 results for each reaction. The circular exit aperture of the target chamber, translating to an angle (polar) of 3.35°, was defined as the angular acceptance of the HYRA for the present experimental setup. Using areas under each curve (shown for two reactions in Fig. 1) within the acceptance while keeping the total area under each curve same, we estimate the transmission efficiency in each case.

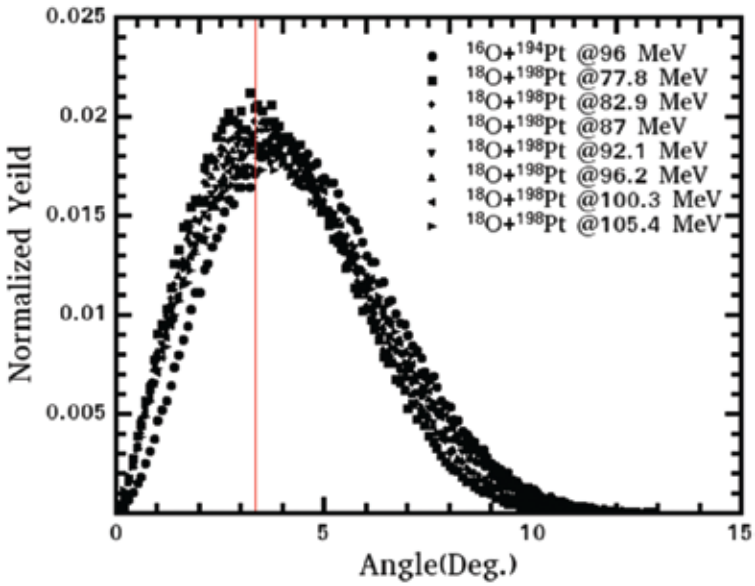

Fig. 1: Normalized ER angular distributions for $^{16}O+^{194}Pt$ and $^{18}O+^{198}Pt$ reactions, simulated using the Monte Carlo code TERS. The vertical line at 3.35° defines angular acceptance in the present set-up.

It was assumed that transmission efficiency relies only on the angular distribution of ERs and angular acceptance of the HYRA. Experimentally extracted ER excitation functions for the systems are shown in Fig. 2. From the Fig. 2 it is clear that ER cross section increases with N/Z value of compound nuclei. Detail statistical model calculation is in progress.

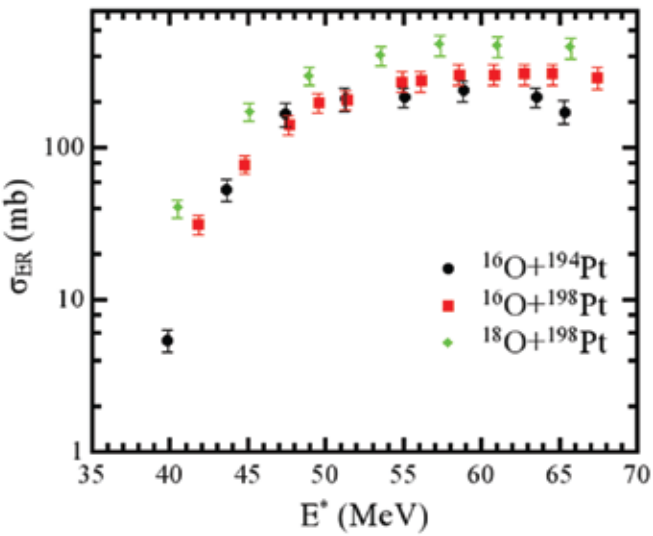

Fig. 2: ER excitation functions for $^{16,18}O+^{198}Pt$ reactions. $^{16}O+^{194}Pt$ data were taken from Ref. [4].

References

[1] M. Beckerman, et al., Phys. Rev. Lett. 45 (1980) 1472.

[2] P. Frobrich and I. I. Gontchar, Nucl. Phys. A 563 (1993) 326.

[3] Rohit Sandal et al., Proc. DAE Symp. Nucl. Phys 55 (2010) 318.

[4] E. Prasad,. et al. Phys. Rev. C 84 (2011) 064606.

[5] N. Madhavan et al., Pramana – J. Phys. 75 (2010) 317.

[6] S. Nath, Comput. Phys. Commun. 180 (2009) 2392.

[7] A. Gavron, Phys. Rev. C 21 (1980) 230.

5.1.3 Evaporation residue excitation function for $^{18}O+^{194}$ Pt reaction

P.V. Laveen[1], E. Prasad[1], N. Madhavan[2], S. Nath[2], J. Gehlot[2], K.M. Varier[3], A.M. Vinodkumar[4], B.R.S. Babu[4,7], B.R. Behera[5], Rohit Sandal[5,8], Varinderjit Singh[5], A. Jhingan[2] , A. Shamlath[1] and S. Kailas[6]

[1]Department of Physics, School of Mathematical and Physical Sciences, Central University of Kerala, Kasaragod 671328, India

[2]Inter University Accelerator Centre, Aruna Asaf Ali Marg, New Delhi 110067, India
[3]Department of Physics, Kerala University, Kariavattom Campus, Trivandrum 695581, India
[4]Department of Physics, University of Calicut, Calicut 673635, India
[5]Department of Physics, Panjab University, Chandigarh 160014, India
[6]Nuclear Physics Division, Bhabha Atomic Research Centre, Mumbai 400085, India
[7]Department of Physics, Sultan Quaboos University, Muscat, Oman
[8]S.V.N. Govt. College, Ghumarwin, Bilaspur 174021, Himachal Pradesh, India

The study of fission hindrance which leads to the increase in the survival probability of Evaporation Residues (ERs) formed in fusion-fission reaction has been the topic of extensive theoretical and experimental work in recent years. ER formation is a clear signature of Compound Nucleus (CN) formation [1] and its survival probability against fission and quasi-fission are important in the production of Super Heavy Elements (SHE). Though the experimental studies of emission rates of neutrons, gamma rays and charged particles show the hindrance of fission relative to the expectation of statistical models description, ER measurement probes this aspect better with greater sensitivity to pre-saddle region. The suppression of fission due to dissipation enhances the survival probability of ERs [2].

The experiment was performed using Hybrid Recoil mas Analyzer (HYRA) operated in gas-filled mode [3]. Pulsed ^{18}O beam (TWD with 4 μs pulse separation) was used to bombard the isotopically enriched target of ^{194}Pt (270μg/cm^2 on 15μg/cm^2 thick carbon backing) in the measurement. The measurements were performed at laboratory beam energies (after correcting for the loss in the pressure window foil (660 ⎡g/cm^2 thick carbon foil), carbon backing and half thickness of the target) of 77.7, 82.8, 86.9, 92.1, 96.1, 100.2 and 105.3 MeV. Two monitor detectors mounted at ± 22.7° were used for registering the Rutherford events and were used for normalizing the absolute cross sections. HYRA was operated at 0.15 Torr helium gas pressure throughout the experiment. The ERs reaching the focal plane were detected using a large area position sensitive MWPC detector of active area 5"×2". A TAC spectrum was generated by taking the "start" from the MWPC-anode signal and "stop" from the TWD-signal, and was used to effectively separate the ERs reaching the focal plane from other background particles.

The $^{16}O+^{194}Pt$ reaction [3] was used as the calibration system to obtain the HYRA transmission efficiency. The normalized angular distributions of ERs from reactions $^{18}O+^{194}Pt$ and $^{16}O+^{194}Pt$ were simulated using the semi-Monte Carlo code TERS [5] and the angular distributions were compared within the geometrical angular acceptance of HYRA. The time-of-flight (TOF) versus energy spectrum for $^{18}O+^{194}Pt$ reaction at 96.1 MeV is shown in Fig. 1. The events shown inside the gate are the ERs reaching the focal plane and are well separated from the other contaminants. The reduced ER cross sections of the $^{16}O+^{194}Pt$ and present reaction are shown in Fig. 2. $^{16}O+^{194}Pt$ reaction (forming the CN ^{210}Rn with neutron number N=124) required a dissipation strength (β) = 1.5 for fitting the experimental data. The present reaction forms CN ^{212}Rn with N =126 shell closure. In this study, we are exploring the role of neutron shell closure in fusion-fission dynamics and on the onset of dissipative forces at high excitation energies. The statistical model analysis is in progress.

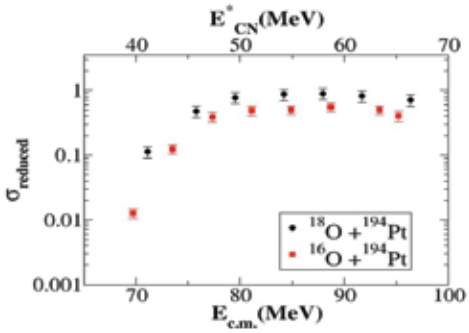

Fig. 1. TOF vs. Energy spectrum for $^{18}O+^{194}Pt$ at 96.1 MeV.

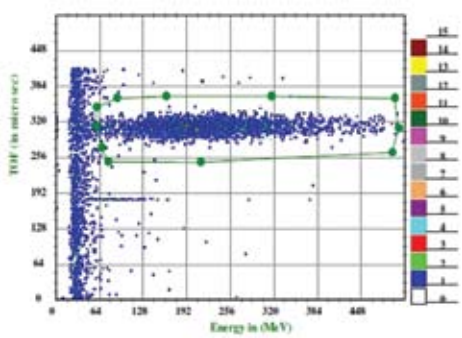

Fig. 2. Reduced ER cross sections for both reactions.

References

[1] N. Bohr, Nature 137 (1936) 344.
[2] B. B. Back et. al., Phy.Rev C 60 (1999) 044602.
[3] N. Madhavan et al., Pramana -J. Phys. 81 (2010) 317.
[4] E. Prasad et.al., Phy. Rev C 84 (2011) 064606.
[5] S. Nath, Comput. Phys. Commun. 179 (2008) 492.

5.1.4 An exploratory experiment to measure evaporation residue cross sections for ^{48}Ti+^{140,142}Ce systems

B.R. Behera[1], N. Madhavan[2], S. Nath[2] , J. Gehlot[2], Maninder Kaur[1],Varinderjit Singh[1], Priya Sharma[1], Meenu Thakur[1], Kushal Kapoor[1], Davinder Siwal[3], I. Mukul[2], A. Jhingan[2] and A. Saxena[4]

[1]Department of Physics, Panjab University, Chandigarh 160014, India
[2]Inter University Accelerator Centre, Aruna Asaf Ali Marg, New Delhi 110067, India
[3]Department of Physics and Astrophysics, University of Delhi 110007, India
[4]Nuclear Physics Division, Bhabha Atomic Research Centre, Mumbai 400085, India

The dynamics of heavy-ion fusion and fission at energies around the Coulomb barrier is an open problem in the field of low energy nuclear physics. In particular, when the compound nucleus is heavy the quasi-fission reaction channel becomes increasingly important and competes with fusion-fission and fusion-evaporation reaction [1]. At energies above the Coulomb barrier fusion hindrance takes place due to various dynamical effects. It is in general believed that an extra energy is required to fuse symmetric target-projectile combination compared to asymmetric target-projectile combination. In some of the recent studies the dependence of the fusion reaction on the nuclear shell structure was investigated and the importance of N=82 in the heavy-ion fusion reaction was proposed [2]. In many cases entrance channel effects in the fusion and fission reactions were also demonstrated [1,3]. The fusion reaction between two large mass nuclei also depends on nuclear structure of the colliding nuclei (coupling with inelastic excitation and transfer channel and deformation, etc.) [1]. In the production of super-heavy nuclei it was demonstrated that in the cold fusion approach normally shell closed target-projectile is chosen for the stability of the compound nucleus formation. Oganessian et al. [3-4], measured the evaporation residue cross section in the fusion reactions ^{130}Xe+^{86}Kr and ^{136}Xe+^{86}Kr, where the nucleus ^{136}Xe has a closed neutron shell N=82 and the neutron number of the nucleus ^{130}Xe is 76. It was found that the measured evaporation residue (ER) cross sections for the fusion reaction ^{136}Xe+^{86}Kr are almost two to three orders of magnitude larger than those for the fusion reaction ^{130}Xe+^{86}Kr. These few experiments suggest that the shell structure plays an important role in the low energy fusion process.

On the other hand, gaps in the single-particle energies of orbitals are responsible for shell stabilization of the super-heavy nuclei. Excited states in heavy nuclei allow us the measurement of the single particle energies. Since the production cross section of heavy nuclei decreases with increasing mass and proton number, in-beam spectroscopy becomes increasingly difficult and structural information are less. In order to perform a gamma or alpha spectroscopy experiment, understanding the ER cross section is essential. One should exploit the accessible beams and projectiles for better understanding the ER cross section for shell closed nuclei. In order to investigate the effect of the nuclear shell structure, the entrance channel effect and the other nuclear structure effect in fusion process, we have started an experimental programme in the gas filled separator HYRA for mapping the ER cross sections for several shell closed nuclei. The primary motivation of the programme is to disentangle the effect of extra-push and shell closure effect in fusion dynamics. In the first part of the experimental series we plan to measure the ER cross-sections for the ^{48}Ti+^{140,136,142}Ce systems. In the first case the target ^{140}Ce is neutron shell closed with N = 82. By measuring the ER cross-sections for the 1st , 2nd and third case we can map the shell closure effect from N=78, 82 and 84. In this write-up we report the ER cross-section measurements for ^{48}Ti+^{140,142}Ce system.

The experiment was performed at the Pelletron+LINAC accelerator facility of the Inter University Accelerator Centre (IUAC), New Delhi. Pulsed ^{48}Ti beams with a pulse separation of either 4 μ s or 250

ns was used for the experiment. The targets used were isotopically enriched ^{140}Ce and ^{142}Ce of thickness 212 ⎡g/cm^2 and 225 ⎡g/cm^2 , each on a 10 ⎡g/cm^2 thick carbon backing, respectively. ER excitation function measurements were performed at laboratory beam energies in the range of (after correcting for the loss in the pressure window foil (1.1 mg/cm^2 of Ni foil) and half thickness of the targets) of 239.6 to 192.9 MeV. Along with these measurements, ER excitation function was also measured for few energy points for ^{48}Ti+^{124}Sn reaction for comparison purposes. The heavy ERs produced in the reaction were separated from the intense beam background by the gas-filled separator, Hybrid Recoil Mass Analyzer (HYRA) [6]. Elastically scattered titanium ions were detected in two silicon surface barrier detectors placed at ±24° with respect to the beam direction. Scanning was performed for two energy points for the optimum helium gas pressure and found to be 0.30 Torr. For all beam energies the helium gas pressure in the HYRA was set at 0.30 Torr and HYRA magnetic fields setting were calculated using a simulation program [7]. Low-energy ERs reaching the focal plane were detected using a position sensitive multiwire proportional counter (MWPC). At each energy point, magnetic field values were also optimized by maximizing the ER yield at the focal plane, keeping the pressure fixed at 0.30 Torr. To get the time of flight signal, the start was taken from the focal plane MWPC anode signal and stop signal was taken from RF used for beam pulsing. The logical 'OR' signal of two monitor detectors and MWPC anode was the master strobe for the data acquisition system. During the actual experiment, the beam current was low, so few measurements were taken with 4 ⎡s repetition rate; otherwise measurements were taken with the normal LINAC beam. Typical representative of the spectra are given below.

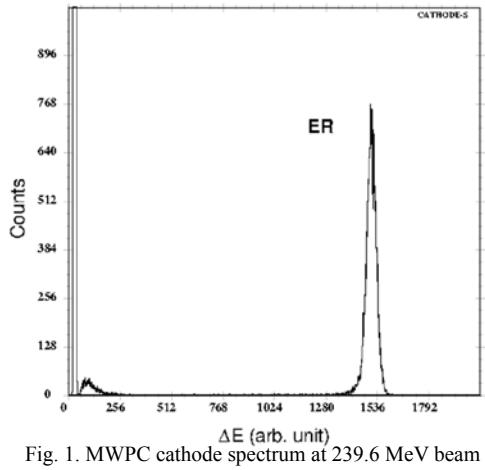

Fig. 1. MWPC cathode spectrum at 239.6 MeV beam energy.

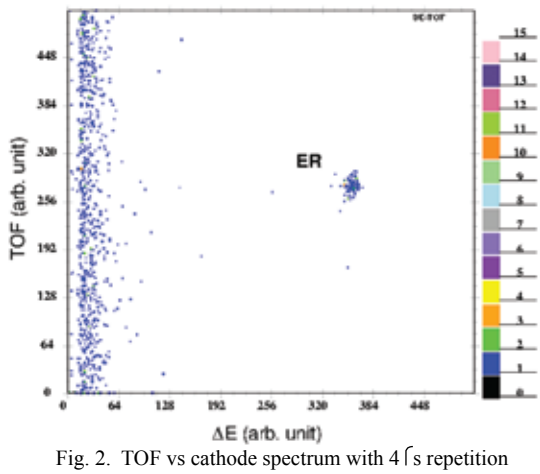

Fig. 2. TOF vs cathode spectrum with 4 ⎡s repetition rate of LINAC beam at 239.6 MeV.

The analysis is in progress and request for beam time for the next set of experiments is already given for the next accelerator user committee meeting.

References

[1] A.M. Stefanini et al., Proc. Fusion-08, AIP Conf. Proc. 1098 (2009) 3.
[2] K. Satou et al., Phys. ReV C 65 (2002) 054602.
[3] Yu.Ts. Oganessian et al., JINR Scientific Report 1995-1996, 1997, 1998-2005.
[4] Yu.Ts Oganessian et al., Nature (London) 400 (1999) 242.
[5] M.G. Itkis et al., Nucl. Phys. A 734 (2004) 136.
[6] N. Madhavan et al., Pramana – J. Phys. 75 (2010) 317.
[7] S. Nath, Comput. Phys. Commun. 180 (2009) 2392.

5.1.5 Measurement of evaporation residue cross section and spin distributions in ^{28}Si+^{176}Yb reaction

R. Tripathi[1], S. Sodaye[1], S. K. Sharma[1], P. K. Pujari[1], J. Gehlot[2], N. Madhavan[2], S. Nath[2], G. Mohanto[2], I. Mukul[2], A. Jhingan[2] and I. Mazumdar[3]

[1]Radiochemistry Division, Bhabha Atomic Research Centre, Mumbai 400085, India

[2]Inter University Accelerator Centre, Aruna Asaf Ali Marg, New Delhi 110067, India
[3]Department of Nuclear and Atomic Physics, Tata Institute of Fundamental Research, Mumbai 400005, India

Study of fusion hindrance in reaction systems with low Z_pZ_T has currently been an active area of investigation [1-4]. Based on the studies of mass distribution, the onset of fusion hindrance has been proposed to be around Z^PZ^T~1000 [1]. In order to investigate fusion hindrance around this region, evaporation residue cross section and spin distribution was measured in $^{28}Si+^{176}Yb$ reaction using the HYRA gas-filled separator coupled to TIFR 4π spin spectrometer [5] at Inter University Accelerator Centre, New Delhi. An electrodeposited target of ^{176}Yb, on a thin aluminium backing, was used for the experiments. Experiments were carried out with ^{28}Si beam of energy 150 to 185 MeV (in steps of 7 MeV) provided by the accelerator facility after the energy boost by LINAC. The corresponding beam energies in the target were 136.7 to 173.0 MeV after the energy degradation. Evaporation residues were separated from the beam particles by the HYRA, operated in the gas-filled mode, and detected by a multi-wire proportional counter at the focal plane. In order to normalize for the target thickness and beam intensity, elastically scattered beam particles were detected using two monitor detectors placed at ±25°. For clear selection of evaporation residues TOF with respect to the beam pulse as well as energy loss signal from the MWPC were recorded. Typical cathode spectrum of MWPC and TAC spectrum obtained at beam energy of 158.5 MeV are shown in Fig. 1 and 2, respectively. In order to determine the residue spin distributions, prompt gamma-rays emitted by the residues were detected by the 4π spin spectrometer consisting of 29 NaI(Tl) detectors. Use of a nearly 4π geometry provided the fold data up to ~20 folds. A typical plot of fold distribution at the beam energy of 158.5 MeV is shown in Fig. 3. Due to the comparable cross sections for evaporation residues and fission in the compound nucleus mass region~200, information about the spin distributions of evaporation residues becomes important. Also, availability of evaporation residue spin data would better constrain theoretical calculations. The results from the present studies on the evaporation residue cross sections and spin distributions along with the results of our earlier study on fission fragment angular distributions [2] would help in understanding the onset of fusion hindrance in the pre-actinide region.

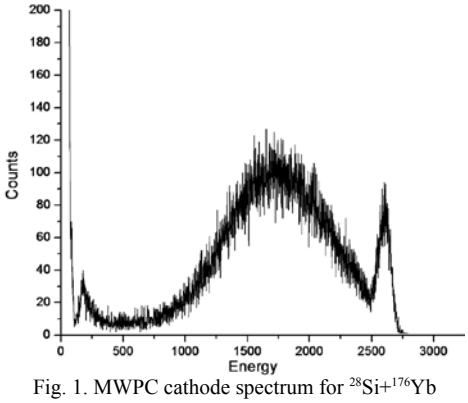

Fig. 1. MWPC cathode spectrum for $^{28}Si+^{176}Yb$ reaction at E_{lab} = 158.5 MeV.

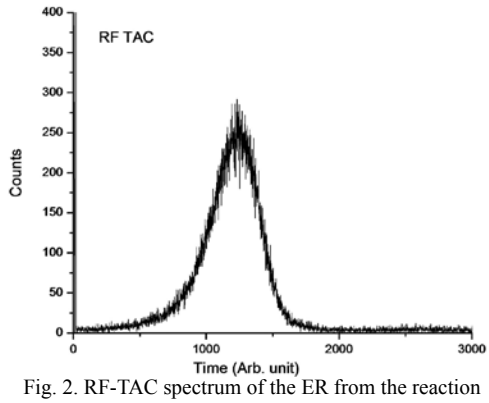

Fig. 2. RF-TAC spectrum of the ER from the reaction $^{28}Si+^{176}Yb$ reaction at E_{lab} = 158.5 MeV.

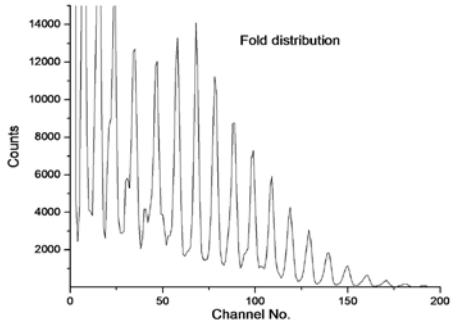

Fig. 3. γ-fold distribution of $^{28}Si+^{176}Yb$ reaction at E_{lab} = 158.5 MeV.

References

[1] R. Rafiei et al., Phys. Rev. C 77 (2008) 024606.
[2] R. Tripathi et al., Phys. Rev. C 79 (2009) 064607.
[3] E. Prasad et al., Phys. Rev. C 81 (2010) 054608.
[4] S. Appannababu et al., Phys. Rev. C 83 (2011) 034605.
[5] N. Madhavan et al., EPJ Web Conf. 17 (2011) 14003.

5.1.6 Spin distribution measurements for $^{16}O+ ^{64}Zn$ and $^{32}S+^{48}Ti$ reactions

Maninder Kaur[1], B.R. Behera[1], Varinderjit Singh[1], N. Madhavan[2], S. Muralithar[2], S. Nath[2], J. Gehlot[2], G. Mohanto[2], I. Mukul[2], Davinder Siwal[3], Meenu Thakur[1], Kushal Kapoor[1], Priya Sharma[1], T. Varughese[2], A. Jhingan[2], Indu Bala[2], B.K. Nayak[4], A. Saxena[4], M.B. Chatterjee, and G. Singh[1]

[1]Department of Physics, Panjab University, Chandigarh 160014, India
[2]Inter University Accelerator Centre, Aruna Asaf Ali Marg, New Delhi 110067, India
[3]Department of Physics and Astrophysics, University of Delhi 110007, India
[4]Nuclear Physics Division, Bhabha Atomic Research Centre, Mumbai 400085, India

Over the past few decades, considerable efforts have been made in understanding the spectra of the light particles evaporated from the various excited compound nuclear systems. These studies yield direct information about the main statistical model ingredients, the nuclear level densities and barrier penetration probabilities. Different studies have shown that the mass symmetric systems deviate from the statistical model at high excitation energies. Several investigations report the use of structure dependent level density as a solution for it [1]. Some of the authors claimed that light charged particle spectra can be explained by lowering the emission barrier [2]. In some of the studies [3], the analysis of alpha spectra through dynamical model code HICOL predicted that the effective l_{max} value for fusion to take place in the case of symmetric system is low as compared to that obtained through Bass systematics [4]. However, in most of the measurements existing in literature, consistent analysis was not performed taking other variables (cross-section, spin distribution, etc.) into account. With this motivation we have proposed the ER cross-section (fusion cross-section) as well as ER-spin distribution measurements for the asymmetric $^{16}O+^{64}Zn$ and symmetric $^{32}S+^{48}Ti$ reactions populating the same compound nucleus, ^{80}Sr. The alpha particle, proton and neutron spectra for the above systems have already been measured [3]. Here, we report the preliminary results of spin distribution measurements.

The experiment was carried out using Heavy ion reaction analyzer (HIRA) [5] + BGO multiplicity filter [6] at IUAC, New Delhi. Pulsed beam of ^{16}O with repetition rate of 2 μs, in the energy range from 66.6 to 91.9 MeV and ^{32}S with repetition rate of 1 μs, in the energy range from 95 MeV to 125 MeV were bombarded on isotopic enriched targets of ^{64}Zn and ^{48}Ti, respectively. The thickness of both of these targets was about 500 μg/cm^2. The targets were placed at the center of the target chamber and two Si surface barrier detectors were mounted at ±25° with respect to beam direction. These detectors were used for monitoring the beam and to normalise the yield to extract the cross-section values. Spin distribution measurement was performed with 14 element BGO multiplicity array (7 detectors above and 7 below the target chamber), placed in a close geometry (at a distance of 24 mm from the target). The multiplicity filter covered 48% of the total 4μ solid angle. The target ladder was tilted at 45° with respect to the beam direction and about a horizontal axis to rule out attenuation of γ-rays in the target ladder. The focal plane detector system consisted of a MWPC detector of dimension 6"×2". A time-of-flight (TOF) spectrum was generated using anode signal of MWPC as start and the RF signal of beam as stop. Further, a two-dimensional plot was generated using TOF and energy loss signal of MWPC. It provides a clean separation of ERs from beam-like components as shown in Fig. 1.

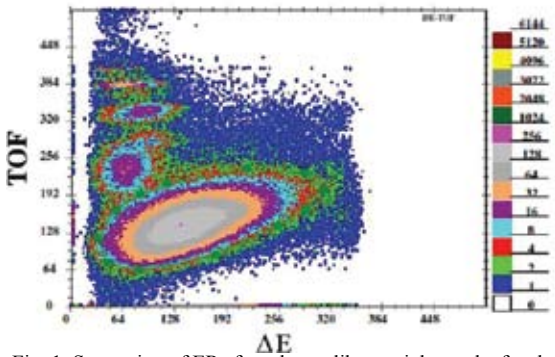

Fig. 1. Separation of ERs from beam-like particles at the focal plane of HIRA.

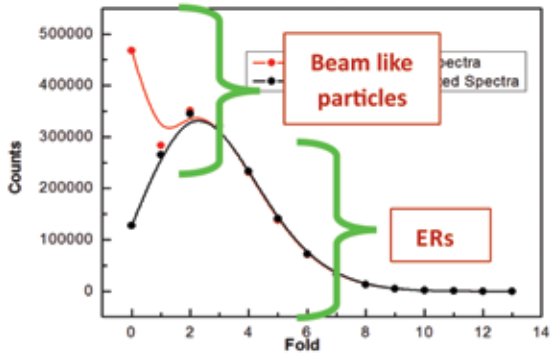

Fig. 2. Comparison of raw and ER-gated fold spectra for the $^{16}O+^{64}Zn$ system at E_{lab} = 91.9 MeV.

The γ-fold distribution was generated offline, from the 14 TDC signals, using CANDLE [7] software. The raw γ-fold spectrum was gated with ER events from the energy versus TOF spectrum for removing the background (see Fig. 2). Experimentally measured γ-fold distribution was converted to corresponding γ–multiplicity distribution using the Van Der Werf prescription [8]. The multiplicity distribution was assumed to be a modified Fermi function of the form

$$P(M_\gamma) = \frac{2M_\gamma + 1}{1 + \exp\left(\frac{M_\gamma - M_{\gamma 0}}{\Delta M_\gamma}\right)}$$

where $M_{\gamma 0}$ and ΔM_γ are two free parameters that were varied at each E_{lab} to obtain the best fit for fold distribution. Values of $M_{\gamma 0}$ and ΔM_γ were found by $\chi 2$ minimization of fold distribution. The comparison of fitted fold distribution and extracted multiplicity distributions for both the systems at two different beam energies are shown in Fig. 3 and Fig. 4.

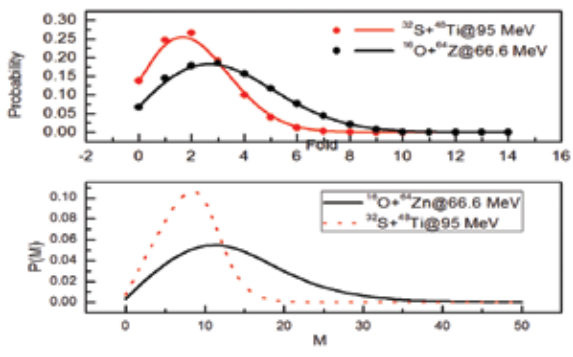

Fig. 3. Comparison of fitted fold distributions (top) and extracted gamma multiplicity distributions (bottom) for both the systems at E*= 52.8 MeV.

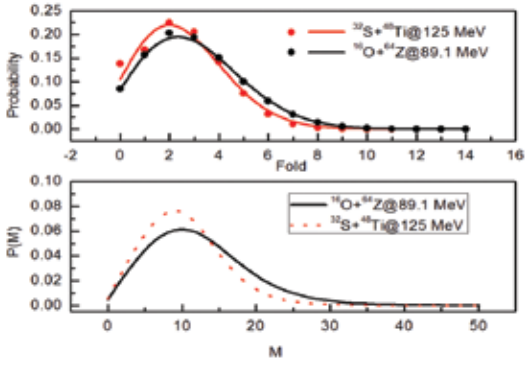

Fig. 4. Same as Fig.3. but at E* = 70.8 MeV.

For performing the detailed theoretical calculation, knowledge of both fusion cross section and spin distribution are required. The cross-section measurements are planned and the experiment will be performed soon. The extracted spin distribution and the experimental fusion cross-section will be fed to the statistical model for explaining the alpha particle spectra measured earlier [3].

References

[1] D.K. Agnihotri et al.,Phy. Lett. B 307 (1993) 283.
[2] B. Fornal et al., Phy. Rev. C 37 (1988) 2624.
[3] J. Kaur et al., Phy. Rev. C 70 (2004) 017601.
[4] R. Bass, Phys. Rev. Lett. 39 (1977) 265.
[5] A.K. Sinha et al., Nucl. Instr. Meth. A 339 (1994) 543.
[6] S. Murlithar et al., Proc. DAE Symp. Nucl. Phys. 34 B (1991) 417.
[7] E.T. Subramaniam, B.P. Ajith Kumar and R.K. Bhowmik, Collection and Analysis of Nuclear Data using Linux nEtwork (unpublished).
[8] S.Y. Van Der Werf, Nucl. Instr. Meth. 153 (1978) 221.

5.1.7 Study of isomer decay in Bi nuclei at the focal plane of HYRA

G. Mukherjee[1], T. Roy[1], Soumik Bhattacharya[1], H. Pai[1], T.K. Rana[1], C. Bhattacharya[1], S. Bhattacharya[1], S. Bhattacharyya[1], N. Madhavan[2], S. Nath[2], R.P. Singh[2], A. Jhingan[2], S. Muralithar[2], R. Kumar[2], J. Gehlot[2], T. Varughese[2], I. Bala[2], A.K. Sinha[3], S.S. Ghugre[3], R. Raut[3], S.S. Bhattacharjee[3], K. Basu[3], R. Palit[4]

[1]Variable Energy Cyclotron Centre, 1/AF Bidhan Nagar, Kolkata 700064, India
[2]Inter University Accelerator Centre, Aruna Asaf Ali Marg, New Delhi 110067, India
[3]UGC-DAE-CSR Kolkata Centre, Sector III/LB-8 Bidhan Nagar, Kolkata 700098, India
[4]Tata Institute of Fundamental Research, Homi Bhabha Road, Colaba, Mumbai 400005, India

Investigation of decay of high spin isomers is one of the interesting aspects in the experimental nuclear structure research. The isomers would dominate for the heavy nuclei with proton and/or neutron numbers close to the shell closure. For Bismuth nuclei (Z = 83) in the A = 190 region, the proton Fermi level lies just above the Z = 82 shell closure and the neutron Fermi level lies below the N = 126 shell closure. Therefore, the high spin states in Bi nuclei are expected to be dominated by isomers. A 750 ns isomer has been known for a long time in ^{195}Bi [1] whose excitation energy and decay path has been reported recently [2]. A rotational band has also been reported in this nucleus based on $13/2^+$ isomer, originated from the deformation driving $i_{13/2}$ state. This band was reported to have prompt feeding through a 457 keV γ-ray apart from a strong feeding from the 750 ns isomer. In ^{193}Bi, the $29/2^-$ state is a 3 μs isomer; apart from this an isomer with half-life > 10 μs is also known in this nucleus. But the excitation energy, spin, or parity of the state is not known [3]. The aim of the present work was to find new isomer in ^{195}Bi and to characterize the isomer decays in ^{193}Bi.

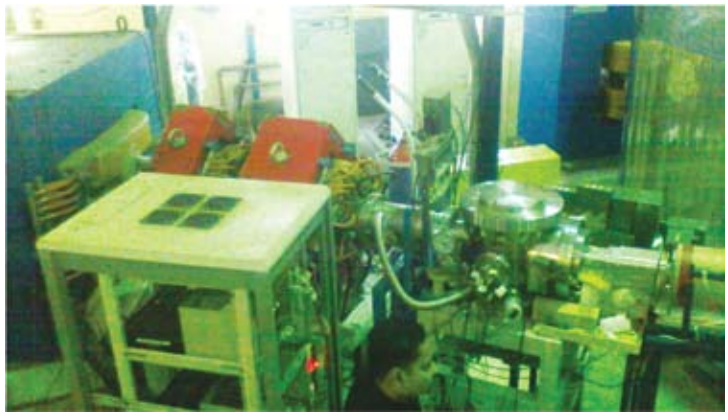

Fig. 1. The experimental set up at the focal plane of HYRA.

The experiment was done at the HYRA facility of IUAC, New Delhi. The fusion evaporation reaction ^{30}Si(^{169}Tm, xn)^{193,195}Bi was used to populate the high spin states in the above two nuclei. The target (mono-isotopic) was a self supporting foil of ~ 0.8 mg/cm^2 thickness made by rolling method at the IUAC target laboratory. The beam of ^{30}Si was provided from the Pelletron-LINAC facility of IUAC. Beam energy was between 155 – 179 MeV. The gas-filled separator HYRA was used to separate the evaporation residues (ERs) from the background events and transport to the focal plane. A Ni foil was used upstream from the target to separate gas-filled (0.15 Torr He) region of the HYRA from the beam line. Beam energy loss in

this foil was ~ 10 MeVl. The focal plane chamber consisted of a MWPC followed by three Si pad detectors in which the ERs were stopped. A Clover HPGe detector was placed behind the focal plane chamber. A re-entrant cup was used to keep the clover detector close to the Si pad detectors to increase detection efficiency. A Clover detector was placed near the target chamber also. ER time-of-flight (from the target to the focal plane) was estimated to be ~ 1.5 μs. The multi-parameter data were recorded in the list mode using the CANDLE software whenever either MWPC or Si pad detectors registered a signal. Time between the MWPC and the Clover detector (OR of all the four crystals) (T1) and between master and the individual crystals were recorded. The latter one ensured that the four crystals could also be used as four individual detectors for γ-γ coincidence measurements.

The states in ^{193}Bi were produced at 179 MeV of beam energy and the known isomeric transitions from the isomers were observed in the add-back spectrum of the focal plane Clover detectors. This ensured that the set up was working well. 155 MeV of beam energy was used for populating ^{195}Bi. The add-back γ-ray spectrum obtained in the focal plane Clover detector is shown in Fig. 2. The top panel shows the spectrum without the gate on ERs. The ERs were identified from a two-dimensional plot of MWPC (cathode) and Si Pad detector. The γ-ray spectrum in the top panel gated by ERs is shown in the bottom panel of Fig. 2. It is evident from these figures that the spectrum is dominated by the background lines without the ER gate. The ER gate ensured a clean spectrum with lines only belonging to the ERs. In the ER-gated spectrum, apart from γ-rays from isomeric decays of ^{195}Bi, some known lines from the isomeric decays of ^{194,195}Pb were also observed.

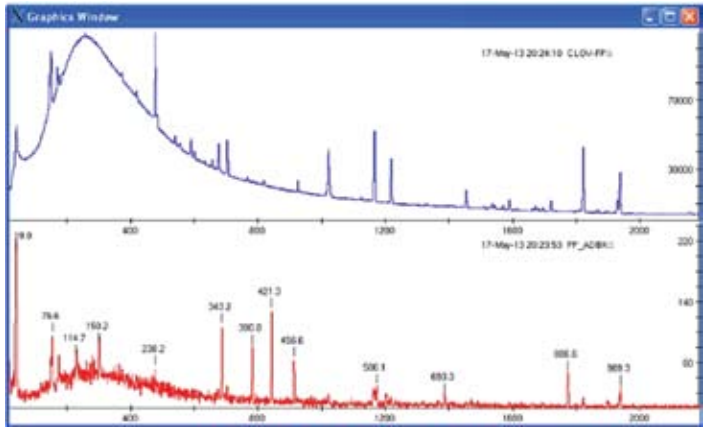

Fig. 2. Add-back spectrum in focal plane Clover detector with (bottom) and without (top) gate on ERs, identified by MWPC and Si pad detectors. The marked peaks are mostly from isomeric decay in ^{195}Bi.

The 115, 150, 343, 391, 421 and 886 keV γ-lines are the known lines in ^{195}Bi which are fed from the 750 ns isomer. It is interesting to see the 456.6 keV line in Fig. 2 (bottom panel) as this is the γ-transition identified as the prompt feeding to the rotational band in ^{195}Bi, as mentioned earlier. The presence of this line indicates that there is another isomer in ^{195}Bi which lies above the 750 ns isomer. The time T1 has been projected with sum energy gate on the lower lying transitions and also with gate on 457 keV transition.

In conclusion, isomer decay studies were successfully demonstrated at the focal plane of HYRA for the first time. The known isomeric decays were clearly observed. Clear indication of a new isomer in ^{195}Bi was obtained. Detailed analysis to measure the half-life and the decay pattern of the new isomer is in progress.

Untiring effort of the Pelletron and LINAC staff for providing good beam and help of Dr. D. Kabiraj and S.R. Abhilash in the preparation of the target foil are gratefully acknowledged.

References

[1] T. Lönnroth et al., Phys. Rev. C 33 (1986) 1641.
[2] H. Pai et al., Phys. Rev. C 85 (2012) 064317.
[3] P. Nieminen et al., Phys. Rev. C 69 (2004) 064326.

5.1.8 Search for high-spin isomer in 188Tl at the focal plane of HYRA

R. Palit[1], J. Sethi[1], D. Choudhury[1], S. Saha[1], S. Biswas[1], P. Singh[1], S.V. Jadav[1], B.S. Naidu[1], S. Tandel[2], S. Kumar[3], S. Mandal[3], Rojita[3], Khushboo[3], N. Kumar[3], V. Singh[4], S. Kumar[4], T. Trivedi[5], A.K. Sinha[6], S. Ghugre[6], G. Mukherjee[7], N. Madhavan[8], S. Nath[8], R.P. Singh[8], A. Jhingan[8], S. Muralithar[8], R. Kumar[8], J. Gehlot[8], T. Varughese[8] and I. Bala[8]

[1]Tata Institute of Fundamental Research, Homi Bhabha Road, Colaba, Mumbai 400005, India
[2]Centre for Excellence in Basic Sciences, Mumbai 400098, India
[3]Department of Physics and Astrophysics, University of Delhi, Delhi 110007, India
[4]Department of Physics, Punjab University, Chandigarh 160014, India
[5]Department of Pure and Applied Physics, Guru Ghasidas University, Bilaspur 495009, India
[6]UGC-DAE-CSR Kolkata Centre, Sector III/LB-8 Bidhan Nagar, Kolkata 700098, India
[7]Variable Energy Cyclotron Centre, 1/AF Bidhan Nagar, Kolkata 700064, India
[8]Inter University Accelerator Centre, Aruna Asaf Ali Marg, New Delhi 110067, India

Nuclei in the vicinity of A~190 lie in a transitional region, where a variety of nuclear deformations are known. The neutron deficient nuclei in this region provide possibility of shape coexistence [1]. In particular, the high spin structure of doubly odd nuclei in this region will give rich variety of information on proton-neutron residual interaction near Z=82, nuclear shape as well as position of energy of the second minimum in the deformation parameter. However, their decay schemes pose complication due to the presence of isomers. This can result from structural changes and also from the reduction of intra-multiplet transition rates as one moves to the middle of the $i_{13/2}$ neutron shell [2]. Search and study of high spin isomeric states in the doubly odd ^{188}Tl nucleus are helpful to study the evolution of nuclear shape. High spin isomers were observed in ^{187}Tl, ^{190,192}Au [2,3]. A prompt spectroscopy measurement was carried out at TIFR using the Pelletron-Linac facility with few Compton suppressed clover detectors using the reaction ^{165}Ho(^{28}Si, 5n) at 158 MeV beam energy. The partial level scheme of 188Tl developed in the experiment is depicted in Figure 1. The reduction of the measured yield of ^{188}Tl compared to other isotopes suggested the presence of long lived isomer in ^{188}Tl at high spin [4]. Search and study of high spin isomeric states in the doubly odd ^{188}Tl nucleus are helpful to study the evolution of nuclear shape. So, it is interesting to search for the high spin isomeric state in ^{188}Tl to complement the results from the prompt spectroscopy.

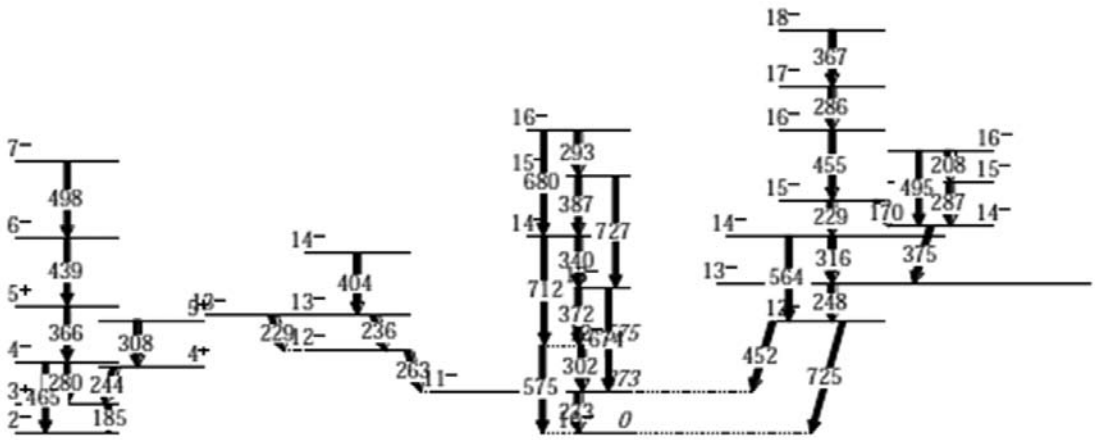

Figure 1: Level scheme of 188Tl (see Ref [4]).

An experiment was performed using the fusion evaporation reaction ^{28}Si(^{165}Ho,5n)^{188}Tl to populate the high spin states in ^{188}Tl. An isotopically enriched self supporting ^{28}Si target of thickness 700 μg/cm^2 was used for the experiment. The ^{28}Si at 168 MeV was provided by the Pelletron-LINAC facility at IUAC. Using the gas filled separator HYRA (Figure 2), the evaporation residues (ER) were separated from the fission products and carried to the focal plane. The He gas used in the HYRA was separated from the beam line using a Ni foil at the upstream of the target. The focal plane chamber consisted of a MWPC followed by three Si pad

detectors in which the ERs were stopped. A clover HPGe detector was placed outside the focal plane chamber. To enhance the detection efficiency, the clover detector was kept close to the Si pad detectors using a re-entrant cup. Another clover detector was placed near the target chamber to detect the prompt gamma rays. The target to focal plane time of flight of the ERs was estimated to be about 1.5 μs. The multi-parameter data were recorded in the list mode form using the CANDLE software whenever either MWPC or Si pad detectors have data. Time between the MWPC and the clover detector (OR of all the four crystals) (T1) and between master and the individual crystals were recorded. The later ensured that the four crystals of the clover can be used as four individual detectors for the γ-γ coincidence measurements.

Figure 2: The experimental set up at the focal plane of HYRA.

The ^{188}Tl recoils observed at the focal plane decayed to ^{188}Hg. The low-lying transitions of ^{188}Hg were observed in the add-back spectrum of focal plane clover detector. Fig. 3. shows the add-back γ-ray spectrum obtained in the focal plane clover detector with (right panel) and without (left panel) gating by the ERs. The ERs were identified from a two-dimensional plot of MWPC (cathode) and Si Pad detector. The add-back spectrum without ER gating (left panel of Fig. 3), though dominated by the background lines, do show the dominant γ-ray transitions of ^{188}Hg (formed by the decay of ^{188}Tl). On the other hand, the ER gated spectrum (right panel of Fig. 3) contains only the dominant background peaks and no known lines (273-,302-,451keV) from the isomeric decays in ^{188}Tl were observed indicating the absence of the isomeric state in the nucleus. The result of the current experiment suggests for the need of future investigation of the decay spectroscopy of 188Tl with improved background shielding and time stamped data acquisition system to search for isomers with wider range of half-life.

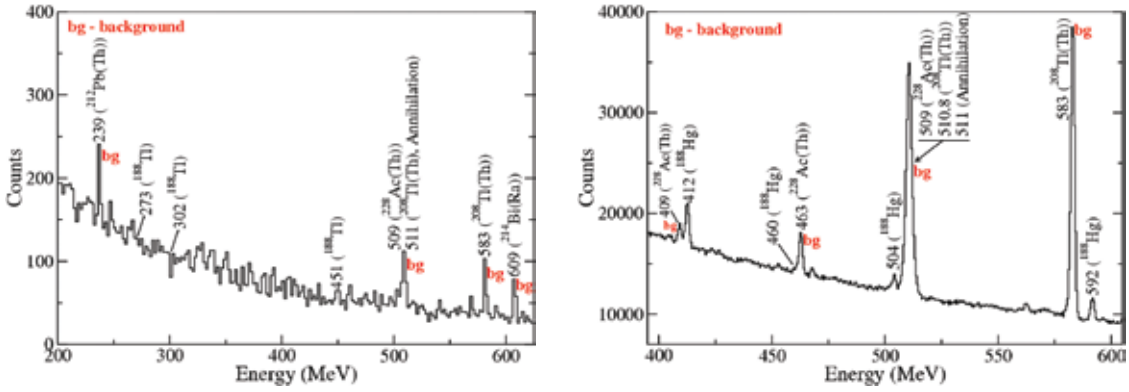

Fig 3: Addback spectrum in focal plane Clover detector with (right) and without (left) gate on ERs identified by the MWPC and Si pad detectors.

References

[1] A.N. Andreyev et al., Nature 405 (2000) 43.
[2] A.P. Byrne et al. EPJ A 7 (2000) 41.
[3] E. Gueorguieva et al., Phys. Rev. C 64 (2001) 064304.
[4] J. Sethi, R. Palit et al. (project report for TIFR graduate school).

5.1.9 Giant dipole resonance in ^{144}Sm

Ish Mukul[1], A. Roy[1], P. Sugathan[1], G. Mohanto[1], J. Gehlot[1], N. Madhavan[1], S.Nath[1], R. Dubey[1], I. Mazumdar[2], D.A. Gothe[2], M. Kaur[3], A.K.R. Kumar[4] and P. Arumugam[4]

[1]Nuclear Physics Group, Inter University Accelerator Centre, New Delhi 110067, India
[2]Department of Nuclear and Atomic Physics, Tata Institute of Fundamental Research, Mumbai 400085, India
[3]Department of Physics, Panjab University, Chandigarh 160014, India
[4]Department of Physics, Indian Institute of Technology Roorkee, Roorkee 247667, India

The phenomenon of giant dipole resonance (GDR) built on excited states in nuclei continues to be a subject of active research by many groups. It has been proven to be the best tool to study nuclear shapes and properties at very high excitation energies and angular momenta [1,2]. GDR decay line shape is sensitive to nuclear deformations and thus several experiments have been carried out to study the dependence of temperature and angular momentum on GDR observables like centroid, width and strength of decay. At IUAC, we study the effect of temperature and angular momentum on GDR observables in medium heavy mass ^{144}Sm nucleus [3]. We will also try to search for nuclear shape changes at high temperature and angular momenta.

The experiments were performed at the 15UD Pelletron + LINAC facility at IUAC, New Delhi. Self-supporting targets of ^{116}Cd were rolled at IUAC target laboratory with thicknesses ranging from 1.8 mg/cm^2 to 2.0 mg/cm^2. The enrichment of the target material was more than 98.3%. We have used ^{28}Si beam at four laboratory energies of 125, 140, 170 and 197 MeV for formation of the compound nucleus (CN), ^{144}Sm. 170 and 197 MeV beam energies were obtained using LINAC booster facility of IUAC. Beam energy loss at the half thickness of target was ~ 5 MeV. The excitation energies populated were in the range of 68 to 120 MeV after taking into account the energy loss through the target. A 4 mm × 4 mm tantalum collimator was placed in the beam line at a distance of nearly 60 cm upstream of the target for focusing the beam. The high-energy γ-rays were detected using High energy Gamma Ray Spectrometer (HiGRaSp) [4]. The spectrometer consists of a single cylindrical crystal of NaI(Tl) as the main detector with the dimensions of 25.4 cm × 30.5 cm. Three plastic detectors surrounded the main detector. These acted as active shields for cosmic muon suppression. Lead bricks and borated paraffin blocks were used for reducing γ-rays and neutrons originating from the collimator. The response function of the detector was determined experimentally using standard radioactive sources. The response of the detector for γ-energy range of 5-40 MeV was generated using Monte Carlo simulation package GEANT4 [5]. Low energy γ-rays were also detected in the TIFR 4π sum-spin spectrometer [6]. The spectrometer consists of 32 NaI(Tl) detectors in soccer ball geometry covering almost 4π solid angle. In present experiments, 27 detectors were used giving 82% solid angle coverage. Each detector of the spectrometer was set with a threshold of ~ 100 keV. The multiplicity signal from the array was fed to ADC for recording γ-hits or fold distribution.

The data acquisition and reduction was done using the CANDLE software developed at IUAC. In offline data reduction, the high-energy γ-rays spectrum, cleaned by gating with prompt γ-peak in the time-of-flight (TOF) and pile-up spectra, was further gated with low energy γ-fold spectrum. The statistical model code CASCADE [7] incorporating the GDR parameters was used for calculations and extraction of GDR parameters. Detailed analysis of data at different beam energies is under process.

We would like to thank the Pelletron group of IUAC, especially Rajan Joshi, for providing beam of excellent quality throughout the experiments and S.R. Abhilash, from IUAC target laboratory, for help in fabrication of self-supporting ^{144}Sm targets. One of the authors (IM) would like to thank the University Grants Commission for providing financial support in the form of a Senior Research Fellowship.

References

[1] K.A. Snover, Ann. Rev. Nucl. Part. Sci. 36 (1985) 545.

[2] J.J. Gaardhoje, Ann. Rev. Nucl. Part. Sci. 42 (1992) 483.
[3] Ish Mukul et al., Proc. of DAE Symp. Nucl. Phys. 57 (2012) 284.
[4] I. Mazumdar et al. Nucl. Instr. Meth. A 417 (1998) 297.
[5] S. Agostinelli et al., Nucl. Instr. Meth. A 506 (2003) 250.
[6] G. A. Kumar et al. Nucl. Instr. Meth. A 611 (2009) 76.
[7] F. Puhlhofer, Nucl. Phys. A 280 (1977) 267.

5.1.10 g–factor of $9/2^-$ and $23/2^+$ isomeric states in ^{129}Ba

Jasmeet Kaur[1], N. Bansal[1], V.R. Sharma[2], H. Sisodia[2], N. Kaur[1], V. Kumar[3], R. Kumar[4], A.K. Bhati[1], R.K. Bhowmik[4] and H.J. Wollersheim[5]

[1]Centre of Advanced Study in Physics, Panjab University, Chandigarh 160014, India
[2]Department of Physics, Aligarh Muslim University, Aligarh 202002, India
[3]Centre for Medical Physics, Panjab University, Chandigarh 160014, India
[4]Inter University Accelerator Centre, Aruna Asaf Ali Marg, New Delhi 110067, India
[5]Helmholtzzentrum für Schwerionenforschung GmbH, Darmstadt, Germany

The transitional nuclei in the A~130 mass region with few valence holes near shell closure manifest rich variety of shapes and structures. This is due to interplay of various multi-quasi-particle excitations and the collective behaviour of underlying core. Many experimental studies based on γ-ray spectroscopy with heavy ion-induced reactions evidenced mainly high-spin level structures, an outstanding one being that due to the unique parity orbital h11/2 both for protons and neutrons [1]. The various deformation driving forces of the valence protons and neutrons occupying low and high Ω states of the $h_{11/2}$ intruder orbital leads to shape coexistence. The knowledge of the static magnetic dipole moments is very important for elucidating the structure of coexisting shapes, as they provide independent information on the underlying configurations. The present work is devoted to the investigation of magnetic moments for two isomeric states with spin- parities $9/2^-$ ($t_{1/2}$ = 14 ns) and 23/2+ ($t_{1/2}$ = 47 ns) in ^{129}Ba [2] with time differential perturbed angular distribution (TDPAD) technique.

The isomeric states in 129Ba were populated and aligned using ^{120}Sn(^{12}C,3n)^{129}Ba reaction with ^{12}C pulsed beam from the 15 UD Pelletron accelerator at 50 MeV energy. The excited ^{129}Ba nuclei recoils were implanted into the ferromagnetic (iron) host material. The internal magnetic field in iron was calibrated through the known g-factor of 10+ ($t_{1/2}$ = 14 ns, g = - 0.159(5)) isomeric level in ^{132}Ba [3] i.e. B_{in} = 6.0(2) T. The target was placed between the pole tips of an electromagnet. A magnetic field of B = 2 kG was applied perpendicular to the beam-detector plane to polarize the iron foil. The γ-rays were detected by two HPGe detectors and two NaI(Tl) detectors placed at ±45° and at ±135° w.r.t the beam direction, respectively. The partial level scheme of ^{129}Ba showing the decay of the presently investigated isomers is shown in the Fig. 1. The γ-gated time spectra for 173 keV and 473 keV from $9/2^-$ and $23/2^+$ isomeric states, respectively, after proper background subtraction and matching T_o, have been `least-squares' fitted assuming an exponential decay. The half-lives for both the states were in agreement with the previous reported values. The spin rotation spectra for $9/2^-$ and $23/2^+$ isomeric states are shown in Fig. 2. The value of g-factor is extracted w.r.t the g-factor of 10^+ isomeric state in ^{132}Ba and is free from any uncertainty in the magnetic field value at Ba ions in iron. The value of g-factor so deduced g($9/2^-$) = − 0.192(6) and g($23/2^+$) = - 0.233(7).

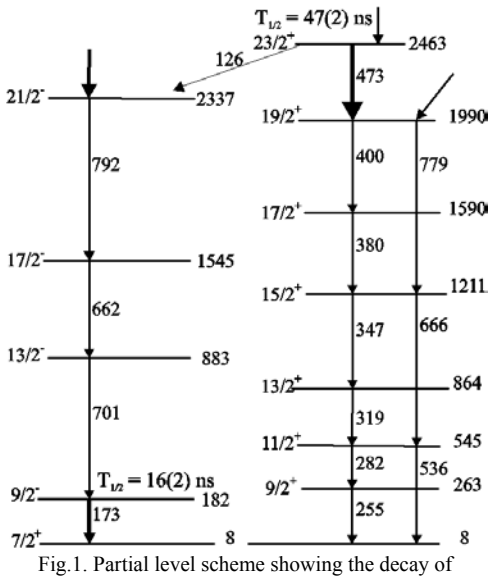

Fig.1. Partial level scheme showing the decay of presently investigated isomeric state.

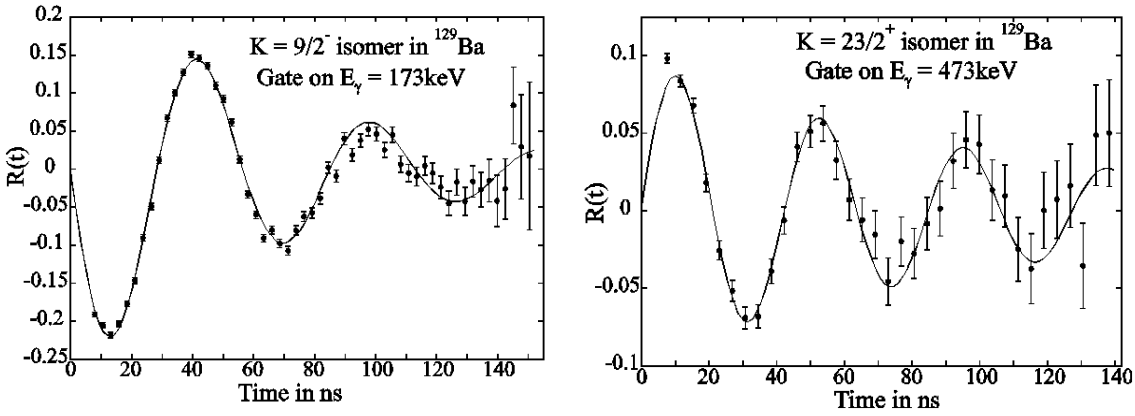

Fig. 2. Spin rotation spectra of $9/2^-$ and $23/2^+$ isomeric states in ^{129}Ba.

References

[1] R.F. Casten and P. von Brentano, Phys. Lett. B 152 (1985) 22.
[2] A.P. Byrne et al., Nuclear Physics A 548 (1992) 131.
[3] P. Das et al., Phys. Rev. C 53 (1996) 1009.

5.1.11 Facility test for g–factor measurement using transient field method

Mansi Saxena[1],*, S. Mandal[1], A. Mandal[2], Rajesh Kumar[2], P. Barua[2], Rakesh Kumar[2], Davinder Siwal[1], Chandan Kumar[1], Savi Goyal[1], Ritika Garg[1], Anisur Rehman[3], Khushboo[1], Minakshi Roy[3], Aman Rohilla[1], Naveen Kumar[1], S. Kumar[1], S. Chamoli[1], R. Gujjar[2], Indu Bala[2] and S. Muralithar[2]

[1]Department of Physics and Astrophysics, University of Delhi, Delhi 110007, India
[2]Inter University Accelerator Centre, Aruna Asaf Ali Marg, New Delhi 110067, India
[3] Saha Institute of Nuclear Physics, 1/AF Bidhannagar, Kolkata 700064, India

Magnetic moments or g–factors [1,2] provide substantial information on the microscopic structure of the nuclei. As the g–factor is very different in sign and magnitude for neutrons and protons, they can serve as a good indicator as to which f them contributes most to the wave function of that state. To measure the g–factor of states having lifetimes ~ ps, we have designed and fabricated a setup [3] based on the transient field measurement technique.

The experiment was carried out in the GDA beam line of the IUAC. 28Si beam at 98 MeV, accelerated from the 15UD Pelletron, was used as the projectile to perform Coulomb excitation reaction. The beam current was limited to 1 pnA to prevent damage to the target. A ferromagnetic host with a thick copper backing was used as the target for the experiment. The target consisted of 6.12 mg/cm^2 ^{nat}Gd stuck to a thick copper backing of 4.98 mg/cm^2 using a thin layer of indium [4]. The motivation for using Gd as the ferromagnetic host came from the fact that it shows better magnetization properties with respect to iron. The targets were prepared at the target laboratory of IUAC.

The de-exciting γ-rays were detected in a pair of germanium detectors and NaI(Tl) detectors. These detectors were placed symmetrically with respect to the beam direction at 45° in the forward and backward direction in the reaction plane, at a distance of 13.6 cm from the target. The back-scattered ^{28}Si ions were detected in a pair of solar cells (10 mm × 10 mm) of thickness 300 μm. The particle detectors were placed at a distance of 36 mm from the target and covered an angular range from 145° to 155°. Opening angle of the particle detectors was 12.2°. The excited Gd ions stopped within the target layer. Data were collected with particle-γ `OR' trigger. A collimator of 2 mm diameter was placed just behind the target chamber to monitor beam current on the target. A Faraday cup was also placed at the end of the beam line.

Analysis of data has been performed using ROOT and Go4. Particle-γ coincidence was performed in the software. The back-scattered ions detected in the particle detectors were used to tag the γ-rays. The gated energy spectra are shown in Fig. 1. We were able to excite the first 2^+ and 4^+ states for ^{154,156,158,160}Gd.

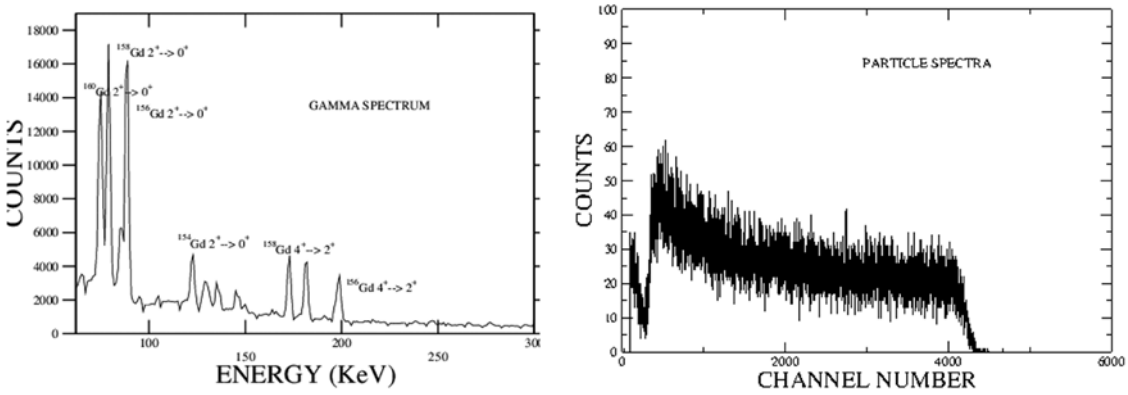

Fig. 1. Gated energy spectrum from one of the germanium detectors (left) and energy spectrum of the back-scattered ^{28}Si ions detected in the particle detector (right).

The authors acknowledge efforts of S.R. Abhilash, J. Zacharias and S. Rao and the Pelletron staff of IUAC for their contribution in preparing the target, fabricating the experimental set up and providing a stable beam, respectively. One of the authors (MS) gratefully acknowledges the financial support from CSIR, New Delhi.

References

[1] K.H. Speidel, Prog in Part and Nucl Phy 49 (2002) 91.
[2] N. Benzer Koller et.al, J.Phys. G. Nucl. Part. Phys. 34 (2007) R321.
[3] Mansi Saxena et.al, Proc. of the DAE Symp. on Nucl. Phys. 55 (2010) 738.
[4] Mansi Saxena et.al, Proc. of the DAE Symp. on Nucl. Phys. 55 (2010) 736.

5.1.12 Study of structure and reaction mechanism near proton drip-line

J. Ray[1], U. Datta Pramanik[1]*, R.K.Bhowmik[2], S.Chakraborty[1], A.Chakraborty[3], R.Garg[4], S. Goyal[4], S. Ganguly[5], S. Kumar[6], S. Mandal[4], B. Mukherjee[3], P. Mukherjee[7], S. Muralithar[2], D. Negi[2], A. Rahaman[1], I. Ray[1], M. Saxena[4], K. Selvakumar[6], P. Singh[6], A. K. Singh[6], and R. P. Singh[2]

[1]1/AF Bidhannagar, aha Institute of Nuclear Physics, Kolkata 700064, India
[2]Inter University Accelerator Centre, Aruna Asaf Ali Marg, New Delhi 110067, India,
[3]Department of Physics, Visva Bharati University, Santiniketan, West Bengal 731235, India
[4]Department of Physics and Astrophysics, University of Delhi, Delhi 110007, India
[5]Chandannagar College, Chandannagar, West Bengal 712136, India
[6]Department of Physics, Indian Institute of Technology, Kharagpur, West Bengal 721302, India
[7]Department of Physics, St. Xavier's College, Kolkata 700016, India

The structure of exotic nuclei is one of the challenging fields of research in low and intermediate energy nuclear physics today. Most of the nuclear structural models are generally derived from the properties of nuclei at or near stability. So this is of fundamental importance to explore the behavior of nuclei as a quantum many body system at the limit of its existence. The macroscopic-microscopic mass model of Moller and Nix predict proton drip-line and deformation of nuclei around drip-line[1]. The nuclei near drip-lines in general are exotic in shape and contain a rich variety of structural information. Various interesting features like shape transition, shape co-existence, octupole deformation etc. have been predicted

in the proton drip-line nuclei. The mass model of Moller and Nix predicts a large prolate deformation in the mass region A ~ 120 near the proton drip-line [1]. So it would be interesting to explore the neutron-deficient ^{121}La, ^{119,120}Cs, ^{114}Te etc. nuclei and the evolution of shapes through in-beam gamma-ray spectroscopy. In addition to that, interesting aspects of reaction mechanism could be explored.

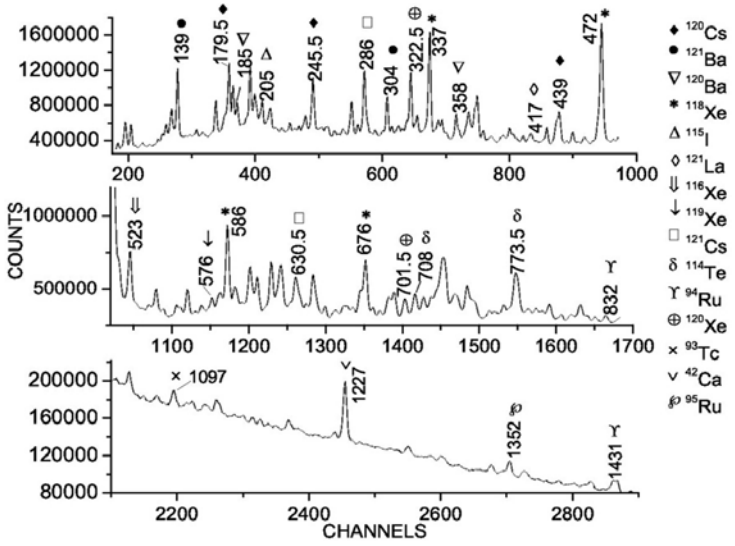

Fig. 1. Gated γ-ray spectra obtained from ^{32}S +^{92}Mo reaction.

For this purpose an experiment has been performed at IUAC, New Delhi using ^{32}S beam on ^{92}Mo target. In the present experiment ^{32}S beam of energy 150 MeV (from 15UD Pelletron accelerator) was bombarded on self supporting ^{92}Mo target with thickness 7.3 mg/cm2. The compound nucleus, ^{124}Ce, was produced in a high excited state with high angular momentum. On evaporation of p, n, α and combination of those from the compound nucleus, a number of exotic loosely bound nuclei such as ^{121}La, ^{120,121}Ba, $^{117\text{-}120}$Xe, $^{118\text{-}121}$Cs, ^{117}I etc. have been populated. These exotic nuclei have been identified by detecting characteristic γ-rays in γ^{-} γ coincidence mode, by 12 Compton suppressed clover detectors of the Indian National Gamma Array (INGA) at IUAC, New Delhi. The detectors were placed at a distance of ~24 cm from the target and at angles $148^0(4)$, $123^0(2)$, $90^0(2)$, $57^0(2)$, $32^0(2)$ with respect to the beam direction. IUAC developed software CANDLE was used for data acquisition. The energy calibration and efficiency measurement of the clover detectors were performed using standard γ^{-} rays (from ^{152}Eu) source of known strength. The list mode data were sorted into different 4096 ⋄ 4096 matrices after gain matching of the spectra obtained from all the detectors. For analysis of data INGASORT software has been used.

Several exotic nuclei have been populated in the present experiment and the populated isotopes are shown in the gated gamma-ray spectra (Fig. 1) obtained from projection of the two dimensional matrix onto one axis. Each isotope has been identified by gating their characteristic gamma-rays and comparing with the previously available literature. The figure shows that the majority of the isotopes have been populated in the mass A~ 120 region, due to particle evaporation from the compound nucleus, ^{124}Ce. In addition to that some nuclei in the target mass region, such as ^{93}Tc, ^{94}Tc etc. have been populated through transfer particle(s) from projectile to target or vice versa. Experimentally obtained result has been compared to the statistical model calculation (PACE4). From the comparison of experimental and theoretical value of relative population it has been observed that population of most of the nuclei like ^{121}La, ^{120}Ba, ^{117}Xe, ^{117}I, ^{114}Te etc. are in agreement with the statistical model calculations. However population of multiple proton evaporation channel are significantly enhanced compared to statistical model predictions [2,3]. Reduction of fission barrier, at times can remove this kind of ambiguity as shown by Wang et al. [4]. However, variation of fission barrier and level density parameter, which are very important input parameters in statistical model calculation, could not reproduce the experimental result.

High spin of states of exotic La [5] and Cs [6] isotopes have been populated. The calculated prolate deformations for most of the neutron deficient Cs and La nuclei are ®$_2$ ~ 0.27-0.33 [7] and ®$_2$ ~ 0.30-0.35 [8], respectively. TRS calculation for ^{119}Cs and ^{121}La have been done for hω = 0.01 to 0.91. It is very interesting to see that there is shape transition from prolate to oblate in ^{119}Cs in higher energy state (hω~0.51) whereas no shape transition in ^{121}La although both the isotopes are having N=64 [6] and almost same band configuration. Details analysis is being carried out to know more information about these interesting isotopes.

References

[1] P. Moller et. al., At. Data Nucl. Data Tables 59 (1995) 185.
[2] J. Ray et. al., Proc. DAE Symp. Nucl. Phys. 56 (2011) 422.
[3] J. Ray et. al., Proc. DAE Symp. Nucl. Phys. 57 (2012) 368.
[4] C. Wang et. al., Phys. Rev. C 84 (2011) 014609.
[5] J. Ray et. al., Proc. DAE Symp. Nucl. Phys. 55 (2010) 52.
[6] J. Ray et. al., Proc. DAE Symp. Nucl. Phys. 56 (2011) 230.
[7] F. Liden et. al., Nucl. Phys. A 550 (1992) 365.
[8] B. Caderwall et. al., Z. Phys A 338 (2011).

5.2 MATERIALS SCIENCE

There were about fifty experiments in materials science beam line in beam hall I and few experiments in materials science beam line in beam hall II utilizing swift heavy ion (SHI) beam. There were about seventy experiments in materials science beam line in low energy ion beam facility. The ion beam irradiation experiments were mainly concerned with electronic sputtering, ion beam modification of materials, engineering of nanostructures etc.

Rhombohedral phase of $BaTiO_3$ was found to be more radiation resistant than tetragonal phase during unique in-situ XRD measurements at 25 K and 300 K with 100 MeV Ag ions. *In-situ* current-voltage measurements were performed during SHI irradiation of quantum dots hetero-junction photodiodes. Continuous degradation in device properties of Schottky barrier junction due to low energy ions irradiation was observed during in-situ electrical transport measurements.

SHI irradiation was found to induce dewetting of Co thin film resulting in formation of high density Co nanostructures. Low energy ion irradiation was utilized to create nanodots and ripples respectively on InP and Si surfaces. Size of TiO_2 nanoparticles, spread on Teflon, increased due to 80 keV Xe ion irradiation.

Mixed conducting solid polymer electrolytes were shown to have enhancement in conductivity of by two orders in magnitude due to low energy ion irradiation. Low energy ion fluence dependent bandgap engineering was demonstrated in rutile TiO_2 crytals.

Semiconductor to metal transition in nanocrystalline ZnO has been observed due to SHI irradiation induced disorder and strain in crystallites. SHI irradiation of graphene was found to induce annealing and purification effects in it. It was demonstrated that SHI irradiation can tailor the ferromagnetic response of Pd nanoparticles embedded in silica.

SHI induced modifications were studied in multiferroic $GdMnO_3$ particles, rare earth doped $CoFe_2O_4$ and Y_2O_3 nanoparticles, micaceous minerals, $YBa_2Cu_3O_{7-\delta}$ thin films, polyethererketone films etc. Ion tracks were observed in SiO_x capped Si-rich a-SiN_x:H films on irradiation with 100 MeV Ni ions. DPPH (diphenylpicryl-hydrazyl) free radical scavenging activity of polypyrrole nanotubes improved on SHI irradiation.

5.2.1 SWIFT HEAVY ION INDUCED STRUCTURAL MODIFICATIONS IN $BaTiO_3$: LOW TEMPERATURE *IN-SITU* XRD STUDY

Renu Kumari[1], P. K. Kulriya[1], S. Mohapatra[2], K. Vasundhara[3], S. N. Achary [3], A. K. Tyagi[3] and D. K. Avasthi[1]

[1]Inter-University Accelerator Centre, PO Box 10502, Aruna Asaf Ali Marg, New Delhi-110067
[2]University School of Basic and Applied Sciences, GGS Indraprastha University, Delhi-110075
[3]Chemistry Division, Bhabha Atomic Research Centre, Mumbai-400085

Barium titanate ($BaTiO_3$) is a high dielectric ferroelectric ceramic material of perovskite structure used in multilayer capacitors, thermistors, piezoelectric transducers and nonlinear medium in integrated optoelectronics. It shows different phases at different temperatures. The phase transition occurs from cubic to tetragonal at 393 K, tetragonal to orthorhombic at 278 K and orthorhombic to rhombohedral at 183 K. The high temperature phase is para-electric and remaining phases are ferroelectric. There are studies on low energy ion irradiation of $BaTiO_3$. However, the studies of the effects of swift heavy ion irradiation on $BaTiO_3$ are limited. In present experiment, $BaTiO_3$ was irradiated with 100 MeV Ag ions at 25 K and 300 K for different fluences ranging from 3×10^{11} ions/cm^2 to 1×10^{14} ions/cm^2. *In-situ* X-ray diffraction (XRD) on the different phases of $BaTiO_3$ was performed at 25 K and 300 K to study the stability of $BaTiO_3$ in two phases under swift heavy ion irradiation. From in-situ XRD results shows that the intensity of diffraction peaks in XRD spectra decreases with increase of ion fluence as shown in Fig.1 (a) and Fig. 1(b) at 25 K and 300 K respectively. It is clear from Fig. 1(a) that $BaTiO_3$ shows some crystalline nature even at 1×10^{14} ions/cm2 at 25 K, whereas $BaTiO_3$ is completely amorphized at 1×10^{13} ions/cm^2 at 300 K as shown in fig. 1(b). So it means that the rate of amorphization is found to be faster at 300 K in comparison to 25 K. The line shape of BaTiO3 (200) diffraction peak at about 2θ=45° is sensitive to temperature change. Single diffraction peak around 45° represents rhombohedral phase of $BaTiO_3$ in case of 25 K as shown in Fig. 1(c) and splitting of peak at 45° confirms tetragonal phase of $BaTiO_3$ at 300 K as shown in Fig. 1(d).

In conclusion, *in-situ* XRD investigation at room temperature and low temperature reveals that $BaTiO_3$ in rhombohedral phase is more radiation resistant than in tetragonal phase. The low temperature *in-situ* XRD, recently installed in beam line, is the only way to examine the irradiation induced structural transformations of the phase existing at low temperature like rhombohedral phase of $BaTiO_3$ as investigated in the present study.

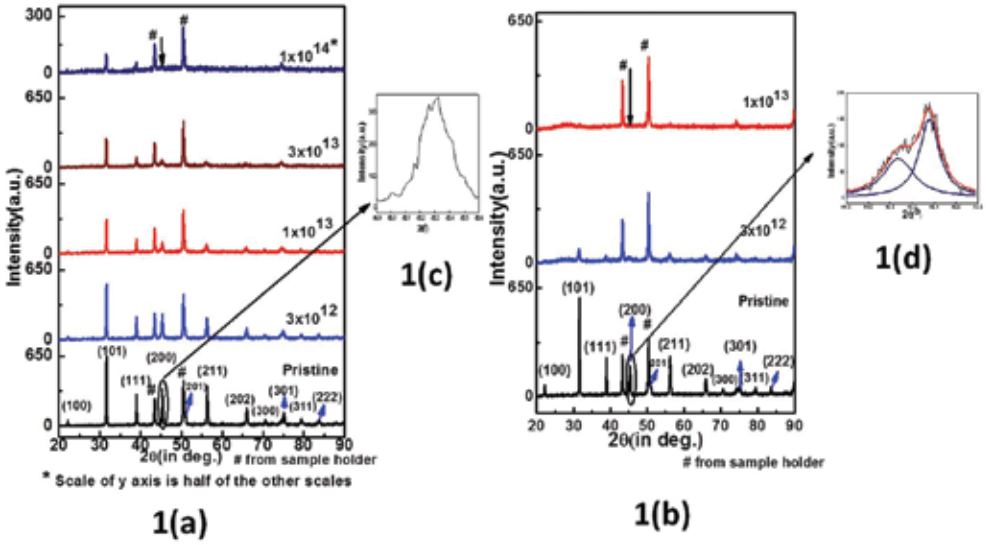

Fig.1 (a) and Fig.1(b) shows XRD patterns of $BaTiO_3$ before and after irradiation with 100-MeVAg ions at different fluences at 25 K and 300 K respectively and Fig. 1(c) and Fig.1 (d) shows effect of temperature change on shape of diffraction peak around angle 45°.

5.2.2 *IN-SITU* CURRENT VOLTAGE (I-V) MEASUREMENTS OF QUANTUM DOTS HETERO-JUNCTION PHOTODIODE UNDER 120 MeV Au^{9+} IONS IRRADIATION

Prabha Sana[1], Shammi Verma[2], K. C. Praveen[3] and M. M. Malik[1]

[1]Physics Department, Maulana Azad National Institute of Technology, Bhopal-461051
[2]Inter-University Accelerator Centre, Aruna Asaf Ali Marg, New Delhi – 110 067
[3]Department of Studies in Physics, University of Mysore, Manasagangotri, Mysore-570006

Semiconducting quantum dots (QD's) based devices have become very important components in modern nano-electronic devices. Due to the concern of device performance in radiation atmosphere, the study of modifications of nanomaterials devices under the irradiation of swift heavy ions (SHI) is an important field of research. Present report is an attempt to address the modifications in a proper prospective, using detailed structural, optical and electrical characterizations of ZnS:TiO_2 core shell colloidal QD's based ZnS:TiO_2/p-Si and ZnS:TiO_2/n-Si heterojunctions under the influence of SHI irradiation. The in-situ current-voltage (I-V) characteristics of prepared QD's heterojunctions have been studied under 120 MeV Au ions irradiation with fluences ranging from 1×10^{11} to 3×10^{13} ions/cm^2. The prime motivation behind performing *in-situ* measurements is to test the electronic properties of heterojunctions as a function of SHI fluence, while all other external parameters are kept unaltered. Good rectifying I-V characteristics of ZnS:TiO_2/n-Si heterojunction was obserced at bias voltages of ±2 V as shown in Fig. 1. The improved rectifying behaviour might be due the removal of interface defects upon annealing. The ion induced crystallization is also confirmed by XRD studies, while SHI irradiation effect on PL spectra have suggested the removal of defect centers. The responsivity for pristine QD's photodiode for ultraviolet (376 nm) detection is 1.8×10^6 A/W, while the responsivity after the irradiation (fluence 3×10^{13} ions/cm^2) is 9.1×10^6 A/W at reverse bias voltage 1.99 volt. It shows the suitability of the photodiode for ultra violet detection under radiation atmosphere [1].

The I-V characteristics of ZnS:TiO_2/p-Si QD's heterojunction, as shown in Fig. 2, shows high reverse leakage current due to low built in potential (V_{bi}) across the p-Si and TiO_2 (shell layer of ZnS) interface. Interestingly, at lower irradiation fluences the ZnS:TiO_2/p-Si diode characteristics is found to deviate from ideal diode nature due to defect production at the interface, while at higher irradiation fluence diode characteristics improved through partial defect annealing. The observed photo responsivity of pristine heterojunction is 2.7×10^{10} A/watt for ultraviolet light detection. The results emphasise the increased responsivity of 4.9×10^{10} A/watt of heterojunction after irradiation at fluence of 3×10^{13} ions/cm^2. The results from x-ray diffraction and photoluminescence spectra analysis also support the above mentioned reasons of modifications in the present heterojunctions under SHI irradiation [2].

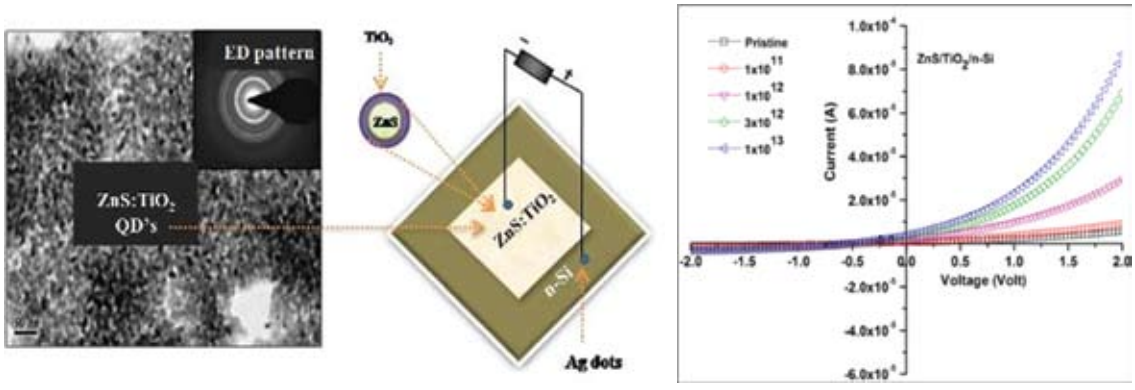

Fig. 1 (a) schematic representation of electrically connected ZnS:TiO_2/n-Si QD's heterojunction,
(b) *In-situ* current-voltage (I-V) characteristics of ZnS:TiO_2/n-Si QD's heterojunction at different SHI fluences.

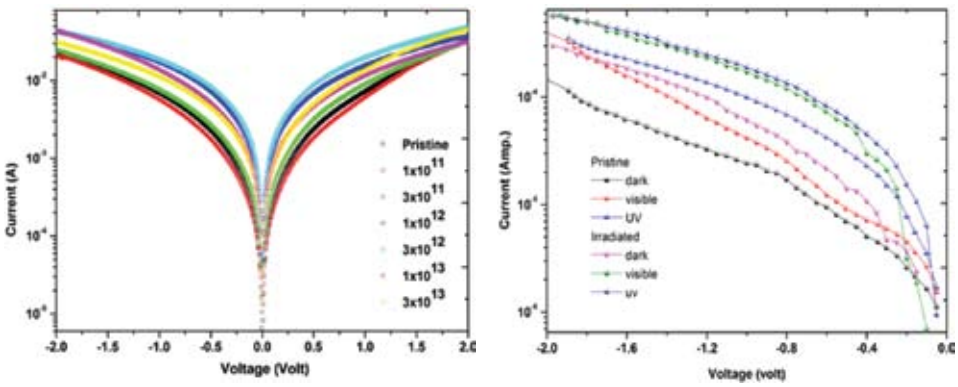

Fig. 2 (a) *In-situ* current-voltage (I-V) characteristics of ZnS:TiO_2/p-Si QD's heterojunction at different SHI fluences (b) current-voltage characteristics under the visible and UV light of the pristine and irradiated ZnS:TiO_2/p-Si QDs heterojunction photo diode

REFERENCES

[1] P. Sana, S. Verma and M. M. Malik, IEEE Transactions on Device and Materials Reliability TDMR, 2013.
[2] S. A. Goodman, F. D. Auret and G. Myburg, Proceedings of the 9th Int. Conf. on Ion Beam Modification of Materials, 1996, p 866.

5.2.3 IN-SITU ELECTRICAL TRANSPORT MEASUREMENTS OF SCHOTTKY BARRIER JUNCTIONS AT LOW ENERGY ION BEAM FACILITY (LEIBF), IUAC

Shammi Verma* and Dinakar Kanjilal

Inter-University Accelerator Centre, Aruna Asaf Ali Marg, New Delhi – 110 067
*Email: shammiktl@iuac.res.in

Metal-Semiconductor (M-S) Schottky contacts are the fundamental part of the semiconductor devices. Formation of a controlled junction barrier known as Schottky barrier (SB) at these M-S interfaces is important from fundamental physics as well as technological point of view [1-2].

In-situ electrical transport measurements like current-voltage (I-V) and capacitance-voltage (C-V) characteristics of Au/n-Si (100) SB diodes were carried out during 700 keV C^{+4} beam irradiation. The SB diodes were fabricated by depositing 100 nm of Au metal as 2 mm circular dots on chemically cleaned and etched n-Si (100) of resistivity ~1 Ω-cm. The irradiation experiment was carried out using 90° beam line of LEIBF, IUAC, New Delhi in an experimental chamber maintained at a vacuum of ~ 10^{-7} mbar. The ion beam current was 50 pnA and was maintained the same throughout the experiment. All the measurements were done at room temperature following the military standards "method: MIL-STD 750". The effect of ion beam on the electrical parameters like ideality factor (η) and Schottky Barrier Height (SBH) (φB) of SB diode is assessed from their current-voltage characteristics [3]. The experimental I-V and C-V characteristics are shown in Fig. 1(a) and 1(b) respectively. The reverse current has been found to increase by about three orders of magnitude at fluence of 5×10^{15} ions/cm^2 as compared to its pre-irradiation (pre-rad) value. Unlike the SHI irradiation effects reported in Ref. 4, there is a continuous degradation in the device properties. The low energy ion beam loses its energy mainly via nuclear energy loss mechanism and is known to create vacancies and other point defects at these M-S interfaces. These defects assist the current transport by contributing to tunneling across the Schottky junction; thereby increasing the reverse leakage current with the ion fluence. The irradiation induced diffusion of Schottky metal into semiconductor and creation of trap centres at M-S interface are the other most plausible mechanisms for these observed deviations in SB diode characteristics [5-6].

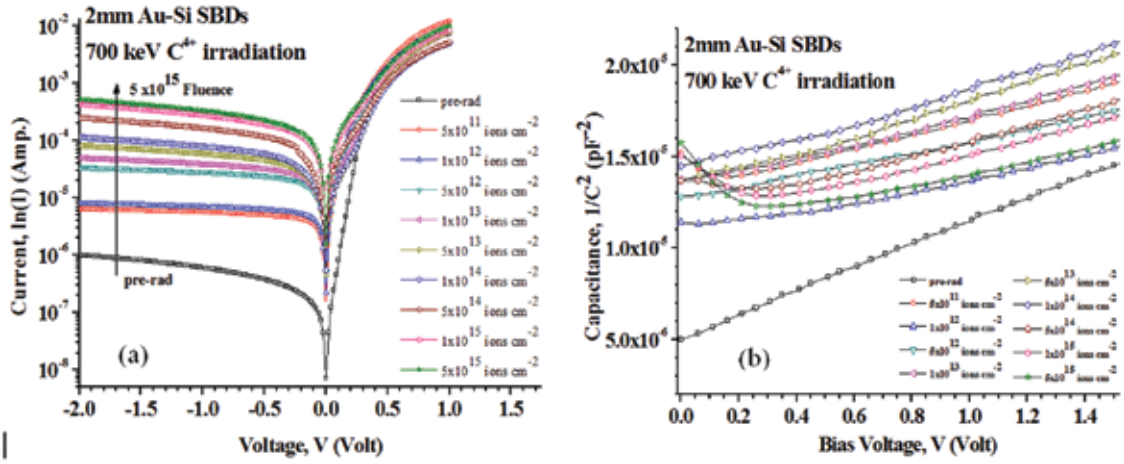

Fig. 1. (a) I-V characteristics of Au/n-Si (100) SB diodes at different ion fluences of 700 keV C^{4+} ion beam, (b) C-V characteristics Au/n-Si (100) SB diodes with different ion fluences of 700 keV C^{4+} ion beam.

REFERENCES

[1] D. K. Schroder, "Semiconductor Material and Device Characterization", New Jersey, Wiley Interscience (2006).
[2] D. V. Lang, J. Appl. Phys. 45 (1974) 3023.
[3] E. H. Rhoderick, "Metal-semiconductor contacts", IEE Proc., 129 (1982).
[4] Shammi Verma et al., IEEE Trans. Device Mater. Rel, Vol. 13, No. 1, March 2013.
[5] R. Singh, S. K. Arora and D. Kanjilal, Mat. Sci. Semicon. Proc. 4 (2001) 425.
[6] Krzysztof Iniewski, "Radiation Effects in Semiconductors", New York, CRC Press (2011).

5.2.4 RE-CALCULATION OF SPUTTERING YIELD OF THICKNESS DEPENDENCE IN LiF THIN FILMS

Manvendra Kumar[1], S. A. Khan[2], Parasmani Rajput[3], F. Singh[2], A. Tripathi[2], D. K. Avasthi[2] and A. C. Pandey[1]

[1] Nanotechnology Application Centre, University of Allahabad, Allahabad 211002 INDIA
[2] Inter University Acclerator Centre, Aruna Asaf Ali Marg, New Delhi 110067 INDIA
[3] Materials Science & Engineering, Northwestern University, Evanston, IL 60208 USA

Electronic sputtering of polycrystalline LiF thin films of different thickness was studied using online ERDA technique and reported in 2007 [1]. Recently, it was observed that the initial areal density of films plotted in one of the figures were erroneous. According to the density (2.64 g/cm^3) of bulk LiF, the areal density of fluorine atoms for the 10 nm and 40 nm thick pristine LiF layers should be $6.1\times10^{16}$and 2.4×10^{17} atoms/cm^2, respectively. In the light of the above error, the areal densities of the films were re-calculated. The error was observed in films having thickness of 10, 20 and 40 nm for which the reported areal density were ~5 times higher. The value of solid angle was wrong in the earlier calculations for these thicknesses due to typographical mistake; it was 10^{-3} sr instead of 5×10^{-3}sr. Sputtering yield was also recalculated for these films. The values for 80, 160 and 265 nm films were found to be correct. The corrected values of sputtering yield for different thickness along with the values reported in the published paper [1] are given in the Table 1.

Table 1: Corrected and reported values of sputtering yield for different thickness.

Film thickness (nm)	Yield (atoms/ion)	
	Reported values [1]	Corrected values
10	2.3×10^{6}	4.6×10^{5}
20	1.1×10^{6}	2.2×10^{5}
40	4.1×10^{5}	8.2×10^{4}
80	8.1×10^{4}	8.1×10^{4}
160	3.8×10^{4}	3.8×10^{4}
265	2.2×10^{4}	2.2×10^{4}

The revised values of sputtering yield are shown in figure 1. The nature of the sputtering yield with film thickness is found to be the same as reported earlier. Also two distinct regimes of thickness dependence on electronic sputtering yield are maintained. The value of sputtering yield for 100 nm thin films, 62000 atoms/ion, (reported in ref. [2]) is also shown in the figure 1 which is consistent with sputtering yield for higher thicknesses.

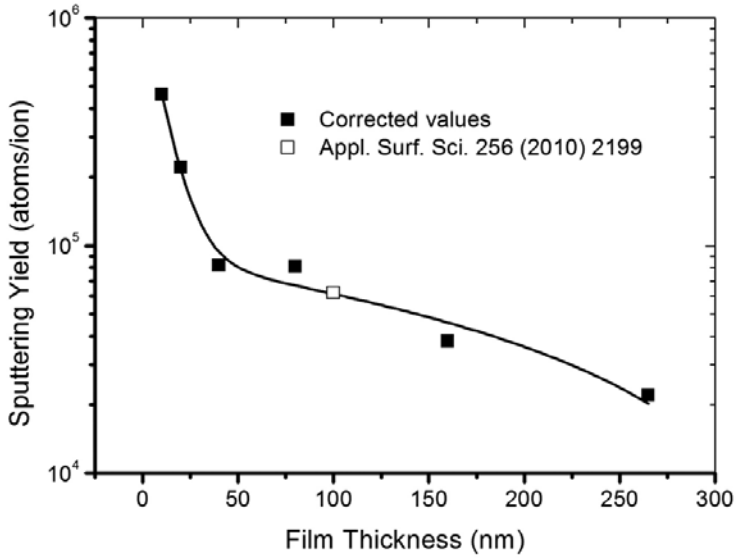

Fig. 1. Sputtering yield of LiF films of different thickness

REFERENCES

[1] Manvendra Kumar, S. A. Khan, P. Rajput, F. Singh, A. Tripathi, D. K. Avasthi and A. C. Pandey, J. Appl. Phys. 102 (2007) 083510.

[2] Manvendra Kumar, Parasmani Rajput, S. A. Khan, D. K. Avasthi and A. C. Pandey, Appl. Surf. Sci. 1256 (2010) 2199

5.2.5 ION BEAM INDUCED MODIFICATIONS IN PROPERTIES OF Zn NANOWIRES

Amandeep Kaur and R.P. Chauhan

Department of physics, National institute of Technology, Kurukshetra-136119
Email: aman2kamboj@yahoo.com, chauhanrpc@gmail.com

During the past decade, nanowires have attracted an enormous interest due to a large variety of promising applications in areas such as nano-electronics, biotechnology, magnetism, thermo-electrics, solar cells, and water splitting, among others [1-4]. Their reduced size, elongated geometry, and high surface to volume ratio turn nanowires into ideal elements for electrical and electrochemical systems [5, 6]. A systematic study on electrical and structural properties of swift heavy ion beam irradiated zinc nanowires has been carried out. Energetic ion beam irradiation is an efficient tool for inducing desired controlled modification in material properties like structural, optical, electrical and magnetic. Irradiation of solids gives rise to

formation of atomic defects in solids [7]. Arrays of zinc nanowire were grown inside the cylindrical nano-pores of polycarbonate track-etch membrane by electrodeposition technique at 0.3 V at room temperature. In these experiments commercially available polycarbonate TEM of Whatman Company with pore size 100 nm and thickness 10 micron were used. The two electrodes electrochemical cell was used for electrodeposition process. Free standing zinc nanowires were synthesized on copper substrate which acts as cathode during electrodeposition process. A zinc rod was used as an anode. The electrolyte solution was prepared from ZnSO4.7H_2O, NH_4Cl, $NaC_2H_3O_2.3H_2O$ and glucose. The pH of the electrolyte was adjusted to 3. After deposition the sample was removed from the cell carefully and washed with distilled water.

Synthesized Zn nanowires were exposed to 40 MeV C^{4+} ions, 80 MeV Si^{7+} and 110 MeV Ni^{8+} ion beams with fluence varying from 1×10^{11} to 3×10^{13} ions/cm^2 at IUAC, New Delhi. The thickness of samples was 10 micron. Using SRIM-2006 software the projected range of ion beam in samples was calculated and larger than length of nanowires. Thus the ion beam passes through the entire sample without any implantation in it.

The analyses of XRD patterns, recorded with Rigaku X-ray Diffractometer, showed no variation in peak positions which indicates no change in shape and size of unit cell after irradiation. The positions of peaks are also used to determine the chemical composition and crystal phase structure. In order to measure the electrical conductivity, I-V characteristics (IVC) of pristine and exposed Zn nanowires were obtained with the help of two probe system using Keithely 2400 series source meter. IVC of exposed nanowires revealed a decrease in electrical conductivity with increase in ion fluence which was found to be independent of applied potential difference. However, the electrical conductivity was found to increase with potential difference in case of high fluence (3×10^{13} ions/cm^2) irradiation with 110 MeV Ni^{8+} beam.

REFERENCES

[1] C. M. Lieber and Z. L. Wang, Mater. Res. Bull. 3(2007) 299
[2] A. I. Hochbaum and P. Yang, Chem. Rev. 110 (2010) 527
[3] D. J. Gargas, M. E.Toimil-Molares and P. Yang, J. Am. Chem. Soc. 131 (2009) 2125
[4] D. Seletskiy et al., Phys. Rev. B. 84 (2011) 115421
[5] C. K. Chan. H. Peng. G. Liu. K. McIlwrath. X. F Zhang. R.A. Huggings and Y. Cui. Nat. Nanotechnol. 3 (2008) 31
[6] J. Sun, C. Liu and P. Yang, J. Am. Chem. Soc. 113 (2011)19306
[7] S. K. Neogi et al., J. Phys.: Condens. Matter. 23 (2011) 205801

5.2.6 HIGH DENSITY Co NANOSTRUCTURES BY ION BEAM INDUCED DEWETTING

Asha[1], K. Asokan[2], Lekha Nair[1]

[1]Department of Physics, Jamia Millia Islamia, New Delhi
[2] Inter-University Accelerator Centre, Aruna Asaf Ali Marg, New Delhi – 110 067

Metallic nano-particles are of great interest for scientific advancements [1] and potential applications mainly in nano-structure magnetism and data storage devices [2], and as catalysts for growth of semiconductor nano-wires and carbon nano-tubes. Cobalt nano-particles were synthesized on silicon (100) substrates by swift heavy ion irradiation of thin film of Co at room temperature. AFM studies showed the formation of bubble shaped cobalt nano-particles as can be seen in Fig. 1. Formation of Co nano particles on the substrate can be explained by thermal spike model which suggests that a local hot molten zone forms along the ion path in matter. Within a time period of picoseconds the metal cools down and agglomerates to form metal nano-particles. Moreover, RBS and XRD suggest that the Co crystalline nano-particles were observed without silicide formation in Co/Si system due to 45 MeV Li^{3+} and 100 MeV O^{7+} ions irradiation. Thus, the present study supports that SHI irradiation is one of the promising ways to grow nano-particles in a clean, controllable, non-toxic, environmentally safe manner.

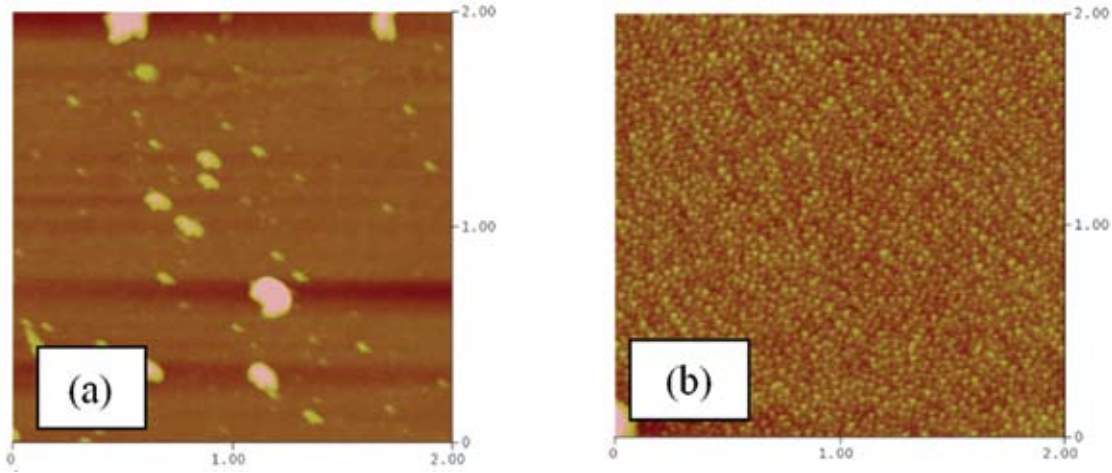

Fig. 1 AFM images of (a) pristine and (b) 1×10^{12} ions/cm2 irradiated samples. The scan size is 2 µm. The initially random pristine surface structure has been transformed into an array of well-developed nanostructures of fairly uniform lateral size of 30-40 nm due to 100 MeV O ion irradiation.

REFERENCES

[1] Y. Huttel et al., J. Appl. Phys. 96 (2004) 1666.
[2] J. Bischof, D. Scherer, S. Herminghaus, and P. Leiderer, Phys. Rev. Lett. 77 (1996) 8.

5.2.7 SWIFT HEAVY ION IRRADIATION INDUCED DEFECTS FOR TAILORING THE FERROMAGNETIC RESPONSE OF PALLADIUM NANOPARTICLE EMBEDDED IN SILICA MATRIX

P. K. Kulriya, [1, 2] B. R. Mehta[1], D. K. Avasthi[2]

[1] Department of Physics, Thin Film Laboratory, Indian Institute of Technology, New Delhi 110 016
[2] Inter-University Accelerator Centre, Aruna Asaf Ali Marg, New Delhi – 110 067

Recently, ferromagnetism like behavior has been reported in nanomaterials such as Pd [1-3], Au [4], and Pt [5] which are normally nonmagnetic in bulk state. The ferromagnetic response of these nanoscale materials cannot be explained on the basis of the unfilled character of 3d or 4f electron energy levels. The Curie, Curie-Weiss, or Bloch law for the paramagnetism, giant paramagnetism and ferromagnetism, respectively, are not obeyed by these materials. The magnetization is found to be almost independent of temperature. Moreover, local anisotropy of these nanomaterials is also extremely high in comparison to well-known harder magnetic materials. Theoretically, magnetic behavior of these materials is explained on the basis of structural defects, high spin-orbit coupling with localized spins or electric charge

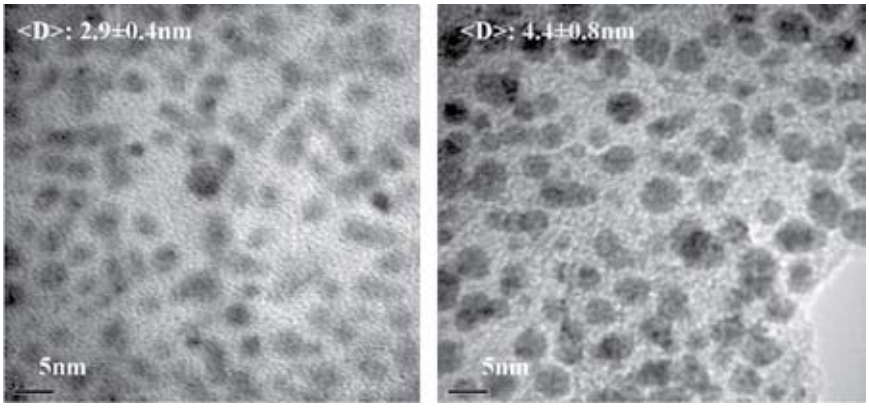

Fig.1. TEM images of as-deposited (left), and SHI ion irradiated (right) the Pd NPs embedded in silica matrix.

distributions and large orbits of the electrons [6]. In the present report, swift heavy ion (SHI) is used for the modifications in the core as well as at nanoparticle-matrix interface which can result in change in the magnetic properties of the Pd. It is well know that as SHI penetrates in a solid, it interacts with the target electrons via inelastic interaction. The resulting intense electronic excitation within ~10^{-12} sec produces a narrow trail of permanent damage along the ion paths which are known as ions track. Therefore, it is expected that irradiation of nanostructures, specifically metal nanoparticles embedded in matrix may give rise to quite unexpected and even counterintuitive results. Track created by the SHI in the surrounding matrix can result in modifications in the magnetic properties of the embedded Pd NPs. Well separated and uniformly distributed Pd nanoparticles (NPs) embedded in silica matrix were synthesized by atom beam sputtering technique. These samples were modified by 120 MeV Au ion irradiation. The electron microscopy images of the as-deposited (AS), and ion irradiated (IS) sample are shown in fig 1. The magnetization measurements on these samples, performed using SQUID magnetometer, (Fig. 2) show an enhancement in the ferromagnetic response on ion irradiation, which is correlated to the change in the electronic structure due to matrix, nanoparticle size, and creation of defects in the nanoparticle core and at NP-matrix interface [2]. In our other study, removal of defects during post-deposition annealing results in decrease in the density of structural defects and decrease in magnetic properties of Pd nanoparticles. The correlation between structural defects and ferromagnetism in Pd nanoparticles is thus clearly established.

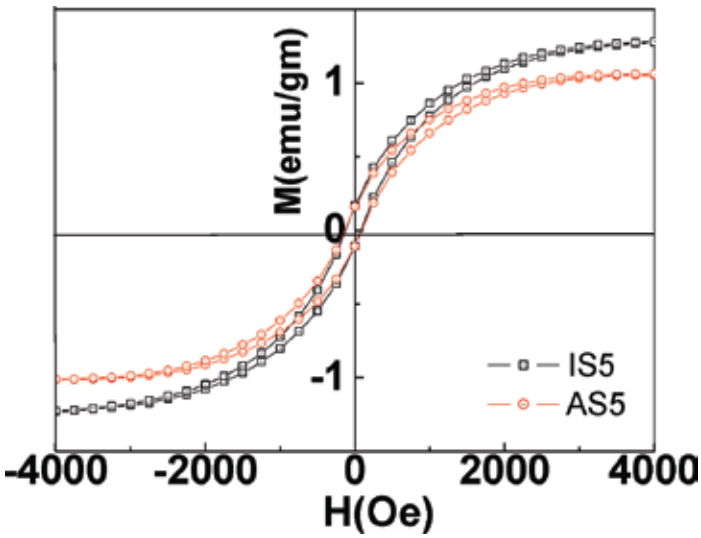

Fig. 2. M-H curves of the (a) AS, and (b) IS samples.

REFERENCES

[1] P. K. Kulriya et al., Appl. Phys. Lett. 96 (2010) 053103.
[2] P. K. Kulriya et al., J. Appl. Phys. 112 (2012) 014318.
[3] B. Sampedro et al., Phys. Rev. Lett. 91 (2003) 237203.
[4] Y. Yamamoto et al., Phys. Rev. Lett. 93 (2004) 116801.
[5] Y. Sakamoto et al., Phys Rev B 83 (2011) 104420.
[6] A. Hernando, P. Crespo and M. A. Garcia, Phys. Rev Lett. 96 (2006) 057206.

5.2.8 SWIFT HEAVY ION IRRADIATION INDUCED FORMATION OF NANOSTRUCTURES IN Si-RICH a-SiN_x:H FILMS

R K Bommali[1], S. Ghosh[1], G. V. Prakash[1], Saif A. Khan,[2] D. Kanjilal [2] and P. Srivastava[1]

[1]Department of Physics, Indian Institute of Technology Delhi, Hauz Khas, New Delhi – 110016
[2] Inter-University Accelerator Centre, Aruna Asaf Ali Marg, New Delhi – 110 067

Silicon quantum dots (QDs) embedded in a dielectric matrix form an attractive system to exploit effects arising due to the quantum confinement effect (QCE) in Si-QDs. Silicon dioxide and silicon nitride are some of the contenders for the choice of a dielectric matrix [1, 2]. We are working towards achieving Si-QDs embedded in silicon nitride matrix. General recipe for obtaining the nanostructures in this matrix consists of depositing thin films of Si rich amorphous hydrogenated silicon nitride (*a*-SiN_x:H) and then

subjecting the films to post deposition treatments (PDTs) like thermal annealing in various gas ambients, plasma treatment or Swift Heavy Ion Irradiation (SHII). In our previous SHII experiments [3] on *a*-SiN_x:H samples containing *in-situ* formed Si-QDs, the dissolution and re-precipitation of Si-QDs with increasing fluence were observed, thereby emphasizing the role of SHI irradiation in tailoring Si-nanostructures in *a*-SiN_x:H.

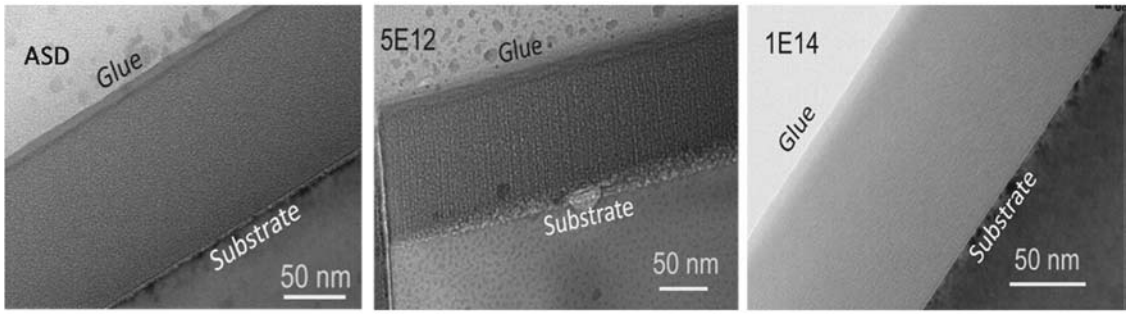

Fig. 1. X-TEM images showing the formation and dissolution of nanostructures within a-SiN_x:H matrix. Ion tracks are observed to appear at a fluence of 5×10^{12} ions/cm^2, whereas upon exposure to a higher fluence of 1×10^{14} ions/cm2 the tracks get dissolved due to possible overlapping.

In continuation of our earlier work, as-deposited and SiO_x capped, Si-rich a-SiN_x:H samples of various compositions prepared by PECVD (Plasma Enhanced Chemical Vapor Deposition) technique were irradiated with 100 MeV Ni^{7+} ions in the present experiments at different fluences using 15 UD Pelletron Accelerator at IUAC, New Delhi. As-deposited and irradiated samples have been characterized by UV-Vis reflectance spectroscopy, photoluminescence spectroscopy and cross-sectional transmission electron microscopy (X-TEM). Reflectance results (not shown here) reveal a compaction of the films with increasing fluence. This is attributed to hydrogen desorption under irradiation as revealed by online residual gas analysis (not shown here). The photoluminescence studies show the formation of Si and nitrogen dangling bond defect centers apart from non-radiative traps. X-TEM studies indicate formation of ion tracks at fluence of 5×10^{12} ions/cm^2 and track dissolution at a higher fluence of 1×10^{14} ions/cm^2 as can be seen from Fig. 1. Further analysis is in progress.

REFERENCES

[1] J. Heitmann, F. Maller, M. Zacharias and U. Gosele, Adv. Mater. 17 (2005) 795.
[2] R. K. Bommali et al., J. Appl. Phys. 112 (2012) 123518.
[3] S. P. Singh et al., Nucl. Instrum. and Meth. B 276 (2012) 51.

5.2.9 PURIFICATION/ANNEALING OF GRAPHENE WITH 100 MeV Ag ION IRRADIATION

Sunil Kumar[1], *, A. Tripathi[1], F. Singh[1], S.A. Khan[1], V. Baranwal[2], and D.K. Avasthi[1]

[1] Inter University Accelerator Centre, Aruna Asaf Ali Marg, New Delhi 110067, India,
[2] University of Allahabad, Allahabad 211002, India
*Email: kumar.sunil092@gmail.com

Graphene is the most promising material in the family of carbon. In recent years it has attracted a lot of interest from researchers due to its unique electronic, mechanical and transport properties [1]. Interaction of graphene with radiation is of particular interest because of nanolithographic processes in graphene based electronic devices and space applications. Earlier studies from our group have shown that swift heavy ion (SHI) irradiation induces annealing and purification effects in fullerenes and carbon nanotubes (CNTs) [2, 3]. In the present work, we report similar effects in graphene films. Commercially available CVD grown 3-4 layers graphene films on Ni/SiO_2 substrate were irradiated with 100 MeV Ag ions (fluences from 3×10^{10} ions.cm^{-2} to 1×10^{14} ions.cm^{-2}) using 15 MV Pelletron accelerator at IUAC, New Delhi. Raman

spectra were recorded for pristine as well as irradiated samples. The disorder parameter α, defined by I_D/I_G ratio, decreases at lower fluences and increases at higher fluences beyond 1×10^{12} ions.cm^{-2} This indicates that SHI induces annealing effect at lower fluences, whereas damage is observed at higher fluences. We also observe that at fluences higher than 1×10^{13} ions/cm^2 the number of graphene layers is reduced. Using thermal spike model calculations, we estimate a radius of 2.5 nm for track core surrounded by a halo extending up to 12 nm. The temperature above melting point in track core results in a permanent damage, whereas lower temperatures in track halo are responsible for the annealing. The results suggest that SHI with optimized energy and fluence may be used as one of the tools for defect annealing and manipulation of number of graphene layers.

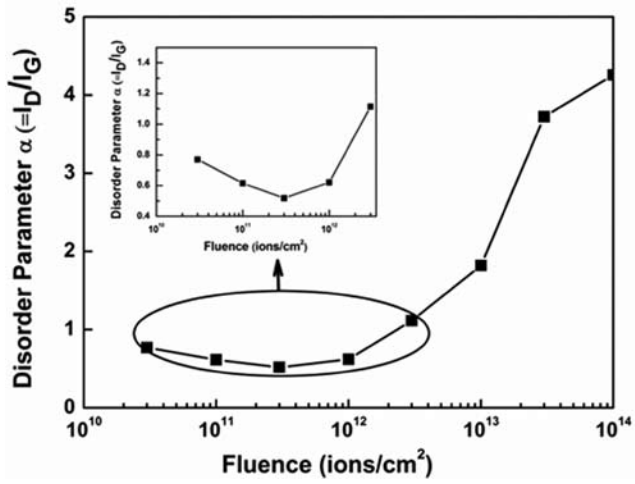

Fig. 1. Variation of disorder parameter with ion fluence

REFERENCES

[1] A. K. Geim, Science 324 (2009) 1530.
[2] Kiran Jeet, V. K. Jindal, L. M. Bharadwaj, D. K. Avasthi and Keya Dharamvir, J. Appl. Phys. 108 (2010) 034302.
[3] Navdeep Bajwa et al., J. Appl. Phys. 104 (2008) 054306.
[4] A. Kumar et al., Appl. Phys. Lett. 92 (2008) 221904.

5.2.10 FREE RADICAL SCAVENGING ACTIVITY OF POLYPYRROLE NANOTUBES IRRADIATED WITH 100 MeV Si $^{9+}$ ION BEAM

J. Upadhyay and A. Kumar*

Dept of Physics, Tezpur University, India
*Email: ask@tezu.ernet.in

Conducting polymers nanostructures have been extensively studied because of the possibilities of different biomedical applications such as artificial muscles, controlled drug release, stimulation of nerve regeneration and as antioxidant materials [1]. The use of swift heavy ion (SHI) beam irradiation is getting high impetus for irreversible physical and chemical modifications of the polymers. In this work we investigate the effect of 100 MeV Si^{9+} ion beam on antioxidant property of polypyrrole nanotubes (Fig.1) by using DPPH free radical assay.

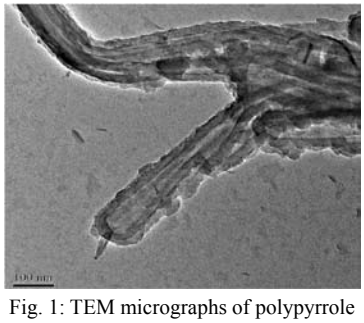

Fig. 1: TEM micrographs of polypyrrole nanotubes.

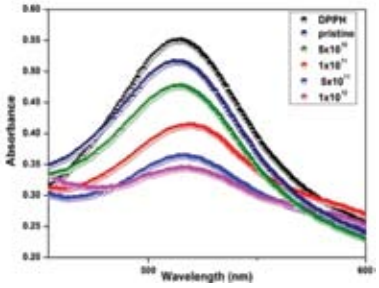

Fig. 2. Uv-Vis absorbance at 516 nm of DPPH solution in methanol after 15 min with 0.6 mg of pristine and irradiated samples with different fluences.

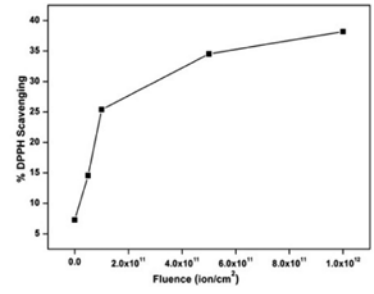

Fig. 3. Percentage of DPPH scavenging activity of 0.6 mg of pristine and irradiated samples

The absorbance of DPPH free radicals at 516 nm with pristine and irradiated polypyrrole nanotubes are presented in the Fig. 2. The absorbance is taken by employing 0.6 mg of each sample in 3 mL of 100 μM DPPH solutions for 15 min. In the absence of conducting polypyrrole, the absorbance of DPPH is around 0.55 units. The decline in the absorbance is observed upon addition of 0.6 mg of pristine as well as irradiated sample and becomes minimum for sample radiated with 1×10^{12} fluence. This decline in the peak intensity is attributed to the interaction of DPPH free radicals with polypyrrole nanotubes resulting in neutralisation of free radicals. The reaction starts with the transfer of hydrogen atom following an electron transfer from polypyrrole to DPPH free radicals. As a result DPPH converts to DPPHH which leads to decolorisation of DPPH [2].

The variation of DPPH scavenging activity with fluence is plotted in Fig. 3. From the plot it is clear that with increase in ion fluence the scavenging activity of the polypyrrole nanotubes increases. During the passage of SHI through the target material, the ion loses its energy either in displacing atoms by elastic collisions or exiting the atoms by inelastic collisions [3]. At the time of irradiation, each ion creates a cylindrical zone of cations, anions, radicals, electrons etc. of the order of few nanometres in diameter. The electrostatic repulsion between these carriers causes the generation of shock waves, which leads to fragmentation of the target material. The higher is the fluence; larger is the time of SHI exposure, higher is the fragmentation. Fragmentation of the nanotubes leads to increase in surface to volume ratio which in turn increases the number of active sites which favor the scavenging of DPPH free radicals.

REFERENCES

[1] U. Lange and V. M. Mirsky, Analytica Chimica Acta 687 (2011) 105-113.
[2] C. F. Hsu, L. Zhang, H. Peng, J. Travas-Sejdic and P. A. Kilmartin, Synthetic Metals 158 (2008) 946.
[3] M. Deka and A. Kumar, J Solid State Electrochem. 17 (2013) 977.

5.2.11 ENERGY DEPENDENCE STUDIES OF NANOSTRUCTURES ON InP(100) USING ENERGETIC ION BOMBARDMENT

Indra Sulania[1,2], Mushahid Husain[2], Dinesh Agarwal[1], Pravin Kumar[1] and D K Avasthi[1]

[1] Inter-University Accelerator Centre, Aruna Asaf Ali Marg, New Delhi – 110 067
[2]Jamia Millia Islamia, New Delhi

In the recent years, special interest is being paid to the study of self-organized nanopattern formation on surfaces by *ion beam sputtering* (IBS) techniques [1]. In general, two types of surface nanostructures can be induced by IBS: (a) nano-ripples and (b) nanodots. In both the cases, the pattern formed by these nanostructures can have dimensions ranging from a few nm to hundreds of nm. These patterns can be produced on variety of materials such as amorphous or crystalline. The generated nanostructures depend upon many parameters such as the angle of incidence, ion fluence and ion energy etc. Studies have shown that with increase in ion energy, the surface nanostrutcures show an increase in the dimension (size/ wavelength) of the structures. There is an increase in ripple wavelength, $\lambda \sim E^n$, where E is the energy of the ions and n is between 0 and 1. There are not many experimental studies to validate this relation. In a study by Facsko et al. for ion beam sputtered IBS nanodot patterns on GaSb, 15 different energy values have been studied [2]. They obtained a value of $m = 0.5 \pm 0.02$ i.e. no power law dependence.

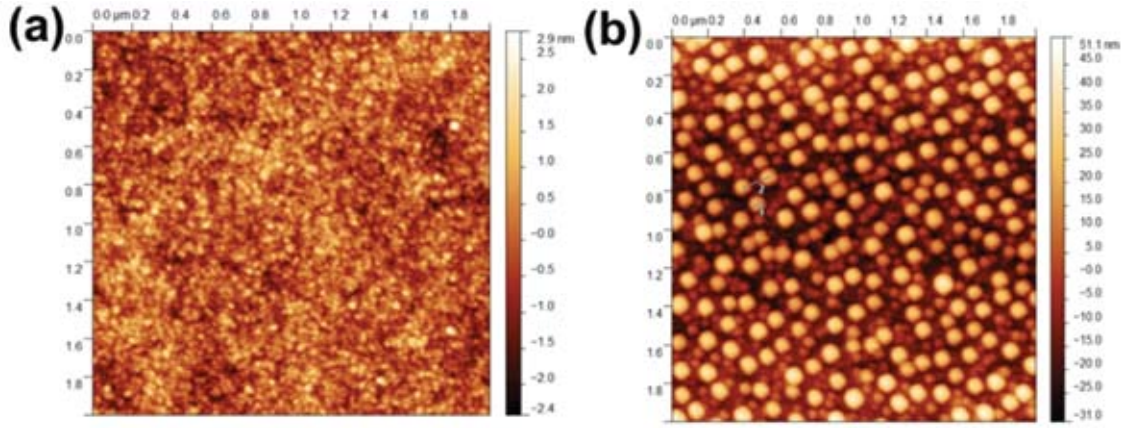

Fig. 1. The AFM image of the (a) pristine InP (100) sample and (b) irradiated sample at an energy of 50 keV

In the present studies, we have used the Ar^+ ions with different energies ranging from 50 keV to 250 keV to bombard the samples of commercially available InP (100) single crystal samples. The bombardment was carried out at an incidence angle of 20º with respect to the surface normal. The studies were carried out at LEIB facility of the Inter-University Accelerator Centre, New Delhi. The commercially available InP(100) wafer was taken and cleaved into smaller pieces of 1×1 cm^2 to be used for irradiation. These small pieces were cleaned with ethanol to remove the traces of impurities from the surface of InP. The AFM images of pristine and irradiated samples at energy of 50 keV are shown in Fig. 1. The images are scanned for 2 µm×2 µm scan size. Pristine sample has no features and the surface is flat with a roughness of ~ 0.2 nm. Upon irradiation, the nanodot formation is clearly visible on the surface. The fluence used for this sample was 8×10^{16} ions/cm^2. The nanodots formed are circular in shape with a small variation in their sizes. The average size of the nanodots was found to be 70 nm. There is an increase in the roughness as compared to the pristine sample to 15.9 nm. Ordering of the naonodots with square symmetry is observed. The irradiated samples show an increase in roughness with increase in energy. The size of the dots also increases with increase in ion energy. The detailed analysis of the energy dependence is still in process.

REFERENCES

[1] S. Facsko, T. Dekorsy, C. Koerdt, C. Trappe, H. Kurz, A. Vogt and H. L. Hartnagel, Science 285 (1999) 1551.
[2] S. Facsko, H. Kurz and T. Dekorsy, Phys Rev B 63 (2001) 165329.

5.2.12 ENGINEERING OF RIPPLE PATTERNS ON Si (100) SURFACE USING LOW ENERGY ION BEAM IRRADIATION

Tanuj Kumar, D.Kanjilal

Inter-University Accelerator Centre, Aruna Asaf Ali Marg, New Delhi – 110 067

Recently, the formation of self-organized nano-structures under the effect of ion-beam sputtering has turned into a highly active research area of surface science. The self-organized surface nano-structures have many technological applications for the development of future optoelectronic, electronic, and magnetic devices in variety of fields [1]. Although, there are several methods to grow surface nanostructures like photolithography, sub-lithography, scanning probe tip, ion beam sputtering etc. Among these, ion beam sputtering of solid surfaces is a very elegant and one-step bottom-up approach. By varying the sputtering parameters in a controlled manner, one can evolve surface topography into well-ordered nanostructures like one-dimensional ripples, regular arrays of dots and pits etc.

In this work ripple patterns were created on the Si(100) surface using 200 keV Ar^+ ion beam irradiation for the fluences ranging from 3×10^{17} ions/cm^2 to 3×10^{18} ions/cm^2. Atomic force microscopic (AFM) images

(Fig. 1) show that the orientation of ripples is perpendicular to the surface projection of the ion beam. Exponential growth of roughness and small variation in wavelength of patterned surfaces with ion fluence is according to the linear continuum/ hydrodynamic models of surface patterning [2-3]. Observed evolution of ripples is in agreement with stress induced hydrodynamic solid flow model. Contact angle measurement demonstrates the possibility of engineering the hydrophilicity of Si (100) surface.

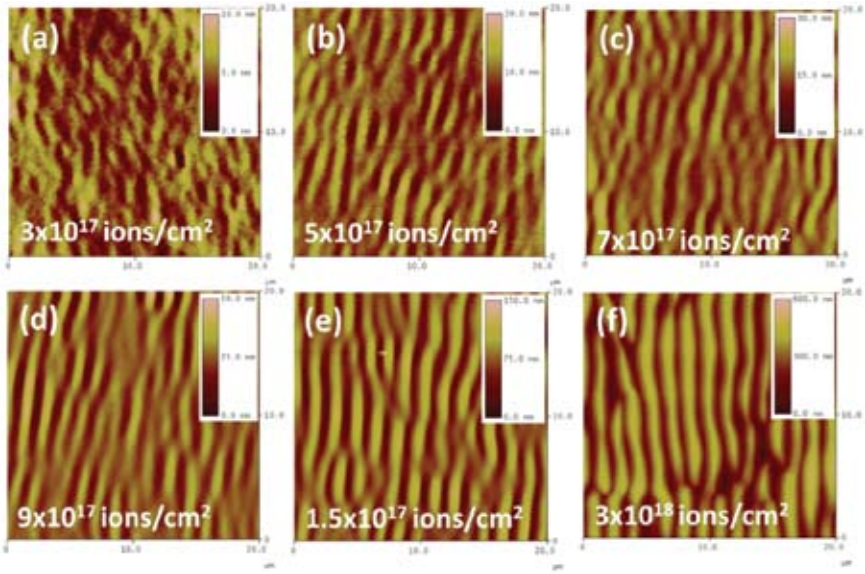

Fig. 1. AFM images of rippled patterns on Si (100) after irradiation with 200 keV Ar^+ at different fluences.

REFERENCES

[1] Y. C. Tseng, A. U. Mane, J. W. Elam and S. B. Darling, Advanced Materials 24 (2012) 2608.
[2] R. M. Bradley and J. M. Harper, Journal of Vacuum Science & Technology A: Vacuum, Surfaces, and Films 6 (1988) 2390.
[3] M. Castro and R. Cuerno, Appl. Surf. Sci. 258 (2012) 4171.

5.2.13 THE EFFECT OF ION BEAM IRRADIATION ON TRANSPORT STUDIES IN POLYMER NANO-COMPOSITE ELECTROLYTES

D. K. Kanchan

Department of Physics, Faculty of Science, The M.S. University of Baroda, Vadodara

Solid polymer electrolytes have drawn considerable attention due to their potential application not only in electrochemical devices but also in electro-luminescence devices and photo-electric devices [1]. Polyethylene oxide (PEO), even being a semi-crystalline polymer, is still an active candidate as a polymer host for solid polymer electrolytes. In terms of ionic conductivity, PEO complexes can achieve good ionic conductivity only when the host polymer is in amorphous phase. However, the amorphous state of these electrolyte films is poorly mechanical stable. Various methods such as polymer blending, addition of plasticizers and the incorporation of inert nano-fillers are reported well to enhance the amorphous phase of PEO Polymer.

In addition to this, irradiation on polymer films by ion beams e.g., electrons, photons, gamma rays and heavy ions has also been proposed to enhance the ion transport properties of polymer host due to irradiative decay, production of new reactive species such as radicals and gases, crosslinking/scissioning of long polymer chains, hardness, strength and wear resistance, electrical conductivity, density, chain length, solubility and optical transmission properties. Change in physical and chemical properties are observed due to energy transfer by the ion to the polymer matrix. Many researchers reported improvement in the

electrical properties in P(VDF-HFP)-(PC+DEC)-$LiClO_4$ [2], PEO-$LiClO_4$ [3], PVA-KOH [4], etc. where P(VDF-HFP) is (-poly(vinylenefluoride-co-hexafluoropropylene), PC is propylene carbonate, DEC is diethyl carbonate, PEO is poly(ethylene oxide), PVA-Poly(vinyl alcohol) and KOH-potassium hydroxide, when these polymer complexes were exposed to the heavy ion irradiations [5, 6].

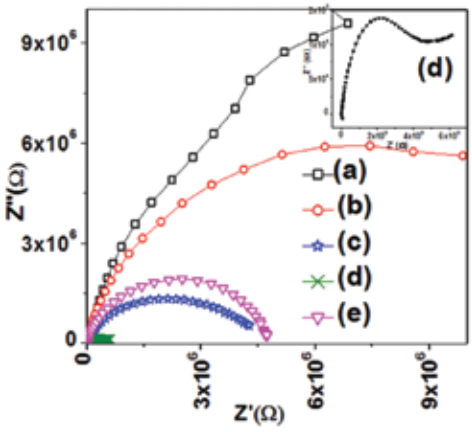

Fig. 1. Impedance Cole-Cole Plot for (a) unirradiated and irradiated blends at fluences of (b) 1×10^{11}, (c) 3×10^{11}, (d) 1×10^{12} and (e) 3×10^{12} ions/cm^2.

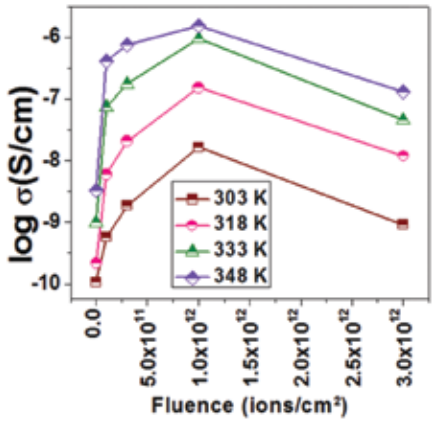

Fig. 2. Variation of conductivity as a function of fluences.

Present work is to study the irradiation effect on PEO-PVA-$AgNO_3$, PEO-PVA-$AgNO_3$-PEG, PEO-PVA-$AgNO_3$-PEG-SiO_2, PEO-$LiCF_3SO_3$-PEG-Al_2O_3 polymer blend electrolytes at different fluences.

In PEO-PVA polymer blend, PVA is a semi-crystalline polymer with a rigid polymer backbone and PEO also shows a low ionic conductivity. It is expected that blending of PVA with flexible PEO may increase the amorphosity of the host polymer. In the present study, polymer electrolyte films of PVA-PEO complexed with $AgNO_3$ and $LiCF_3SO_3$ and plasticized with poly ethylene glycol (PEG) and ethylene carbonate (EC) blend electrolyte films, prepared by solution cast technique, were irradiated with a 80 MeV O^{7+} ions at four different fluences of 1×10^{11}, 3×10^{11}, 1×10^{12} and 3×10^{12} ions/cm^2. Study of the electrical properties of the irradiated polymer films were carried out using complex impedance spectroscopy at different temperatures in the frequency range 1MHz-100Hz. Upon irradiation, the bulk resistance values (obtained from impedance spectroscopy) are observed to shift towards origin (Fig.1 for PEO-PVA- $LiCF_3SO_3$- EC polymer electrolyte system) with the increase in fluence i.e. conductivity (calculated from bulk resistance value) increases gradually with increasing fluence. The optimized conductivity is obtained at the fluence 1×10^{12} ions/cm^2 (Fig. 2). At a higher fluence of 3×10^{12} ions/cm^2, the conductivity drops.

REFERENCES

[1] L. Lee, S.J. Park, S. Kim Solid state Ionics 234 (2013) 19.
[2] A.Kumar, D. Saikia, F. Singh, D.K. Avasthi, Solid State Ionics 177 (2006) 2575.
[3] P. Ferloni, et al. Radiat. Phys. Chem. 37 (1991) 615.
[4] V. M. Nikolic etal. Electrochem. Communi. 9 (2007) 2661-2665.
[5] A. Biwas, et al. Nucl. Instru. Methods in Phys. Res. B 159 (1999) 40.
[6] X. Song, S. Wu, X. Jing, J. Sun and D. Chen, Radiat. Phys. Chem. 49 (1997) 541.

5.2.14 DISORDER INDUCED SEMICONDUCTOR TO METAL TRANSITION AND MODIFICATIONS OF GRAIN BOUNDARIES IN NANOCRYSTALLINE ZINC OXIDE THIN FILM

Fouran Singh*, [1], Babloo Chaudhary[2], Vinod Kumar[1], R. G. Singh[3], Sanjeev Kumar[4], A. Kapoor[4]

[1]Materials Science Group, Inter-University Accelerator Centre, Aruna Asaf Ali Marg, New Delhi-110067

[2]Centre of Excellence in Material Sciences and Nanomaterials, Z. H. College of Engineering & Technology, Aligarh Muslim University, Aligarh (U.P.) –202001
[3]Department of Electronic Science, Maharaja Agrasen College, University of Delhi, New Delhi- 110096
[4]Department of Electronic Science, University of Delhi South Campus, New Delhi - 110023

In the last decade, zinc oxide (ZnO) has been investigated very intensively due to its potential applications such as transparent conducting electrodes, electro-optical devices, thin film transistors, gas sensors, varistors, light emitting diodes, and piezoelectric transducers [1-4]. However, the response of these devices depends on the pronounced nonlinear current-voltage characteristics. The nonlinear current-voltage properties of these devices are controlled by a potential barrier, which originates from interface defects at the grain boundary (GB) of nanocrystalline ZnO (nc-ZnO). Energetic ion irradiation has been proven to be a potential tool for creating defects and disorder in such oxides for the manipulations in their physical properties. Therefore, we report on the disorder induced Semiconductor to Metal Transition (SMT) and modifications of grain boundaries in nanocrystalline zinc oxide thin film. Disorder is induced using energetic ion irradiation. It eliminates the possibility of impurities induced transition. However, it is revealed that some critical concentration of defects is needed for inducing such kind of SMT at certain critical temperature.

Origin of the observed SMT at around a certain temperature is a topic of current research interest and can be explained by the formation of a degenerate band appearing in highly defected semiconductor likely for the heavily doped semiconductors as suggested by Mott [5]. Similar observations of high conductivities and positive temperature coefficient of resistance (TCR) have also been reported in the Ga doped ZnO by Bhosle et al. [6]. They attributed such transition to the impurity induced enhanced ionization efficiency of carriers. Nevertheless, they have not completely ignored the possible role of defects. While, Si et al., by doing first principle calculations, have reported that SMT can be induced under proper axis strain in zigzag-edged ZnO nanoribbons [7]. So, the possibility of SMT in present investigations can be attributed to the high degree of disorder and strain induced by high density of defects in the Ag irradiated films, which could form the degenerate levels as discussed above. Energetic ion irradiation induced disorder and strain in the similar films have been reported in our previous studies [8-9]. However, the decrease in carrier concentration also shifts the Fermi level below the conduction band which explains the observed semiconducting behavior of the films. Moreover, such high density of defects and defect clusters can lead to high degree of disorder in a degenerate semiconductor and result in localization of the electronic states and corresponding increase in resistivity with a negative TCR [10]. Above transition temperature, electrons are delocalized due to thermal activation and the conductivity is dominated by conventional phonon scattering.

In summary, semiconductor to metal transition in nanocrystalline ZnO is demonstrated and the possible defects responsible for such transition are identified. The transition is explained by the defects induced disorder and strain in crystallites created by high density of electronic excitations. Therefore, it is concluded that energetic ions can be used efficiently for a deeper understanding of the transport of carriers in such nanocrystalline films, which are having applications in optoelectronic, photovoltaic and electric field controlled switchable devices. For details, see the full paper *[Fouran Singh et al. J. Appl. Phys. 112 (2012) 073101]*.

REFERENCES

[1] Ü. Özgür et al., J. Appl. Phys. 98, 041301 (2005).
[2] A. Tsukazaki et al., Nat. Mater. 4 (2005) 42.
[3] K. Nomura, H. Ohta, K. Ueda, T. Kamiya, M. Hirano and H. Hosono, Science 300 (2003) 1269.
[4] R.G. Singh, Fouran Singh, D. Kanjilal, V. Agarwal and R.M. Mehra, J. Phys. D: Appl. Phys. 42/FTC (2009) 06200.
[5] N. F. Mott, Metal-Insulator Transition (Taylor and Francis, London, 1974).
[6] V. Bhosle, A. Tiwari and J. Narayan, Appl. Phys. Lett. 88 (2006) 032106.
[7] H. Si and B. C. Pan, J. Appl. Phys. 107 (2010) 094313.
[8] Fouran Singh, R. G. Singh, Vinod Kumar, S. A. Khan and J. C. Pivin, J. Appl. Phys. 110 (2011) 083520.
[9] Fouran Singh, P.K. Kulriya and J.C. Pivin, Solid State Commun 150 (2010) 1751.
[10] Thomas Moe Børseth et al., Appl. Phys. Lett. 89 (2006) 262112, ibid Phys. Rev. B 77 (2008) 045204.

5.2.15 STRUCTURAL AND OPTICAL PROPERTIES OF TEFLON-IMPREGNATED TiO_2 NANOPARTICLES IRRADIATED BY 80 keV Xe^+ ION

Rizwin Khanam[1], Nibedita Paul[1], Pravin Kumar[2], D. Kanjilal[2], Gazi. A. Ahmed[1], Dambarudhar Mohanta[1],*

[1]Nanoscience and Soft Matter Laboratory, Department of Physics, Tezpur University, Tezpur,-784 028, Assam, India
[2]Inter-University Accelerator Centre, Aruna Asaf Ali Marg, New Delhi – 110 067
* Email: best@tezu.ernet.in

In this work, we highlight the influence of 80 keV Xe+ ion irradiation on the morphological and optical response of TiO2 nanoparticles spread over commercially available polytetrafluorothylene (PTFE, Teflon). The nanoparticles were synthesized via a cost-effective sol-gel method whereas the teflon support was made using a hot-press. X-ray diffraction studies have revealed anatase phase of the system with an average crystallite size ~9 nm. The formation of nanoparticles was also confirmed from the high resolution transmission electron microscopy (HRTEM). For irradiation experiment, the teflon-impregnated TiO2 nanoparticles were subjected to 80 keV Xe+ ion irradiation using low-energy ion beam facility (LEIBF) available at IUAC, New Delhi. The beam current was kept at ~1 eμA, while the fluence was varied in the range of 1015-1020 ions/cm^2.

As shown in the micrograph Fig. 1A, the average size of the unirradiated nanoparticles was ~7 nm which tend to increase slightly (size of ~12 nm, Fig. 1B) at a lower fluence but increase drastically (size of ~28 nm, Fig. 1C) when subjected to very high fluence. Point defects generated by low energy ion beam due to nuclear energy loss might act as nucleating agent for the growth of these crystallites [1]. Moreover, nanoscale surface ripples have been observed due to the ion impact (Fig. 1D). Recently, we have demonstrated that the size of the particles is highly dependent on the nature of solid state quenching process [2]. UV-visible optical absorption spectra of teflon impregnated unirradiated and irradiated TiO2 nanoparticles are shown in Fig. 2. The absorption band at ~370 nm is ascribed to the interband *1s-1s* carrier transition from the valence band to the conduction band [3]. The optical band gap *(E_g)*, as calculated for direct and allowed carrier transitions, followed a decreasing trend (from 3.15 eV to 2.70 eV) with increasing fluence (not shown). The reduced band gap, at a higher fluence is expected to appear as a result of the introduction of defect energy levels within the original band gap and possibly, below the bottom of the conduction band.

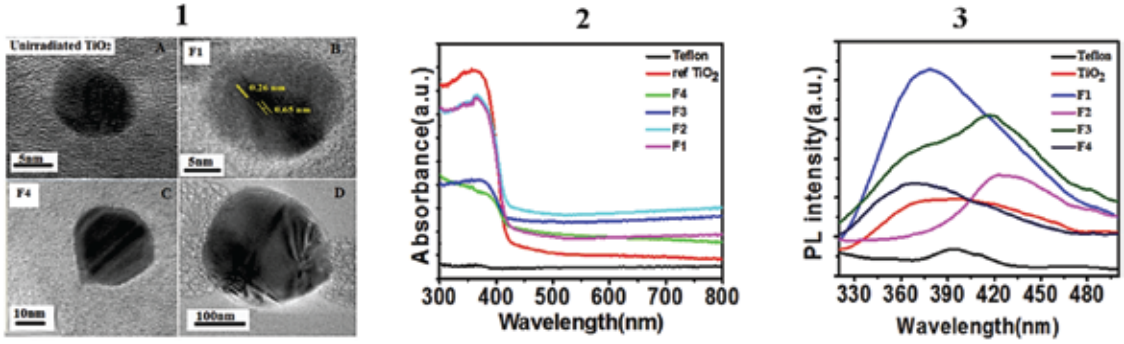

Fig. 1. TEM micrograph of un-irradiated A) and irradiated TiO2 nanoparticles with fluences of B) F1 and C) F4. The formation of ripples is shown in D). Fig. 2. UV-Vis optical absorption spectra and Fig. 3. PL spectra of irradiated and un-irradiated particles.

The photoluminescence response was studied utilizing the excitation at ~270 nm (Fig. 3). Upon irradiation, significant modification of the emission spectra was observed due to drastic variation in the radiative processes. The characteristic peaks could be obtained through deconvolution process (after Gaussian fitting, not shown). The first peak was located at ~ 376 nm and is ascribed to the emission via band gap transitions in TiO_2. Additionally, a peak at ~ 490 nm is assigned to the charge transfer transition from Ti^{3+} to oxygen anion in TiO_6^{2-} octahedra associated with oxygen vacancies. Moreover, the emission peak located at ~ 423

nm is due to the self trapped excitons (STE) localized on TiO_6^{2-} octahedral sites [4]. Whereas, the peak positioned at ~ 458 nm might have occurred due to the color centers associated with the oxygen vacancies with two trapped electrons (*F* center). The peak positions though similar for all the samples, the strength of the emission was dictated by the modification of the localized defect states introduced by irradiation of definite ion fluence.

REFERENCES

[1] T. Mohanty, S. Dhounsi, P. Kumar, A. Tripathi and D. Kanjilal. Surf. Coat. Tech. 203 (2009) 2410.
[2] N. Paul, M. Patowary, B. Pegu & D. Mohanta. Nanosci. Nanotechnol. Lett. 5 (2013) 452.
[3] H. S. Chen, C. Su, C.K.Lin, Y. F. Hsieh, C. K.Yang, & W. R. Li, J Chem. Eng. Jpn. 42 (2009) 36.
[4] D. Li. H.Haneda. N. K. Labhsetwar. S. Hishita and N. Ohashi, Chem. Phys. Lett. 401 (2005) 57.

5.2.16 FLUENCE DEPENDENT BANDGAP ENGINEERING OF RUTILE TiO_2 (110) SINGLE CRYSTAL

Vanaraj Solanki [1], Subrata Majumder[1], Indrani Mishra[1], Shalik R. Joshi[1], Dinakar Kanjilal [2] and Shikha Varma[1]*

[1] Institute of Physics, Bhubaneswar- 751005
[2] Inter-University Accelerator Centre, Aruna Asaf Ali Marg, New Delhi – 110 067
*corresponding author: shikha@iopb.res.in

Ion beam sputtering is a useful technique to produce self-assembled regular arrays of close-packed nanostructures on thin films or substrates, in a large scale, in a single technological step [1, 2]. Ion beam irradiation has gained immense attention due to the technological demand for large arrays of nanostructures. In the case of ion beam irradiation, the close-packed regular arrays of nanostructures are formed through competition between curvature dependent sputtering that roughens the surface and smoothening by different relaxation mechanisms. In our previous work on ion beam irradiation of TiO_2 single crystals, we have demonstrated high absorbance of UV-Vis radiation at high fluence [2,3].

Room temperature sputtering experiments were performed on rutile TiO_2 single crystal by utilizing low energy ion beam facility (LEIBF) at IUAC New Delhi. Singly charged Ar^+ ion beam with energy 60 keV and flux 1.8×10^{14} ions/cm^2.s from electron cyclotron resonance source was used for this study. The ions were bombarded on the surface at an incident angle of 60° from the surface normal. The samples were sputtered with different fluences ranging from 5×10^{15} ions/cm^2 to 5×10^{17} ions/cm^2. The morphological study reveals the formation of self-assembled nanostructures on the sputtered surfaces. The evolution of the TiO_2 nanodots (size varying from 5 to 26 nm) has been observed as a function of irradiation fluence. The changes in the surface chemical states after sputtering were studied by X-ray Photoelectron Spectroscopy (XPS). The XPS results show the creation of Ti-rich zones near the surface due to preferential sputtering of low mass oxygen atoms [4]. The optical absorption studies on the sputtered surfaces show increase in absorbance in the full UV-Visible region along with bandgap widening of ~0.1 eV, compared to the pristine sample. The enhancement in defect related emission is also observed in Photoluminescence studies. The observed Ti-rich zones and oxygen vacancies (created due to preferential sputtering of oxygen) near the surface, are responsible for the enhanced absorption and luminescence properties of the sputtered surfaces while smaller size of the nanostructures is responsible for the bandgap widening [5].

We would like to thank Pravin Kumar for providing the ion beam. We would also like to thanks Santosh Choudhary.

REFERENCES

[1] F. Frost, A. Schindler and F. Bigl, Phys. Rev. Lett. 85 (2000) 4116.
[2] S. Majumder, D. Paramanik, V. Solanki, B. P. Bag and Shikha Varma. Appl. Phys. Lett. 98 (2011) 053105.
[3] Subrata Majumder, D. Paramanik, V. Solanki, I. Mishra, D.K. Avasthi, D. Kanjilal and Shikha Varma, Appl. Surf. Sci 258 (2012) 4122.

[4] Vanaraj Solanki, Subrata Majumder, Indrani Mishra, Shalik R. Joshi, Dinakar Kanjilal and Shikha Varma, Rad. Eff. Def. Solids (2013).
[5] Vanaraj Solanki, Subrata Majumder, Indrani Mishra, Shalik R. Joshi, Dinakar Kanjilal and Shikha Varma, (To be submitted)

5.2.17 STUDY OF AMORPHIZATION OF Ge USING 100 keV Ar IONS

Sonu Hooda, S. Ojha, D. Kanjilal, D. Kabiraj

Inter-University Accelerator Centre, Aruna Asaf Ali Marg, New Delhi – 110 067

The damage evolution in germanium (100) crystal has been studied. For this study Ge (100) crystal were irradiated with 100 keV Ar^+ ion beam using LEIBF facility at IUAC. The damage formation has been investigated with the help of Rutherford Backscattering Spectroscopy in Channeled condition (c-RBS).

Polished undoped Ge (100) samples were cleaned using TCE, alcohol and acetone and used as target. The samples were irradiated by 100 keV Ar^+ ions in the fluence regime of 1.6×10^{12}- 8×10^{14} ion/cm^2 at room temperature. To avoid channeling of Ar ions during irradiation, ions were bombarded at an angle of 5° with respect to the surface normal of the target. In order to get actual beam current on the target the enclosure around the target was kept at a negative potential for suppressing the secondary electrons which were produced by the impact of energetic ions. The beam current was stabilized at 400 nA during experiment. The beam was scanned uniformly over the entire sample. Irradiation was performed in a vacuum chamber and pressure inside the chamber was 10^{-7} mbar. Samples were mounted on a target ladder using conducting glue. Target ladder is made up of thick copper material. This ensures negligible temperature rise of sample during irradiation. The fluence was evaluated considering constant current and the duration of irradiation. Thus, the fluence was varied by varying the time. C-RBS was performed using 2 MeV He ions at IUAC facility. A 2-axis goniometer was used in this setup and a solid-state surface barrier detector was used at an angle of 170° to detect the back-scattered particles. The channeled spectra of irradiated and pristine Ge samples are shown in Fig. 1. This shows the dependence of damage formation in Ge on the number of incident Ar ion and it is clear from the figure that damage fraction increases with increase in ion dose.

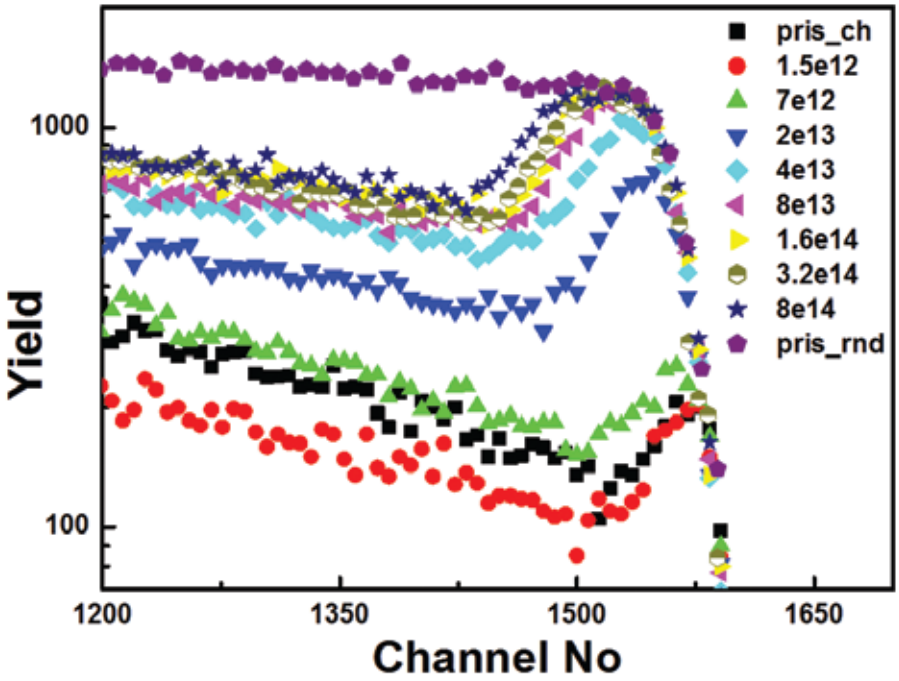

Fig. 1 Channeled spectra of irradiated and pristine Ge samples

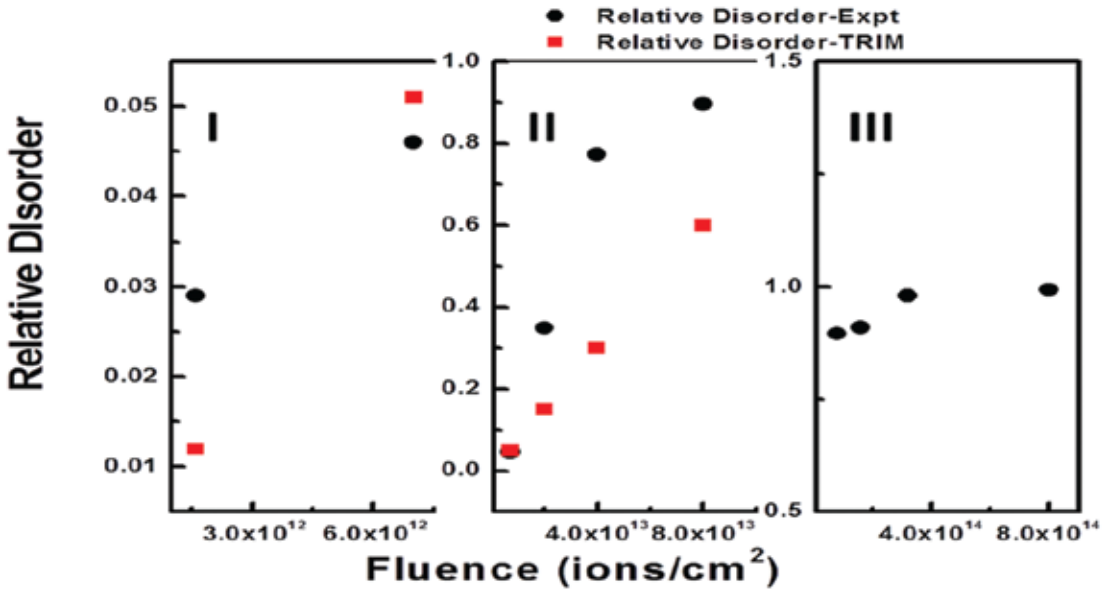

Fig. 2. Comparison of experimentally evaluated relative disorder with TRIM calculation

The experimentally evaluated relative disorder is shown in Fig. 2. On comparing the experimental results with TRIM calculations (Fig. 2) three different regimes of damage accumulation were observed. In regime (I) rate of damage formation with fluence is less than TRIM value; in regime (II) rate of damage formation is higher than TRIM value and in the (III) regime saturation was observed.

5.2.18 LAYER TRANSFER AND BLISTERING STUDIES OF H-IMPLANTED SEMICONDUCTORS

U. Dadwal, S. Chandra and R. Singh

Indian Institute of Technology Delhi, Hauz Khas, New Delhi 110016, *India*

Layer transfer studies were carried out in 100 keV H^+ ion implanted silicon (Si) wafers (2-inch diameter) at room temperature (RT). The H-implantation was performed with the scan area of 1.5×1.5 cm^2 and 3.5×3.5 cm^2 at different fluences from 1.5×10^{17} cm^{-2} to 2.8×10^{17} cm^{-2}. In addition, H-implantation was also carried out in germanium (Ge) samples (1×1 cm^2) at liquid nitrogen (LN_2) temperature and RT for the blistering investigation. The beam current was kept at either 10 μA or 20 μA.

H-implanted Si wafer at a fluence of 2.2×10^{17} cm^{-2} was bonded directly with the oxidized Si wafer (oxide thickness ~80 nm) in the micro-clean room setup. Direct wafer bonding was performed at RT followed by thermal annealing in air ambient. The post-implantation annealing was done in the temperature range 200–500 °C with different annealing steps: 250 °C for 6 h, 300 °C for 6 h, 350 °C for 10 h and 400 °C for 4 h. This resulted in the transfer of thin Si layer (mm × cm) from the H-implanted wafer onto an oxidized Si wafer (Fig.1a and 1b). Thus, the fabrication of silicon-on-insulator (SOI) substrate could be realized. Atomic force microscopy (AFM) measurements revealed that root mean square surface roughness of the transferred Si layer was ~8 nm over the scan area of 5×5 μm^2 (Fig. 1c). The thickness of the transferred Si layer was ~770 nm (Fig. 1d).

In the case of H-implanted Ge samples, post-implantation annealing studies were carried out in the temperature range 400–600 °C for different durations. The investigations showed that the surface blistering/ exfoliation occurred only after post-implantation annealing.

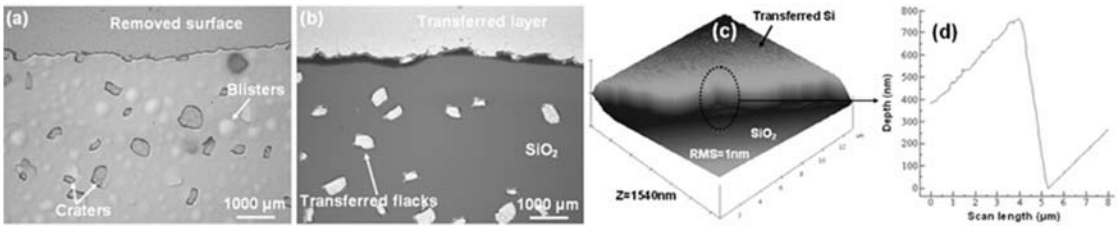

Fig. 1. Nomarski optical images of the surfaces of Si wafers after debonding/splitting following the annealing steps; (a) H-implanted Si wafer and (b) oxidized Si wafer. (c) Shows the AFM image of the transferred Si layer and (d) represents its thickness.

REFERENCES

[1] U. Dadwal and R. Singh, Appl. Phys. Lett. 102, 081606 (2013).
[2] U. Dadwal, M. Reiche and R. Singh (2012). Ion Implantation-Induced Layer Splitting of Semiconductors, Ion Implantation, Prof. Mark Goorsky (Ed.), InTech (2012) DOI: 10.5772/35956

5.2.19 ROLE OF SWIFT HEAVY ION IRRADIATION FOR THE DEVELOPMENT OF $Zn_{1-X}In_XO$ AS TRANSPARENT CONDUCTING OXIDE

Subodh K. Gautam[1], R.G. Singh[2], V.V. Siva Kumar[1], S. Ojha[1] and Fouran Singh[1]

[1] Inter-University Accelerator Centre, Aruna Asaf Ali Marg, New Delhi – 110 067
[2]Maharaja Agrasen College Delhi University, Delhi – 110 017

Transparent conducting oxides (TCOs) are electrically conductive materials and are of great importance due to their applications in various electronic and optoelectronic devices such as solar cells, gas sensors, flat panel displays, heat mirrors and diodes etc as cited in Ref. 1-2. Various types of dopants such as group-III elements like In^{3+}, Al^{3+}, Ga^{3+} have been exploited to improve and/or control the optical and electrical properties [3]. Therefore, for the present experiment multi-layers consisting of two thin Indium (In) layers sandwiched between three zinc oxide (ZnO) layers were deposited using RF magnetron sputtering at room temperature. Effects of swift heavy ion (SHI) and thermal annealing in controlled environment were studied using various characterization techniques such as Grazing incidence X-ray diffraction (GIXRD), UV-visible spectroscopy and Rutherford backscattering spectrometry (RBS) analysis. GIXRD pattern as shown in Fig. 1(a) reveals that as-deposited films have imputity phase of In_2O_3 around the interface, which gets pronounced by thermal annealing at 850 °C; while the irradiation for 3×10^{13} ions/cm^2 by 120 MeV Ag ions leads to the formation of single phase $Zn_{1-x}In_xO$. Films are polycrystalline in nature with wurtzite crystal structure. UV-visible absorption spectra (Fig. 1(b)) shows that irradiation does not leads to deterioration of near band edge (NBE) absorption, while the annealed sample shows very sharp NBE and strong exciton absorption peak. Observation of exciton peak and sharp NBE signified the high quality of ZnO crystallite, well phase separated with impurity phase of In_2O_3 at the interface region. The evolved phase of In_2O_3 is oriented along (222) plane. The observations of GIXRD and UV-vis spectroscopy are further corroborated by RBS measurements and their simulations as shown in Fig. 1(c) and (d). It has to be pointed out that only simulated spectrum of as-deposited film is shown in Fig. (d) for the clarity and brevity of writeup.

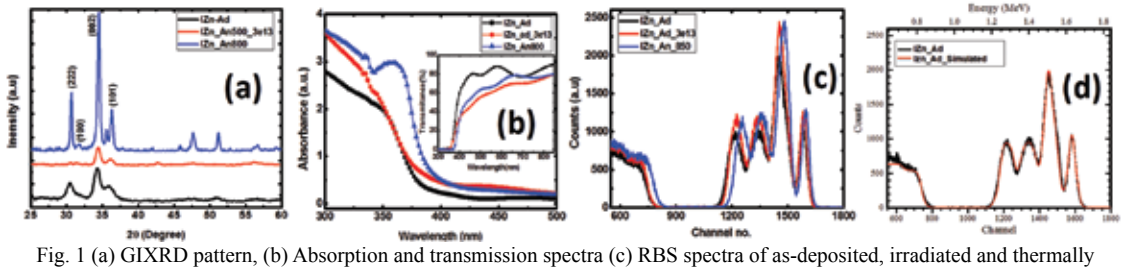

Fig. 1 (a) GIXRD pattern, (b) Absorption and transmission spectra (c) RBS spectra of as-deposited, irradiated and thermally annealed ZnO/In/ZnO/In/ZnO on silicon and/or silica substrate, (d) experimental and simulated RBS spectra of as-deposited sample on silicon substrate.

A simulated RBS result reveals the evolution of about 20 nm In_2O_3 layer around both the In layers. However, this layer which is not well crystallized and has diffused interface with ZnO layers gets crystallized and well phase separated after annealing at 850 °C. This annealing also improves the crystalline quality of ZnO layers. It would be better to remark that the remaining In diffuse in the ZnO layers which leads to the formation of $Zn_{1-x}In_xO$ single phase besides the formation of In_2O_3 phase. However, SHI irradiation of this multilayer film leads to the formation of single phase $Zn_{1-x}In_xO$ film without any inclusion of In_2O_3 or metallic In. These results are well corroborated with GIXRD and UV-vis results. These $Zn_{1-x}In_xO$ films also show interference fringe patterns in their transmission spectra with high transmittance of 75-80 % in the whole of the visible spectral region. Interference fringes of the transmittance curves also reveals that the film surface was highly reflecting and free from scattering or absorption losses in the films. However, the transmission spectra of the annealed and irradiated films show that the amplitude of the fringe pattern became flatter and the average transmittance is also reduced. This can be ascribed to the formation of a grainy surface leading to large scattering loss. The large red shift of NBE of the annealed film is attributed to the formation of good quality In_2O_3 phase at the interface which is having a band gap of about 3 eV. However, the small contribution from In impurities in the films for the formation of new recombination centers with lower energy state of shallow donor nature responsible for band narrowing cannot be completely ignored [4]. Therefore, these preliminary experiments show that SHI irradiation can be used as an efficient tool for the formation of doped single phase metal oxide film with very high transparency and conductivity [5]. Detailed experiments are in progress for the better understanding for the mechanisms.

REFERENCES

[1] Fouran Singh et al., J. Appl. Phys. 112 (2012) 073101.
[2] Vinod Kumar and Fouran Singh et al., J. of Alloys and Compounds 544 (2012) 120.
[3] P. M. Ratheesh Kumar et al., Semicond. Sci. Technol. 20 (2005) 120.
[4] S.Y. Bae, H.C. Choi, C.W. Na and J. Park, Appl. Phys. Lett. 86 (2005) 033102.
[5] Ravi Kumar and Fouran Singh et al., J. Appl. Phys. 100 (2006) 113708.

5.2.20 100 MeV O^{7+} ION IRRADIATION INDUCED EFFECT ON MULTIFERROIC $GdMnO_3$ NANOPARTICLES

Puneet Negi[1], H. M. Agarwal[1], R. C. Srivastava[1] and K. Asokan[2]

[1]G. B. Pant University of Ag. and Technology Pantnagar-263145
[2] Inter-University Accelerator Centre, Aruna Asaf Ali Marg, New Delhi – 110 067

For the last two decades, swift heavy ion (SHI) received attention in the modification of structural, magnetic and electrical properties of manganites [1]. Here we report the 100 MeV O+7 ion irradiation induced effects on multiferroic GdMnO3 nanoparticles.

The nanoparticles of GdMnO3 were synthesized by sol-gel method and irradiated with 100 MeV O^{+7} beams at fluences of 1×10^{12}, 5×10^{12}, 1×10^{13}, 2×10^{13} and 5×10^{13} ions/cm^2. X-ray diffraction (XRD) of pristine sample confirms the pure phase of $GdMnO_3$. After irradiation, the XRD pattern shows no significant shifting of peaks upto the fluence of 2×10^{13} ions/cm^2. However, at the fluence of 5×10^{13} ions/cm^2, the peak (121) is shifts to a lower angle side (Fig. 1). The crystallite size (D) and lattice spacing (d) of $GdMnO_3$ corresponding to most instance peak (121) are shown in the Table 1. Fig. 2 shows the low temperature dielectric constant of pristine and irradiated (at 5×10^{13} ions/cm^2) samples of GdMnO3 nanoparticles at the frequency of 610 Hz. The real part of the dielectric constant increases after irradiation. The temperature dependent real part of the dielectric constant exhibits an anomaly at T_1~13 K and indicates the phase transition from the incommensurate antiferromagnetic to canted A-type antiferromagnetic (ICAFM-cAAFM) in both pristine and irradiated samples [2].

An anomaly also observed at T_2~28 K in the irradiated sample. The observed changes may be due to the strain as well as the semi amorphous nature of the GdMnO3 nanoparticles induced by SHI. The detailed analysis of these features in these samples is underway.

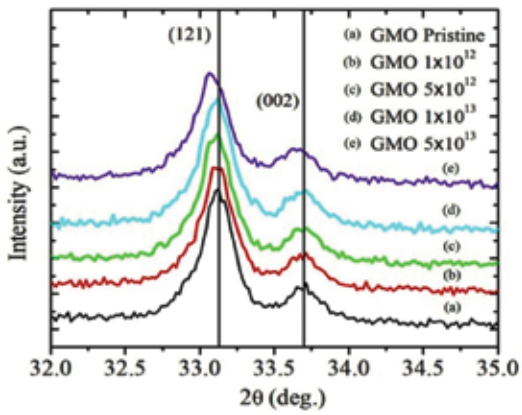

Figure 1: XRD pattern of pristine and irradiated nanoparticles of Multiferroic $GdMnO_3$

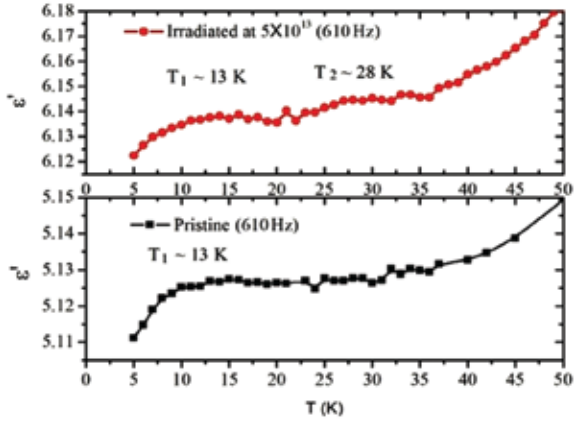

Figure 2: Dielectric constant of pristine and irradiated $GdMnO_3$ nanoparticles.

Table 1. The crystallite size (D) and lattice spacing (d) of $GdMnO_3$ nanoparticles before and after irradiation.

		Irradiated (by 100 MeV O^{+7} ions) at fluences				
	Pristine	1×10^{12}	5×10^{12}	1×10^{13}	2×10^{13}	5×10^{13}
2θ±0.002	33.118	33.113	33.106	33.107	33.102	33.077
D ± 0.8 (nm)	33.5	32.5	32.8	31.7	32.9	31.4
d (Á)	2.705	2.705	2.706	2.706	2.706	2.708

REFERENCES

[1] R. N. Parmar, J. H. Markna, D. G. Kuberkar, R. Kumar, D. S. Rana, V. C. Bagve and S. K. Malik, Appl. Phys. Lett. 89 (2006) 202506.

[2] W. S. Ferreira, J. A. Moreira, A. Almeida, M. R. Chaves and J. P. Araujo, Phys. Rev. B 79 (2009) 054303.

5.2.21 EFFECT OF IRRADIATION OF 100 MeV O^{7+} BEAM ON THE COBALT FERRITE NANOPARTICLES

Grish Chandra[1], R. C. Srivastava[2], H. M. Agrawal[2] and K. Asokan[3]

[1]Deptt. of Physics D.S.B. Campus, Kumaun University, Nainital
[2]Deptt. of Physics, G.B. Pant University of Ag. & Tech., Pantnagar
[3]Inter-University Accelerator Centre, Aruna Asaf Ali Marg, New Delhi – 110 067

Ferrites are the most important magnetic materials for both commercial and industrial purpose and no other magnetic material can take its place due to their low coercivity and high resistivity [1-2]. Cobalt ferrite $CoFe_2O_4$ and $CoFe_{1.96}Ce_{0.04}O_4$ sintered at 700°C were irradiated with 100 MeV O^{+7} beams. The fluences 5×10^{12}, 1×10^{13}, 3×10^{13} and 5×10^{13} ions/cm^2 were taken for $CoFe_2O_4$ and 1×10^{13}, 2×10^{13}, 3×10^{13} and 5×10^{13} ions/cm^2 were taken for $CoFe_{1.96}Ce_{0.04}O_4$.

Due to reduction in the particle size, specific surface area increased after irradiation. For pristine sample, the specific surface area is 32.67 m^2/g. After irradiation, it increases to the value of 47.46 m^2/g for the

fluence of 5×10^{12} ions/cm^2. However the variation of specific surface area has no consistent relationship with the fluence. Also, lattice parameter increased slightly after irradiation.

A measurable change is observed in magnetic parameters: saturation magnetization, remanence and coercivity after irradiation with 100 MeV O^{7+} beam. For pure cobalt ferrite, saturation magnetization value decreased at high fluences. The remanent magnetization increased by substantial amount. The saturation magnetization of cerium doped cobalt ferrite decreases by an appreciable amount after irradiation. However, as the fluence is increased further the saturation magnetization again starts to increase and the sample behaves like a pristine sample. These effects after irradiation may be due to the produced disorder in the system [3]. The overall effects of irradiation on magnetic parameters are dominant for cerium doped cobalt ferrite.

Table 1. Saturation magnetization, remanence and coercivity of the samples after irradiation with 100 MeV O^{7+} beam

Composition	Fluence (ions/cm^2)	MS (emu/g)	Remanence (emu/g)	Coercivity (kOe)
$CoFe_2O_4$	Pristine	78.0	30.0	0.93
	5×10^{12}	79.0	34.8	1.29
	5×10^{13}	76.9	34.6	1.17
$CoFe_{1.96}Ce_{0.04}O_4$	Pristine	76.9	29.6	0.30
	1×10^{13}	71.8	32.8	1.17
	5×10^{13}	74.8	35.1	1.15

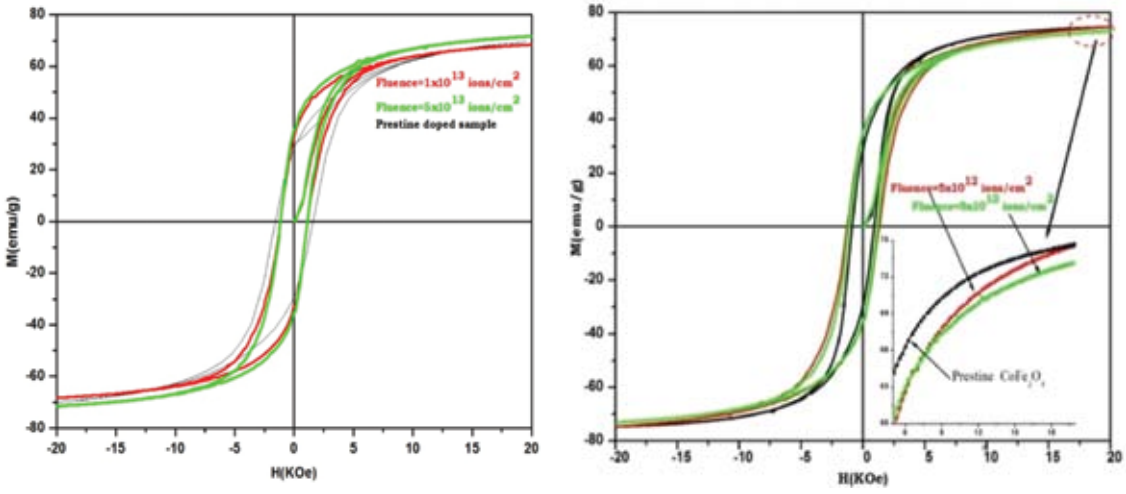

Fig. 1. M-H curves for (left) pristine and (right) irradiated cobalt ferrite at different fluencies.

REFERENCES

[1] Wafaa Bayoumi, J. Mater Sci 42 (2007) 8254.
[2] T. Raghvender and K. M. Jadhav, Bull. Mat. Sci. 32 (2009) 575.
[3] B. P. Rao et al., Nucl. Instr. Meth. Phys. Res. B 244 (2006) 27.

5.2.22 EFFECT OF 100 MeV OXYGEN ION BEAM IRRADIATION ON DYSPROSIUM DOPED COBALT FERRITE NANOPARTICLES

Hemaunt Kumar[1], R. C. Srivastava[1], H. M. Agrawal[1] and K. Asokan[2]

[1]Department of Physics, G.B. Pant University of Ag. & Tech. Pantnagar, Uttarakhand-263145
[2]Inter-University Accelerator Centre, Aruna Asaf Ali Marg, New Delhi – 110 067

Ferrimagnetic spinel ferrites constitute an important class of magnetic materials. The magnetic, electrical and optical properties of these ferrites depend on the nature and distribution of the cations in the tetrahedral (A) and octahedral (B) sub-lattice. $CoFe_2O_4$ is an important magnetic material having inverse spinel structure, which finds use in a wide range of applications including electronic devices, ferro-fluids, drug delivery, microwave devices, and high – density information storage [1]. Swift heavy ion (SHI) beam is widely used for modification of the structural and magnetic properties of the spinel ferrites. For this purpose, the $CoFe_{1.90}Dy_{0.10}O_4$ was synthesized by using the nitrates routes. The precursor materials in the present study were sintered at 500 °C for 2 hr. The sample was irradiated by 100 MeV oxygen beam with fluence of 1×10^{12}, 5×10^{12}, 1×10^{13}, 5×10^{13} and 1×10^{14} ions/cm^2. The electronic stopping (S_e), nuclear stopping (S_n) and the projected range (R_p) values for oxygen beam, calculated by using SRIM code are: S_e = 1.1 keV/nm, $S_n = 6.5\times10^{-4}$ keV/nm and R_p = 61.5 μm. The value of threshold electronic stopping for producing the columnar defects in cobalt ferrite is ~13 keV/nm [2]. This shows that only point/cluster defects are expected due to irradiation. The crystallographic phase and particle size of the pristine and irradiated samples were determined by the XRD. Further, magnetic measurement at room temperature and 10 K were carried out in order to observe the changes in magnetization after irradiation.

Fig. 1 shows the XRD patterns of the pristine and irradiated samples. They contain the peaks corresponding to the cubic spinel phase. The crystallite size of the sample are 13, 10, 8, 9, 7 and 9 nm for the fluence of 0 (pristine),1×10^{12}, 5×10^{12}, 1×10^{13}, 5×10^{13} and 1×10^{14} ions/cm^2 respectively. The magnetization versus applied magnetic field curve was recorded for the pristine and irradiated samples. The saturation magnetization changes after irradiation at room temperature as well as at low temperature (10 K). Fig. 2 shows the M-H curve at 10K.

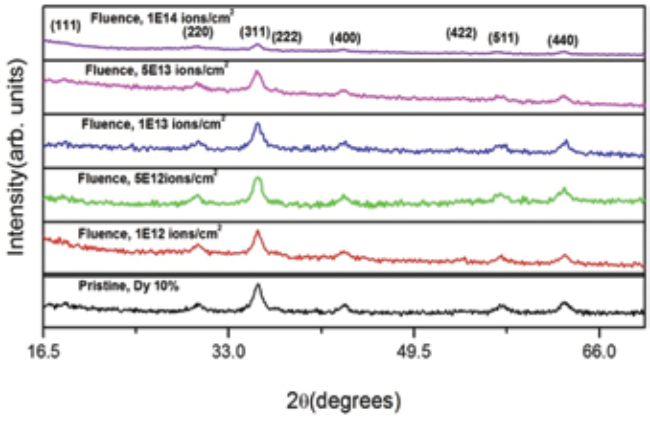

Fig. 1. XRD pattern of pristine and irradiated sample of $CoFe_{1.90}Dy_{0.10}O_4$.

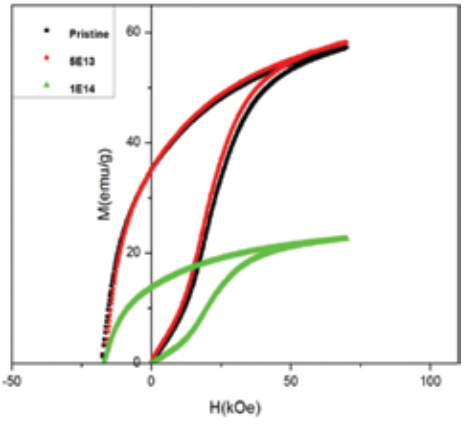

Fig. 2. M-H curve at 10 K.

The magnetic moment of the system are 1.84, 1.89 and 1.98 μ_B at room temperature and 2.50, 2.50 and 1.01 μB at 10 K for the fluence of 0 (pristine), 5×10^{13} and 1×10^{14} ions/cm^2 respectively.

REFERENCES

[1] G. D. Dwivedi et al., Phys. Rev. B 82 (2010) 134428.
[2] R. Kumar et al., Hyperfine Interaction 160 (2005) 143.

5.2.23 EFFECT OF GAMMA AND HEAVY ION IRRADIATIONS ON STRUCTURAL, OPTICAL, ELECTRICAL AND DIELECTRIC PROPERTIES OF MICACEOUS MINERALS

Sukhnandan Kaur[1], Surinder Singh [1], Lakhwant Singh[1] and S.P. Lochab[2]

[1]Department of Physics, Guru Nanak Dev University, Amritsar-143005, Punjab
[2] Inter-University Accelerator Centre, Aruna Asaf Ali Marg, New Delhi – 110 067

The experiment is to study radiation effects on structural, optical, electrical and dielectric properties of micaceous minerals. These studies will be helpful to utilize these minerals for innovative applications in radiation rich environment. Irradiation of minerals by charged particles leads them to several applications like solid state nuclear track detection [1], microfiltering [2] and fission track dating in geology [3, 4]. In addition to their main applications in insulation systems of high power rotating machines, these minerals are susceptible to ionizing radiation and are presently being used as dosimeter for monitoring absorbed doses in radiation rich environments. Thin sheets of these minerals of $1\times1cm^2$ having a thickness of 20 μm were irradiated with various fluences (1×10^{12} to 5×10^{13} ions/cm^2) of 80 MeV O and 100 MeV Ag ion beams. The range of incident ion as calculated from SRIM 2008 is more than the thickness of the sample.

An ion beam of energy ~MeV produces latent tracks in most dielectrics. These ion tracks in turn produce various modifications in their structural, optical and dielectric properties. These modifications are monitored using various techniques viz. Ultraviolet-Visible (UV-Vis) spectrometer, X-Ray Diffraction (XRD), LCR meter and Fourier Transform Infra-Red (FTIR) in natural phlogopite mica. Thin sheets (~ 20 μm) of phlogopite mica were exposed to 80 MeV of oxygen ions. A systematic decrease of optical band gap with ion fluence is observed. Increase in the Urbach energy indicates increase in disorderness in phlogopite mica. Dielectric constant has been found to decrease with increasing ion fluence while tanδ, ac conductivity and dielectric loss (□□□) show an increase. Obtained data reveal that the value of ac conductivity depends linearly on the frequency, with slope n ranging between 0.62 and 0.77. The XRD diffraction analyses of pristine and irradiated phlogopite mica have demonstrated that the crystallite size decreases while lattice strain and dislocation density increases with increase in ion fluence. The FTIR spectra show the shifting of OH stretching band and disappearance of Si-H bands due to irradiation. The different causes of these modifications are discussed in the present paper. The results are published in Nucl. Instrum. and Meth. 301 (2013) 17.

REFERENCES

[1] R. L. Fleischer, P. B. Price and R. M. Walker, Annu. Rev. Nucl. Sci. 15 (1965b) 1.
[2] G. Shi-Jun, R. Brandt, P. Vater and R. Dersch, Nucl. Tracks and Radiat. Meas. 15 (1988) 751.
[3] S. P. Ahlem, Rev. Mod. Phys. 52 (1980) 121.
[4] R. L. Fleischer, P. B. Price, E.M. Symes and D. S. Miller, Science 143 (1964) 349.

5.2.24 SWIFT HEAVY ION INDUCED STRUCTURAL AND LUMINESCENCE STUDIES OF RARE EARTH DOPED YTTRIUM OXIDE NANOPHOSPHORS

Sudipta Som[1], S K Sharma[1], S P Lochab[2]

[1]Solid State Physics Laboratory, Department of Applied Physics, ISM, Dhanbad
[2]Inter-University Accelerator Centre, Aruna Asaf Ali Marg, New Delhi – 110 067

This research work is focused on the comparative investigation on structural and optical modifications of rare earth doped/ codoped Y_2O_3 phosphors after swift heavy ions irradiation to find its suitability in colour tunable devices and as heavy ion dosimeters. Eu^{3+}, Tb^{3+} and Dy^{3+} doped, Eu^{3+}/ Tb^{3+} and Tb^{3+}/ Dy^{3+} codoped Y_2O_3 phosphors were prepared by varying rare earth concentration, annealing temperature using combustion synthesis method. The prepared phosphors were characterized by X-Ray diffraction,

Fourier transform Infrared spectroscopy and Transmission electron microscopy techniques. Different optical properties such as diffuse reflectance, photoluminescence and thermoluminescence were studied. The prepared phosphors were irradiated with swift Ni, Ag and Au ions and γ-ray.

A comparison among the various structural and optical properties of un-irradiated, ion-irradiated and γ-irradiated phosphors was made. The structural characterization confirms the formation of the desired compound in crystalline form having body centred cubic phase. The phosphors lose their crystallinity after swift heavy ion irradiation [1]. The richness of colour emission was observed after swift heavy ion irradiation. Tunable colour emission, richness of colour, near white light emission and tunning of bandgap with ion fluence indicate the applicability of phosphors in different lighting, display optoelectronics devices [2].

The response of a TL dosimeter to heavy ions is very important for air crew and space dosimetry. So, TL response with ion fluence was checked for different ion irradiation. Good TL sensitivity and linear TL response of swift heavy ion irradiated Y_2O_3 phosphor shows its suitability as TL dosimeter [3].

REFERENCES

[1] S. Som, S. K. Sharma & S. P. Lochab, Materials Research Bulletin 48 (2013) 844–851
[2] S. Som, S. K. Sharma & S. P. Lochab, Ceramics International, in press
[3] S. Som, S. K. Sharma & S. P. Lochab, PSS a, accepted

5.2.25 EFFECT OF 200 MeV Ag IONS ON THE TRANSPORT PROPERTY OF $YBa_2Cu_3O_{7-\delta}$ THICK FILMS

A. Kujur[1], K. Asokan[2], D. Behera[1]

[1]Department of Physics, National Institute of Technology, Rourkela-769 008
[2]Inter-University Accelerator Centre, Aruna Asaf Ali Marg, New Delhi – 110 067

$YBa_2Cu_3O_{7-\delta}$ composite thick films are prepared by diffusion reaction technique and subjected to irradiation with 200 MeV Ag ions with fluences $\Phi = (5\times10^{10}, 1\times10^{11}, 3\times10^{11}, 1\times10^{12}, 5\times10^{12}$ ions/cm^2). The effect of columnar defects generated by swift heavy ions on electrical transport property is studied and some of the results are shown in Fig. 1. The crystallographic modification is analyzed with x-ray diffraction technique. The addition of columnar defects marks the shifting of XRD peak [1]. The track radius is calculated to be 2.54 nm. Temperature dependent electrical resistivity highlights increment of residual resistivity and decrement of transition temperature with significant broadening in transition width as a function of ion fluence. A widespread value of T_{c0} and broadening is explained by stress model [2]. The excess conductivity has been analyzed within the framework of Aslamazov-Larkin (AL) and Lawrence-Doniach (LD) theories. A shift from 2D to 3D transition to higher temperature was observed with increasing fluences. The variation in T_{LD} with Φ indicates that intragranular region is modified by the invading ion tracks. The thermodynamically activated Cooper pairs are generated within the grains at a comparatively higher temperature however due to intragranular structural deformities of columnar track and its associated stressed region mean field transition temperature records lower value. The coherence length and the Josephson coupling have been estimated from LD theory. Psuedogap temperature (T*) regime [3] is affected by irradiation. At T* fermions couple into pairs forming bosons which condense at T_c. Phase coherence of the condensed bosons result in global superconductivity at T_{c0}. Introduction of columnar defects due to amorphized latent tracks enhances critical current density and flux pinning.

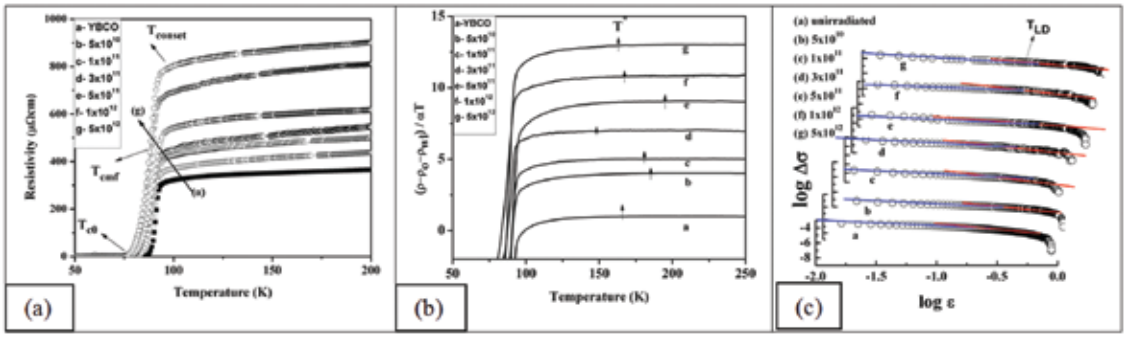

Fig. 1. (a) Illustrates dependency of resistivity on temperature for pristine and irradiated YBCO thick.
(b) Variation of Psuedogap temperature (T*) as a function of fluence.
(c) Log–log plot of excess conductivity as a function of reduced temperature $\varepsilon = (T - T_c) / T_c$ for various Φ.

REFERENCES

[1] R. Biswal et al., J. of Appl. Phys. 106 (2009) 053912.
[2] B. Hensel et al., Phys. Rev. B 42 (1990) 4135.
[3] H. Alloul, T. Ohno and P. Mendels, Phys. Rev. Lett. 63 (1989) 1700.

5.2.26 ION-INDUCED OPTICAL TREATMENT OF AMORPHOUS CHALCOGENIDE THIN FILMS FOR NEXT GENERATION PHOTONIC/OPTICAL COMPONENTS

R. Chauhan[1], K. K. Srivastava[2], A. K. Srivastava[3] and D. K. Avasthi[4]

[1]Department of Physics, DAV College, CSJM University, Kanpur – 208001
[2]Department of Physics, DBS College, CSJM University, Kanpur – 208006
[3]Material Science Programme, Indian Institute of Technology, Kanpur – 208016
[4]Inter-University Accelerator Centre (IUAC), Aruna Asaf Ali marg, New Delhi-110067

Amorphous chalcogenides are IR transparent, optically nonlinear (100 to 1000 times then Si), low-phonon energy materials, hence suitable for IR integrated optics/photonics. Due to flexible structural arrangement, these can be easily tuned according to desired application by external treatment i.e. annealing, photo/ion exposure etc. [1]. Some recent studies report that swift-heavy ion irradiation is a more effective technique to make optical/photonic components with improved performance [2]. Ge-As-Se chalcogenide glassy system has a broad glass formation region; hence a lot of compositions are available within this system [3]. Systematic study of this system can be done in terms of glass network connectivity, which is defined in terms of Mean Coordination Number (MCN), where MCN is the sum of product of coordination number and atomic percentage of constituent elements. It is observed that compositions within the MCN range 2.42 to 2.55 have finest attributes i.e. high optical nonlinearity with low optical losses in IR range along with thermal stability and highest possible glass transition temperature (250 °C). Hence, compositions within this range of MCN are suitable for IR photonic applications [4-6].

The present work investigates changes in optical properties of Ge-As-Se amorphous chalcogenide ($2.4 \leq MCN < 2.55$) thin films on 100 MeV Ag swift-heavy ion irradiations for ion fluence ranging from 3×10^{10} to 1×10^{13} ions/cm^2. The compositions selected for this study are $As_{40}Se_{60}$ [MCN = 2.4] and $Ge_{7.533}As_{38.698}Se_{53.769}$ [MCN = 2.54]. The changes in optical properties with swift-heavy ion irradiations are understood in terms of structural changes in order to optimize it for the next generation optical/photonic devices. Optical transmission and micro-Raman measurements were performed before and after irradiation in order to understand optical and structural changes due to irradiation. In amorphous $As_{40}Se_{60}$ and $Ge_{7.533}As_{38.698}Se_{53.769}$ thin-films, it is observed that optical bandgap reduces as shown in Fig. 1 and 2, while refractive index increases after irradiation [7, 8]. These changes are consequence of increment of

disorder caused by SHI irradiation. This is supported by reduction in Tauc parameter. This is also supported by Raman measurements of amorphous $Ge_{7.533}As_{38.698}Se_{53.769}$ thin films as shown in Fig. 3, where FWHM corresponding to GeSe4/2 CST mode increases after irradiation till fluence 3×10^{12} ions/cm^2. In addition, stability in $GeSe_{4/2}$ CST units indicates that optical elasticity remains almost unchanged upon 100 MeV Ag swift-heavy ion irradiations for ion fluence up to 3×10^{12} ions/cm^2.

The present study is helpful in understanding the threshold limits and tuning of optical/structural properties of amorphous Ge-As-Se compositions under ion irradiations.

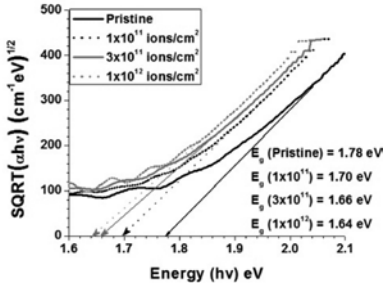

Fig.1. Tauc's Plot of As40Se60 thin films.

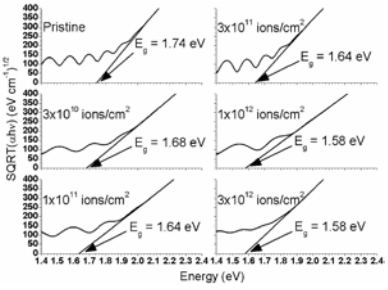

Fig. 2. Tauc's Plot of Ge7.533As38.698Se53.769 thin films.

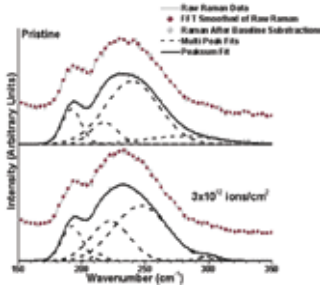

Fig. 3. Raman plots of Ge7.533As38.698Se53.769 thin films.

REFERENCES

[1] B. J. Eggleton, B. Luther-Davies and K. Richardson, Nature Photon. 5 (2011) 141.
[2] F. Qiu, T. Narusawa and J. Zheng, Appl. Opt. 50 (2011) 733.
[3] Z. U. Borisova, Glassy Semiconductors, Plenum Press, Newyork (1981).
[4] A. Prasad, C.J. Zha, R. P. Wang, A. Smith, S. Madden and B. Luther-Davies, Opt. Express. 16(4) (2008) 2804.
[5] D. A. P. Bulla, R. P. Wang, A. Prasad, A. V. Rode, S. J. Madden and B. Luther-Davies, Appl. Phys. A 96 (2009) 615.
[6] A. Tripathi, R. Chauhan and K. K. Srivastava, AIP Conf. Proc. 1536 (2013) 663.
[7] R. Chauhan, A. K. Srivastava, A. Tripathi and K. K. Srivastava, AIP Conf. Proc. 1536 (2013) 599.
[8] R. Chauhan, A. K. Srivastava, A. Tripathi and K. K. Srivastava, Chalc. Lett. 10(2) (2013) 63.

5.2.27 EFFECT OF IRRADIATION OF Si^{5+} ION ON Fe DOPED HYDROXYAPATITE

V. Sarath Chandra[1], K. Elayaraja[1], R. V. Suganthi[1], M. I. Ahymah Joshy[1], I. Sulania[2], P. K. Kulriya[2], K. Asokan[2], D. Kanjilal[2] and S. Narayana Kalkura [1],*

[1]Crystal Growth Centre, Anna University, Chennai – 600 025
[2]Inter-University Accelerator Centre, Aruna Asaf Ali Marg, New Delhi – 110 067
*Corresponding author's email: kalkurasn@annauniv.edu, kalkura@yahoo.com

Hydroxyapatite (HAp - $Ca_{10}(PO_4)_6(OH)_2$) is extensively used for hard tissue replacement of bone and teeth, owing to its excellent biocompatibility and bioactivity. The pure HAp has low bonding ability, poor mechanical properties and no magnetic properties. The mechanical properties of HAp could be enhanced by the fabrication of composites of HAp and doping with different metal ions like iron. Magnetic ion (Fe, Co, Ni, etc.) incorporated HAp, exhibit strong ferromagnetic properties. Nowadays, magnetic HAp (Fe-HAp) is used for cell separation, targeted drug delivery, magnetic resonance imaging (MRI) and as heat mediator for the hyperthermia treatment of cancer [1]. Ion beam irradiation (O^+, Si^{++}, Ar^+ and Ag^{7+}) on HAp was found to improve the surface roughness, wettability, mechanical properties, cell adherence and drug loading/release [2-5]. The swift heavy 100 MeV O^{7+} ion irradiation on HAp enhanced the in vitro bioactivity. 125 MeV Si^{9+} ion irradiated HAp thin films showed no cytotoxycity. Here, we report the effect of Si^{5+} ion irradiation on hydrothermally synthesized Fe-HAp. The physical and *in vitro* biological responses of pristine and irradiated samples were investigated.

The Fe-HAp powder was synthesized by hydrothermal method using $Ca(NO_3)_2.4H_2O$ (Merck), $(NH_4)_2HPO_4$ (Merck), $FeCl_3$, (Qualigens) and ammonia solution (Merck). Fe-HAp pellets of 8 mm diameter and 1 mm

thickness were irradiated with 60 MeV Si^{5+} ions and fluences ranging from 1×10^{11}, 1×10^{12} and 1×10^{13} ions/cm^2 at IUAC. Based on SRIM 2009 calculations, electronic energy loss (S_e), nuclear energy loss and the projected range of the 60 MeV Si^{5+} on Fe-HAp pellets was found to be 4.1×10^{2} eV/Å, 4.1×10^{-1} eV/Å and 14.5 μm respectively.

The GXRD analysis of irradiated samples revealed no secondary phases other than that of HAp. The average crystallite size, crystallinity and lattice parameters, calculated from XRD patterns, gradually decreased with an increase in ion fluence as shown in Table 1. AFM images of the pristine samples showed smooth surface while those of irradiated samples showed formation of pores whose size increased with an increase in fluence as shown in Table 1. Phase shift calculated from Magnetic Force Microscopy (MFM) was found to be 0.40° for pristine and for the irradiated samples it decreased from 0.33° to 0.17° with an increase in ion fluence. MFM also indicated the presence of magnetic regions distributed uniformly along the plane of the Fe-HAp matrix.

For bioactivity test the samples were immersed in simulated body fluid (SBF) and scanning electron microscopy was performed which indicated the increase in growth of apatitle layer on the surface with increase in fluence. Acid Citrate Dextrose (ACD) human blood was used to study the blood compatibility by haemolytic assay. The percentage of haemolysis of pristine and irradiated samples was less than 10%, which was within the acceptable limit as per the ASTM standards. These studies revealed that the irradiation of Fe^{3+} did not affect the biocompatibility of the samples. The antibacterial activity of amoxycillin (AMX) free and loaded pristine and irradiated samples was determined by agar diffusion test against gram positive bacteria (*S. aureus*). Drug free pristine and irradiated samples showed no inhibition zone against *S. aureus* whereas AMX loaded pristine and irradiated samples inhibited bacterial growth of *S. aureus*. In addition, the irradiated samples showed gradual increase in the diameter of inhibition zone as mentioned in Table 1, indicating the enhanced drug release from the irradiated samples. The presence of pores, increase in surface roughness and wettability due to irradiation would have led to an increased absorption of drugs and their subsequent release.

Table 1. Effect of irradiation on the properties of Fe-HAp samples

	Pristine	**1×10^{11} ions/cm^2**	**1×10^{12} ions/cm^2**	**1×10^{13} ions/cm^2**
Lattice parameter (Å) a (± 0.02) c (± 0.01)	 9.45 6.86	 9.44 6.86	 9.43 6.85	 9.42 6.84
Crystallite size (± 1 nm)	33	32	23	13
Crystallinity (%) (± 0.1)	95	94	84	72
Pores size (±1 nm)	-	300	351	360
Diameter of inhibition zone (± 0.5 mm)	0.7	1.0	1.2	1.3

REFERENCES

[1] Z. Stojanovic, L. Veselinovic, S. Markovic, N. Ignjatovic and D. Uskokovic, Mater. Manuf. Processes 24 (2009) 1096.
[2] A. Sagari et al., Nucl. Instrum. Methods Phys. Res., Sect. B. 266 (2008) 2515.
[3] C. M. Lopatin, T. L. Alford, V. B. Pizziconi, M. Kuan and T. Laursen, T. Nucl. Instrum. Methods Phys. Res., Sect. B. 145 (1998) 522.
[4] V. Nelea, H. Pelletier, D. Müller, N. Broll, P. Mille, C. Ristoscu and L.N. Mihailescu, Appl. Surf. Sci. 186 (2002) 483.
[5] K. Elayaraja et al., Mater. Chem. Phys. 134 (2012) 464.

5.2.28 INVESTIGATIONS OF PHYSICAL AND BIOLOGICAL PERFORMANCE OF SWIFT HEAVY ION IRRADIATION ON CALCIUM PHOSPHATE BASED BIOCERAMICS AND ITS POLYMER COMPOSITES

G.M. Shanthini[1], Catherine Ann Martin[1], N. Sakthivel[1], Sarath Chandra Veerla[1], K. Elayaraja[1], P.K. Kulriya[2], K. Asokan[2], D. Kanjilal[2], S. Narayana Kalkura[1]

[1]Crystal Growth Centre, Anna University, Chennai
[2]Inter – University Accelerator Centre, New Delhi

Dense and porous hydroxyapatite (HAp–$Ca_{10}(PO_4)_6OH_2$) have been vigorously investigated as implant materials for orthopedic and dental applications showing excellent bioactivity, osteoconductivity and osteoinductivity [1, 2]. PMMA is a thermoplastic polymer demonstrating good biocompatibility [3]. The gamma irradiation of PMMA induces physical and structural changes [4]. Antibiotic loaded PMMA has been successfully used as a local drug delivery system [5].

The samples of PMMA and PMMA-HAp, prepared by solvent evaporation technique, showed smooth surface which may be unsuitable for cell attachment and proliferation hence, the surface was modified by swift heavy ions. The samples were irradiated with Si^{7+} ion of energy 100 MeV and fluences 1×10^{11} ions/cm^2, 5×10^{11} ions/cm^2 and 1×10^{12} ions/cm^2 with current of 1 pnA. There was creation of pores and clusters on the surface of the scaffolds without any change in chemical structure. Decrease in crystallinity and crystallite size was observed along with decrease in glass transition temperature. In addition, the irradiation led to improvement in wettability and blood compatibility. These results confirm that swift heavy ion irradiation plays a vital role in enhancing the surface properties which could favour better cell attachment and proliferation in biomaterials.

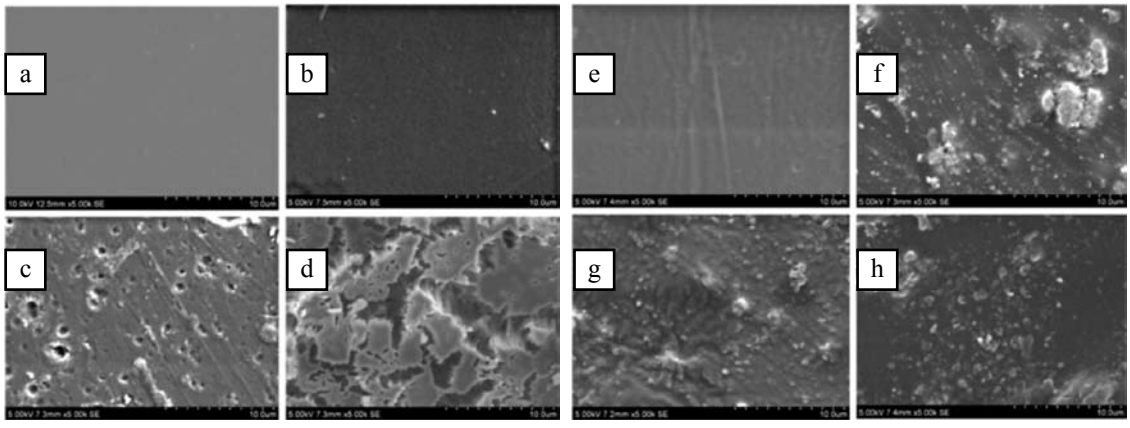

Fig. 1. SEM micrograph of PMMA a) Pristine b) 1×10^{11} c) 5×10^{11} d) 1×10^{12} ions/cm^2 and PMMA – HAp e) Pristine f) 1×10^{11} g) 5×10^{11} h) 1×10^{12} ions/cm^2

Table 1. Average crystallite size and crystallinity of PMMA-HAp composites

Samples Avg	Crystallite Avg Size (nm)	Crystallinity
PHpris	5.295	0.793
PH1e11	5.378	0.818
PH5ell	4.203	0.481
Ph1e12	4.003	0.364

REFERENCES

[1] Nebahat Degirmenbasi, D.M. Kalyon and E. Birinci, Colloids Surf. B (2006) 48.
[2] M. Boutinguiza, J. Pou, R. Comesana, Lusquinos, A. De Carlos and B. Leon, Mater. Sci. Eng. C (2012) 32.
[3] Viet van thai, Young-Ki Min and Byong-Taek Lee, Bioceramics development and applications (2011) 1.
[4] P. Silva, C. Albano, R. Perera and N. Dominguez, Radiat. Phys. Chem. (2010) 79.
[5] R. Vani et al., Nanotechnology (2011) 22.

5.2.29 AC CONDUCTIVITY STUDIES OF 160 MeV Ni^{12+} ION IRRADIATED POLYANILINE NANOFIBERS

J. Hazarika, Chandrani Nath and A. Kumar

Materials Research Laboratory, Department of Physics, Tezpur University, Tezpur- 784028

The polyaniline (PAni) nanostructures have drawn considerable attention owing to their potential applications such as in optical devices, actuators, sensors etc. [1]. Recently, PAni nanofibers have been widely studied because of their ease of synthesis, good processability and solubility, unique applications in fabrications of nanoscale devices. PAni nanofibers can be used for the design and fabrication of novel devices with advanced potential properties. Swift heavy ion (SHI) irradiation of conducting polymers has been used as a novel technique for the modification of their physico-chemical properties such as crystallinity, electrical conductivity, optical and mechanical properties, density, solubility, chain length etc. [2]. The interaction of energetic heavy ions with polymers result in cross-linking, chain-scission and emission of atoms, molecules and some reactive species along the cylindrical ion trajectories. In the present work, PAni nanofibers have been irradiated with 160 MeV Ni^{12+} ion with a view to improve their morphology and ac conductivity using different ion fluence 10^{10}, 5×10^{10}, 10^{11} and 3×10^{11} ions/cm^2.

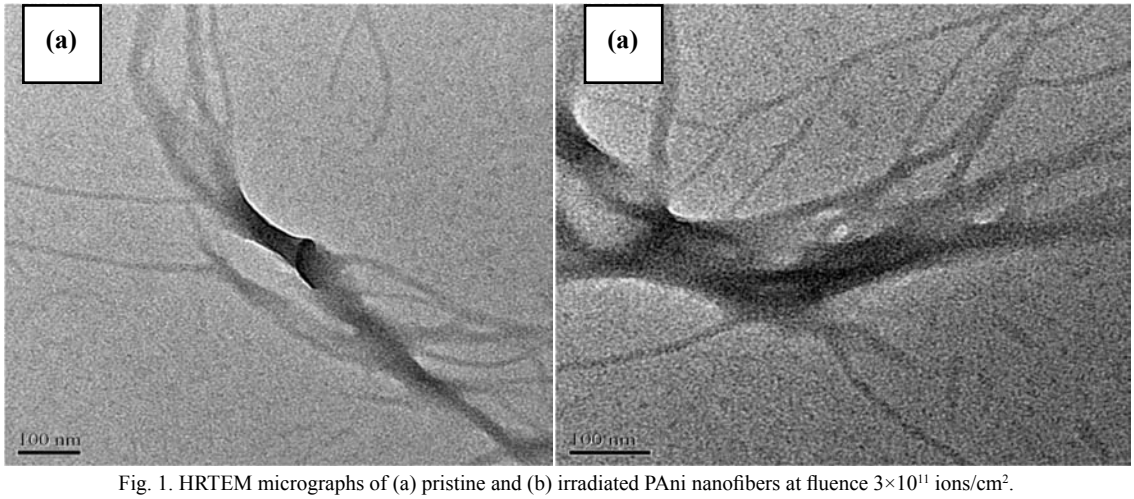

Fig. 1. HRTEM micrographs of (a) pristine and (b) irradiated PAni nanofibers at fluence 3×10^{11} ions/cm^2.

HRTEM micrographs of the pristine and irradiated PAni nanofibers are shown in Fig. 1. It is evident that upon SHI irradiation both the diameter and length of PAni nanofibers increase as compared to that of the pristine PAni. Moreover with increasing fluence, more branching networks of PAni nanofibers result which may be due to the fragmentation and rearrangement of the polymer chains due to large electronic energy deposition by interacting with SHI irradiation which also results in more ordered arrangement of PAni nanofibers at higher ion fluence that are clearly observed from the above TEM micrographs.

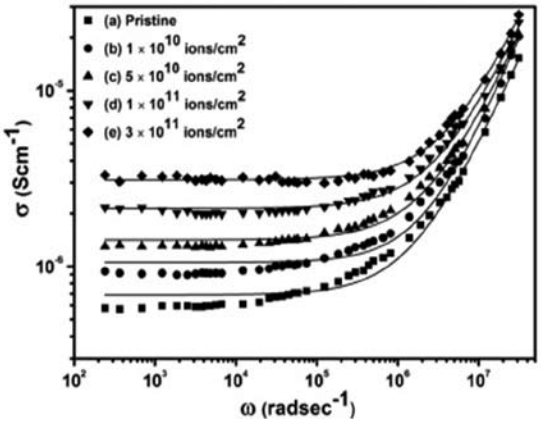

Fig. 2. ac conductivity of pristine and irradiated PAni nanofibers at fluence 10^{10}, 5×10^{10}, 10^{11} and 3×10^{11} ions/cm^2 at 313 K.

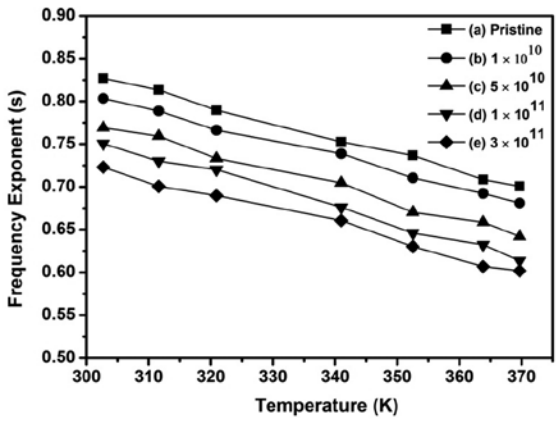

Fig. 3. Temperature dependent of frequency exponent *s* of the pristine and irradiated PAni nanofibers at fluence 10^{10}, $5\times10^{10,}$ 10^{11} and 3×10^{11} ions/cm^2.

The ac conductivity of pristine and irradiated PAni nanofibers at temperature 313 K are shown in Fig. 2. In lower frequency region, total conductivity corresponds to the dc conductivity and in the higher frequency region, conductivity increases exponentially obeying the power law, $\sigma_{ac}=A\omega^s$ where A is the pre-exponential factor and s ($0< s <1$) is the frequency exponent [3]. Furthermore, upon SHI irradiation ac conductivity increases appreciably with increasing fluence and this may be due to the increased number of trapped charges generated by cross-linking in the system [4]. The frequency exponent s decreases with temperature as shown in Fig. 3 which suggests the correlated barrier hopping (CBH) of charge carriers [5]. The polaron binding energy decreases from 0.871 eV to 0.712 eV with increasing ion fluence. The decrease in the binding energy with increasing fluence may be due to more cross-linking of polymer chains that forms new crystalline domains and thereby making favourable charge transport in PAni nanofibers which is consistent with the XRD results.

REFERENCES

[1] J. Huang, M. Wan and J. Polym. Sci. A 37 (1999) 151.
[2] J. Davenas, G. Boiteux, X. L. Xu and E. Adem, Nucl. Instr. and Meth. B 32 (1988) 136.
[3] A. K. Jonscher, Universal Relaxation Law (London: Chelsea Dielectric Group, chapter 5, 1996).
[4] S. Chandra, S. Annapoorni, F. Singh R. G. Sonkawade, J. M. S. Rana and R. C. Ramola, Nucl. Instr. and Meth. B 268 (2010) 62.
[5] S. R. Elliott, Adv. Phys. 36 (1987) 135.

5.2.30 EFFECT OF LOW ENERGY IRRADIATION ON THE TRANSPORT PROPERTIES OF MIXED CONDUCTING SOLID POLYMER ELECTROLYTES

H. Manjunatha[1], D. Praveen[1], G.N. Kumaraswamy[1] and R. Damle[2]

[1]Department of Physics, Amrita School of Engineering, Bengaluru-560 035
[2]Department of Physics, Bangalore University, Bengaluru-560 056

Solid polymer electrolytes have attracted the attention of researchers worldwide for application in various electrochemical devices particularly in solid state rechargeable lithium batteries, mainly because of their flexibility and shape versatility. However, one of the major drawbacks of PEO based solid polymer electrolytes is their low ionic conductivity at ambient temperature. We planned to investigate the enhancement of ionic conductivity of PEO based polymer electrolyte by two methods

a) Introducing two different conducting species (salts) in to the polymer (PEO).

b) Irradiating the solid polymer electrolyte with low energy ion beam.

Weighed proportions of polymer and salts are mixed together in a common solvent and stirred for 10-12 hours at room temperature and at elevated temperatures for removal of solvent content. Thin film of thickness (0.3 mm) is prepared by solution casting technique. The thin film is cut into samples of circular shape (diameter = 10mm.). The samples were irradiated with low energy oxygen ion (100 keV, 1 μA) at different fluencies (1×10^{13}, 5×10^{13}, 1×10^{14}, 5×10^{14}, 1×10^{15}, 5×10^{15}) at low energy ion beam facility [LEIBF] in IUAC New Delhi. Ionic conductivity of the irradiated samples has been measured by ac impedance spectroscopy.

Five different salt concentration polymer electrolytes were irradiated to different fluences, one concentration was not irradiated properly. Four concentrations which were well irradiated have shown enhancement in conductivity by two orders. The details of the experimental results are shown in Fig. 1 and 2. The effect of ion irradiation on the morphology of the polymer could be well understood from the X-ray diffraction patterns of irradiated and unirradiated SPEs. A careful observation reveals that, the intensity of the peak in case of X-ray diffractograms of irradiated SPEs has decreased indicating the decrease in crystallinity.

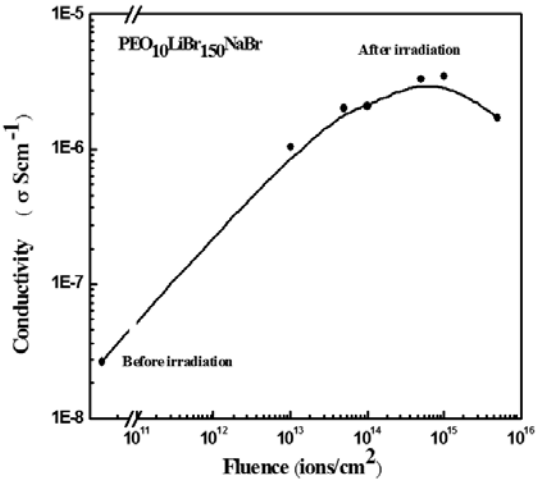

Fig. 1. Variation of conductivity of samples with irradiation fluence

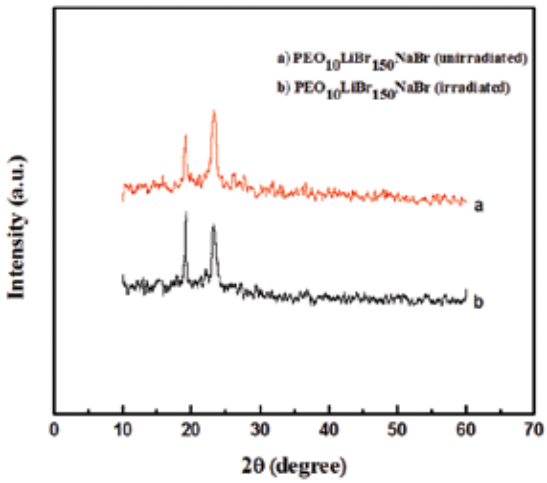

Fig. 2. XRD pattern of unirradiated and irradiated samples

REFERENCES

[1] F. M. Gray, Solid Polymer Electrolytes: Fundamental and Technological Applications, VCH Publishers, New York, 1991.
[2] M. Gaafar, Nucl. Instrum. Methods B, 174 (2001) 507.
[3] Z. H. Li, G. Y. Su, X. Y. Wang and D. S. Gao, Solid State Ionics 176 (2005) 1903.
[4] A. Kumar, M. Deka, S. Banerjee, Solid State Ionics, 181 (2010) 609.

5.2.31 INVESTIGATION OF THERMALLY STIMULATED DEPOLARIZATION CURRENT IN PRISTINE AND IRRADIATED POLYETHERETHERKETONE (PEEK)

Rajesh Kalia[1]*, Sapna Kalia[1], Vandana Sharma[1], Indra Sulania[2] and J. K. Sharma[1]

[1]Department of Physics, Maharishi Markandeshwar University, Mullana (Ambala)-133207
[2]Inter-University Accelerator Centre, Aruna Asaf Ali Marg, New Delhi – 110 067
*Email: rajkalia23@gmail.com

Organic polymers have been broadly used as electrical insulating materials and have large applications in power supply industries. The electrical performance of these materials is affected by their working

environments such as nuclear reactor and radiation facilities [1]. These properties are retained at temperature as high as 200 °C. Due to the symmetry of benzene rings along the polymer backbone and almost linear chemical structure, PEEK offers a good mechanical strength, thermal, chemical, mechanical strength and radiation resistance [2]. The glass transition temperature of PEEK is around 143°C and it melts around 343°C. Therefore, PEEK is expected to be applied in electrical insulation as well as in various other industrial fields [3]. The charge storage mechanism in polymer electrets is strongly dependent on the structure of electrets material [4]. TSDC technique is employed to understand the dielectric relaxation in the present work.

PEEK films of 50 μm [EK301050] were procured from Good Fellow Cambridge limited, UK. These films are transparent pale amber in color. For TSD current measurements the sample is placed in a specially designed furnace. The Aplab dc power supply is used to charge the sample at a desired field for a period of one and half hour. The sample is shorted for 24 hrs at room temperature. The thermally stimulated discharge current (TSDC) is measured by Electrometer [Keithley 6514]. To study the TSDC behavior of irradiated samples, the samples of PEEK (50 μm) were irradiated with 70 MeV C^{5+} ion beam for fluence 1×10^{12} ions/cm^2 at IUAC, New Delhi.

In this paper, we present the study of pristine and irradiated samples at poling temperature T_p = 100 °C and at different poling fields (E_p) 200 kV/cm, 300 kV/cm, 400 kV/cm and 500 kV/cm. The TSD current is measured at a linear heating rate of 2 °C / min in the temperature range [60–230 °C] (Fig. 1 & Fig. 2). The most pronounced peak occurring in both the spectra named α-relaxation is observed around glass transition temperature (Tg) indicating a strong relaxation process at glass transition temperature owing to the increased mobility of dipoles. The α-dipolar relaxation is taking place because of the movement of main chain segment of the polymer [1]. In case of PEEK the depolarization of ketone (> C = O) dipoles linked to the main chain are responsible for α-relaxations.

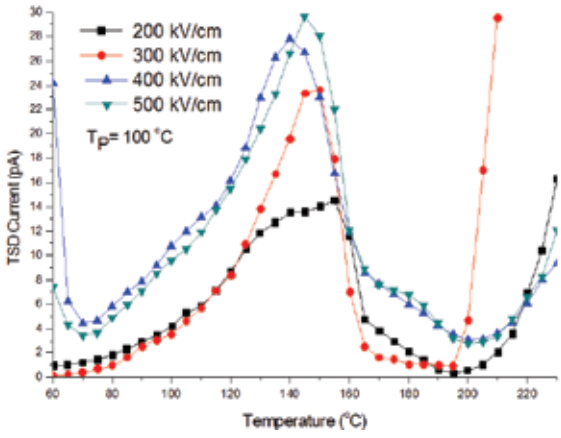

Fig. 1. TSDC spectra of pristine PEEK

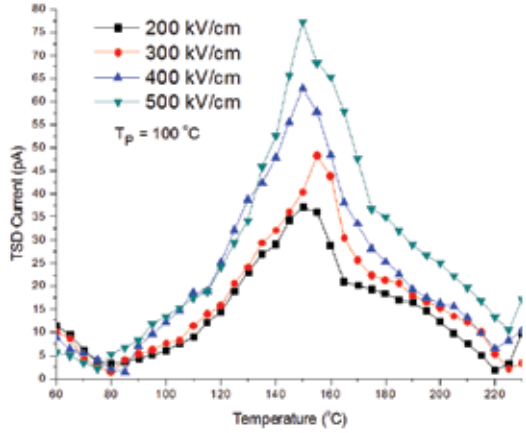

Fig. 2. TSDC spectra of irradiated PEEK

Li et al. studied the Differential Scanning Callorimetery (DSC) thermographs of PEEK of thickness 50 μm and confirmed occurrence of glass transition temperature Tg around 145 °C [5] . The comparison of TSDC spectra of pristine and irradiated samples shows that, the magnitude of α-relaxation peak in irradiated samples has increased as compared to that in pristine samples at similar conditions. The possible mechanisms for this increase may be either an increase in dipole concentration within the polymer, or increase in either electronic or ionic mobile charge concentration near the glass transition temperature. The reason for this is that subsequent chemical reactions after irradiation cause creation of excessive double bonds and cross-linked structures. The creation of excessive double bond formation imparts more dipole nature to the electrets media and cross-linked structure increases mechanical as well as thermal strength [6, 7]. The present study suggests that electric fields of irradiated electrets are enhanced as compared to pristine samples, so the filtration properties of the irradiated samples are likely to be improved over pristine

samples. However, further experimental investigation is needed to see the effect of variety of factors that influence the efficiency of filtration media for example humidity, exposure to certain chemicals, aging, temperature etc.

REFERENCES

[1] R. Kalia, V. Sharma and J. K. Sharma, Journal of Polymer Research 19(2) (2012) 9826.
[2] W. K. Sakamoto, Electica Quimica 28(2) (2003) 49.
[3] J. R. Atkinson, J. N. Hay and M. J. Jenkins, Polymer 43 (2002) 731.
[4] M. M. Perlman, The Electro-Chemical Society, Princeton (1973).
[5] H. M. Li, R. A. Fouracre, D J. Tedford, H. M. Banford and W. Shu, IEEE 1 (1994).
[6] F. Grinnell, M. K. Feld, J. Biol. Chem. 257 (1982) 4888.
[7] L. Calcagno, G. Compagnini and G. Foti, Nucl. Instr. Meth. B 65 (1992) 413.

5.3 RADIATION BIOLOGY RESEARCH

5.3.1 Role of PARP-1 in programmed cell death induced by heavy ion radiation in Human Cervical Epithelial Carcinoma (HeLa) cells

A. Ghorai[1], A. Sarma[2], N.P. Bhattacharyya[3], U. Ghosh[1]

[1]Department of Biochemistry & Biophysics, University of Kalyani, WB-741235
[2]Inter-University Accelerator Center, Aruna Asaf Ali Marg, New Delhi, 110067
[3]Saha Institute of Nuclear Physics, 1/AF Bidhannagar, Kolkata- 700064

We found that PARP-1 knocked down HeLa cells (HsiI) were more sensitive to $^{12}C^{6+}$ beam (62 MeV, average LET 287 kev/μm) than normal HeLa cells as depicted by survival assay (Fig. 1). Further we investigated whether PARP-1 has any role in apoptosis induction after heavy ion beam irradiation or not. We observed significantly more caspase-3 activation in HsiI cells than HeLa (Fig. 2) and more nucleosomal ladder formation in HsiI than parental HeLa after carbon ion beam irradiation in dose dependent manner (Fig. 3).

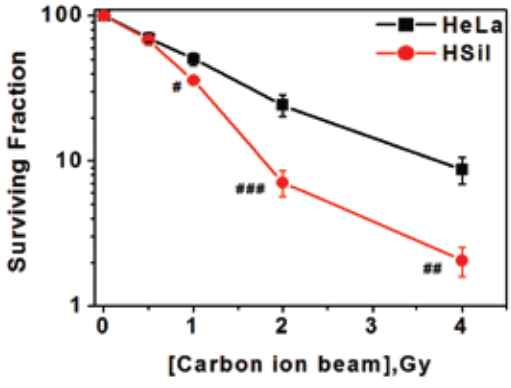

Fig. 1. Survival Assay by different doses of $^{12}C^{6+}$ in HeLa & HsiI. p-values at each dose in HeLa and HsiI were calculated as '#' ($0.01<p\leq0.05$), '##' ($0.001<p\leq0.01$) and '###' ($p\leq0.001$). p-values greater than 0.05 left blank.

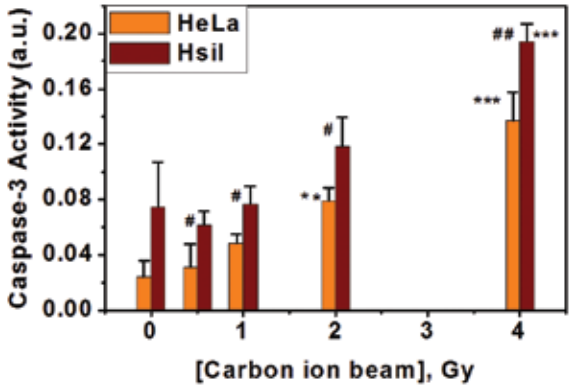

Fig. 2. Activation of caspase-3 in HeLa & HsiI cells after 24 hrs post irradiation of $^{12}C^{6+}$. Each bar diagram represents the mean of 3 independent experiments with the standard deviations (vertical lines). p-values at each dose in HeLa and HsiI were calculated ('#' denotes $0.01<p\leq0.05$ and '##' denotes $0.001<p\leq0.01$). p-values at each dose of $^{12}C^{6+}$ radiation in HeLa and HsiI were also calculated with respect to untreated control of the respective cells and the significant p-values were denoted as '**' ($0.001<p\leq0.01$) and '***' ($p\leq0.001$). p-values greater than 0.05 left blank.

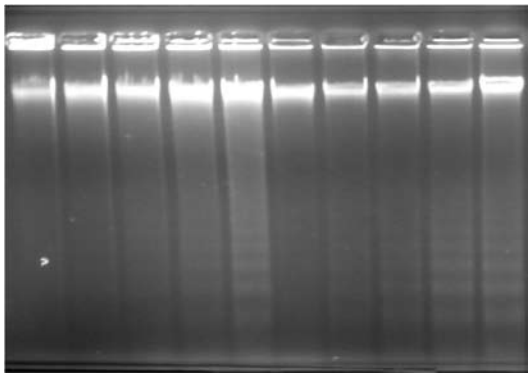

Fig. 3. Nucleosomal ladders induced by ^{12}C ion beam in HeLa and HsiI cells. Lanes 1 to 5 are for HeLa and Lanes 6 to 10 for HsiI. Lanes 1 & 6 – untreated control; Lanes 2 & 7 – 0.5 Gy; Lanes 3 & 8 – 1 Gy; Lanes 4 & 9 – 2 Gy; Lanes 5 & 10 – 4 Gy respectively.

5.3.2 Synthesis of Au nanoparticles and its conjugation with anti EGFR to target A549 lung cancer cell

Geetanjali Pujari, A Sarma, DK Avasthi

Radiation Biology Laboratory, Inter University Accelerator Centre, Aruna Asaf Ali Marg, New Delhi 110067

We have made an approach to synthesize Au nanoparticles and conjugate it with anti EGFR in order to inhibit the expression of Epidermal Growth Factor Receptor (EGFR) and to attach or internalisation of Au naoparticles in A549 lung cancer cells.

Gold Nanoparticles are synthesized by reduction of chloroauric acid by sodium citrate. Characteristic surface plasmon resonance (SPR) band of gold nanoparticles was observed by UV-Vis spectroscopy. We could observe the characteristic signature at 540 nm. The size of Au nanoparticle is 30-40 nm as determined by Scanning Electron Microscopy (SEM) and Transmission Electron Microscopy (TEM).

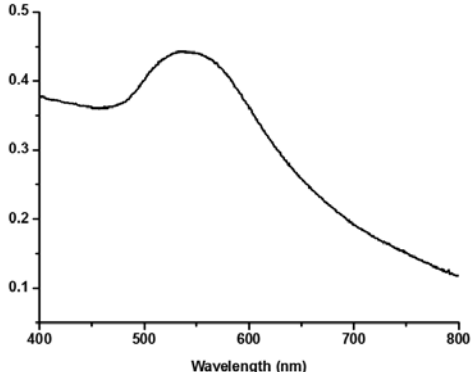

Fig. 1. UV UV-Vis absorbance spectrum of AuNP showing characteristic surface plasmon resonance peak at 540 nm.

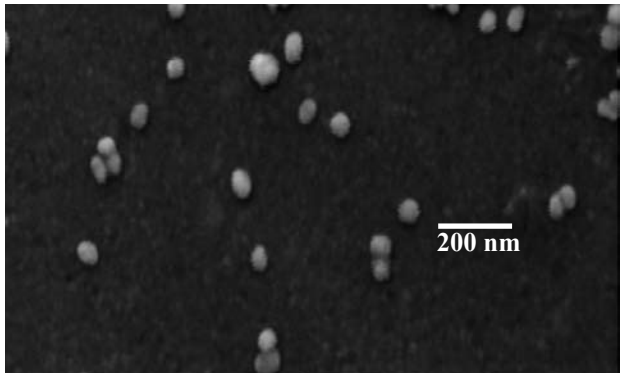

Fig. 2. Scanning Electron Microscopy (SEM) of AuNP.

The synthesized Au nanoparticles are conjugated with anti EGFR. The binding of AuNP to the anti EGFR is by non covalent binding. The complex formation is irreversible and stable. Specific optical changes in UV-Visible spectrum of gold nanoparticles indicate binding of antibodies.

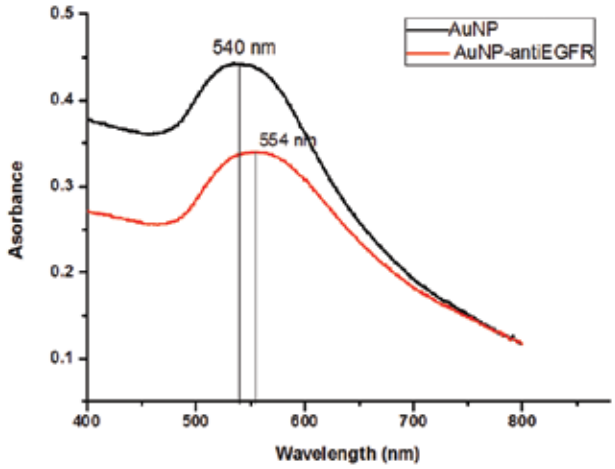

Fig. 3. UV-Vis absorbance of Au nanoparticles and Au nanoparticle conjugated with anti EGFR.

Lung cancer cell line , A549, are treated with the conjugated Au nanoparticles. In order to confirm the attachment and internatlization of AuNPs, TEM of ultrathin cross section of A549 cells were carried out. We could observe that the AuNPs are internalised into the cells.

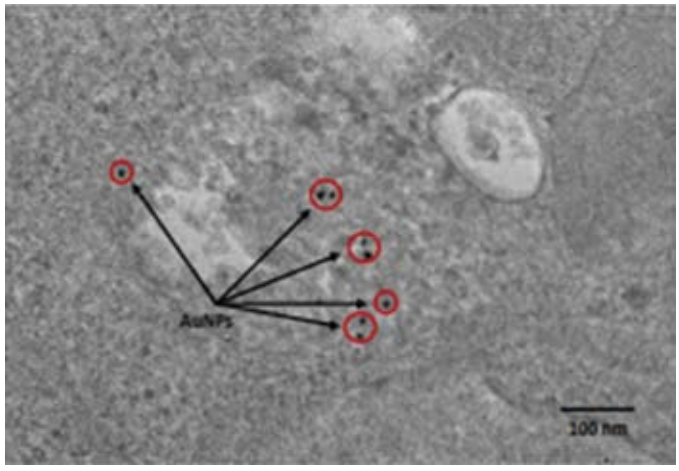

Fig. 4.

With these experiments and findings, we would like to further study the radiosensitization property of Au nanoparticles in A549 lung cancer cells by inhibiting the EGFR expression by binding it to AuNP-anti EGFR.

5.4 ATOMIC & MOLECULAR PHYSICS RESEARCH

5.4.1 Fast Ion Surface Energy Loss in the Surface Wake Fields

T. Nandi[1], K. Haris[2], Hala[2], Pankaj Kumar[1], S. A. Khan[1], Rajesh Kumar[1], S.K. Saini[1], Akhil Jhingan[1], Gurjeet Singh[3], D. Mehta[3] and H G Berry[4]

[1] Inter-University Accelerator Centre, JNU New Campus, New Delhi 11 0067, India.

[2] Dept. of Physics, Aligarh Muslim University, Aligarh 20 2002, India.
[3]Dept. of Physics, Panjab University, Chandigarh 160014, India.
[4] Dept. of Physics, University of Notre Dame, Notre Dame, Indiana 46556

One of our atomic lifetime measurements has found the existence of surface wake field at the exit surface due to passage of highly charged ion beam through a solid thin foil [1]. Further, another study shows that highly charged slow ions lose a lot of its energy at the entry surface [2].

Recently, we have measured the stopping powers of fast, highly ionized atoms passing through thin bi-layer targets made up of metals and insulators. We were surprised to find that the energy losses depend on the ordering of the target (PP-Al or Al-PP) and have small but significantly different values on bi-layer reversal. We ascribe this newly found difference in energy loss to the surface energy loss field (**SELF**) effect to the differing surface wake fields as the beam exits the target in the two cases [3]. This energy loss is greater when the metal part is the exit foil section, i.e. the energy losses for the PP-Al targets are more than the reversed Al-PP targets and we observed similar trends for few other targets such as PET-Ge and PP-Au. Similarly, both partners of the diatomic molecular ions also display similar results (see the table 1).

Table 1. Measured surface energy loss field (SELF) differences for different bi-layer targets and estimates of the range of the surface wake field (SWF) at Al, Ge and Au surfaces. (-dE/dx) is estimated using the formula from Ref. [4].

Ion species	Incident beam energy (MeV)	Energy loss (ΔE) (MeV)		Diff. in ΔE (keV)	(-dE/dx) (keV/Å)	Range of SWF (Å)
	PP-Al	Al-PP			Al-side	
$^{56}Fe^{9+}$	86.908 ± 0.005	30.887 ± 0.011	30.555 ± 0.010	332 ± 15	7.41	45 ± 2
$^{56}Fe^{10+}$	107.258 ± 0.006	30.193 ± 0.011	29.981 ± 0.012	212 ± 16	5.85	36 ± 3
$^{56}Fe^{12+}$	154.473 ± 0.006	28.219 ± 0.009	27.988 ± 0.009	231 ± 13	3.98	58 ± 3
	PET-Ge	Ge-PET			Ge-side	
$^{56}Fe^{9+}$	86.908 ± 0.005	39.951 ± 0.014	39.541 ± 0.013	410 ± 19	5.64	73 ± 3
$^{56}Fe^{10+}$	107.258 ± 0.006	39.120 ± 0.012	38.923 ± 0.013	197 ± 18	4.30	46 ± 4
$^{56}Fe^{12+}$	154.473 ± 0.006	37.018 ± 0.014	36.841 ± 0.011	177 ± 17	2.80	63 ± 6
	PP-Au	Au-PP			Au-side	
$^{56}Fe^{9+}$	86.908 ± 0.005	29.340 ± 0.012	29.222 ± 0.012	118 ± 17	2.38	50 ± 7
	PP-Al	Al-PP			Al-side	
$^{16}O^{q+}$	18.824 ± 0.003	7.426 ± 0.001	7.400 ± 0.002	26 ± 2	0.89	29 ± 2
$^{1}H^{+}$	1.176 ± 0.0002	0.409 ± 0.0002	0.407 ± 0.0003	2 ± 0.4	0.01	200 ± 36

On the passage of 20 MeV $^{16}OH^{+}$ beam on Al-PP bi-layer target, SELF energy loss differences was found to be of 26 ± 2 and 2±0.2 keV for oxygen and hydrogen ions, respectively. This difference in oxygen ions was attributed to Polarization wake, whereas, self-wake [5] could be responsible for the energy loss difference of hydrogen ions.

Theoretical calculations were performed using the SRIM [5] and ATIMA codes [6] for a bi-layer target of PP and Al for the two different geometries. From both theoretical calculations, the energy loss in Al-PP is higher than that in PP-Al, which is in contrast with the experimental results. Hence the SELF differential energy loss cannot be explained by the present theories.

We have scaled the Neelavathi wake potential for O and S ions to our case of Fe ions. In contrast, our measured wake potential is about 15 kV for PP-Al bi-layer, which is at about 2 orders of magnitude higher than the theoretical predictions of Neelavati et al. However, our differential energy loss results show

reasonably close agreement with theoretical estimates, from the work of Vager and Gemmell [4]. We have evaluated the mean range of the potential and found that the range varies from 30–60 Å for PP-Al, 40–80 Å for PET-Ge and the similar trend for PP-Au for heavy ions, which is consistent with the surface potential range as predicted by Echenique and Pendry [7]. In contrast the H ions show a large range.

Measured SELF energy loss depends on the metal layer thickness. The Ge layer thickness in Ge-PET is much thicker whereas the Au layer in Au-PP was smallest 15 nm only. The measured SELF differential energy loss differences was found to be maximum (200-400 keV) for Ge-PET whereas for Au-PP it was minimum [3].

REFERENCES

[1] Nandi and B.P. Mohanty, "Measurement of Wake Field Intensity", J. Phys. B: At. Mol. Opt. Phys, 42, 225402 (2009)
[2] T. Nandi,"Role of Ion-Surface Interaction at the Entry Surface on the Energy Loss of Highly Charged Slow Ions in Solids" Open Journal Microphysics, Vol. 1, 53-57 (2011).
[3] T. Nandi, K. Haris et al, Phys. Rev. Lett. 110, 163203 (2013)
[4] Z. Vager and D. S. Gemmell, Phys. Rev. Lett. 37, 1352(1976).
[5] P. M. Echenique, W. Brandt, and R. H. Ritchie, Phys. Rev. B 33, 43 (1986).
[6] Current version of the SRIM code by F. Ziegler and J. P.Biersack was obtained from http:\\www.srim.org.
[7] ATIMA, http:\\www-linux.gsi.de\~weick\atima\.
[8] P. M. Echenique and J. B. Pendry, J. Phys. C 8, 2936(1975).

5.4.2 Energy loss straggling due to SELF

K. Haris[1], T. Nandi[2], and H. G. Berry[3]

[1]Dept. of Physics, Aligarh Muslim University, Aligarh 20 2002, India.
[2] Inter-University Accelerator Centre, JNU New Campus, New Delhi 11 0067, India.
[3] Dept. of Physics, University of Notre Dame, Notre Dame, Indiana 46556

The statistical fluctuation of the energy-loss of projectile ions with the targets is known as the energy-loss straggling [1]. Apart from its fundamental theoretical interest, the straggling is an important quantity in ion-beam based techniques for material structuring, and in hadrons' therapy. Experimental energy-loss straggling data are sparse and scattering does exist within these limited data also. This process is a complex phenomenon. Besides the energy spread of the ion-beam, target thickness non-uniformity, and charge state of the ion-beam several other factors such as I) the shell correction accounting for the orbital motion of target electrons, II) the Barkas-Andersen effect accounting for binding induced deviations from free-Coulomb scattering, III) a screening correction accounting for electrons bound to the projectile, IV) a bunching correction accounting for the spatial proximity of electrons in a target atom, V) a packing correction accounting for spatial correlations between the target atoms, VI) a projectile excitation, and VII) charge exchange have been considered [2] to understand the ion energy-loss straggling mechanism. We made an attempt here to investigate the effect of another factor called surface energy loss field (SELF) on energy-loss straggling [3] and results are shown in the table below. Our E-loss experiment showed that SELF introduces 7%-18% additional straggling when the beam is exiting from metal layers. We measured the straggling of fast, highly ionized atoms passing through thin bi-layer targets made up of metals and insulators and found that straggling depends on the ordering of the target (PP-Al or Al-PP) and have small but significantly different values on bi-layer reversal. Theoretical calculation of straggling for bi-layer target with an insulator on the exit side predicts larger straggling; however we observe the opposite trend. Measured straggling for the PP-Al targets are more than the reversed Al-PP targets and we observed similar trends for PET-Ge and PP-Au. Also straggling is metal layer thickness dependent and the thicker metal layer exhibits larger difference.

Table 2: Differential energy loss straggling in bi-layer targets for Fe ions.

Beam Energy (MeV)	FWHM (MeV)			Straggling Ω^2 (MeV^2)		Difference in Ω^2 (MeV^2)
	Blank	PP-Al	Al-PP	PP-Al	Al-PP	
86.908 ± 0.005	1.306±0.052	2.370±0.038	2.271±0.032	3.912±0.029	3.451±0.022	0.461±0.037
154.473 ± 0.006	1.032±0.013	1.938±0.020	1.864±0.017	2.690±0.023	2.411±0.020	0.279±0.031
		PET-Ge	Ge-PET	PET-Ge	Ge-PET	
86.908 ± 0.005	1.306±0.052	2.155±0.045	2.049±0.044	2.939±0.043	2.491±0.045	0.448±0.062
		PP-Au	Au-PP	PP-Au	Au-PP	
86.908 ± 0.005	1.384±0.044	2.449±0.040	2.393±0.052	4.079±0.033	3.812±0.049	0.267±0.059

The energy loss straggling data corroborate the differential energy loss data. Since the exit Wakefield for the metal part is predicted to be larger than that for polypropylene or PET (insulator), we propose that the differential energy loss as well as the differential straggling is due to the exit wake field.

Interestingly it is observed that bi-layer order-dependent energy loss straggling in Ge [3] is larger than that in Au [4] and this fact is in agreement with the results obtained with even light ions with single layer targets. Further observations have been planned to elucidate the mechanism in greater detail.

REFERENCES

[1] N. Bohr, K. Dan Vidensk. Selsk., Mat. Fys. Medd.18, No. 8 (1948).
[2] P. Sigmund and A. Schinner, Eur. Phys. J. D58, 105 (2010).
[3] T. Nandi, K. Haris et al, Phys. Rev. Lett. 110, 163203 (2013)
[4] J.B. Malherbeand H.W. Alberts, Nucl. Instru. Meths. 192, 559 (1982).
[5] H. W. Alberts and J. B. Malherbe, Rad.Effs.69, 231 (1983).

5.4.3 Radiative resonant energy transfer process in projectile-like ion formed in beam-foil interaction

Adya P. Mishra [1]*, T. Nandi [2], B. N. Jagatap [1]

[1]Atomic and Molecular Physics Division, BARC, Trombay, Mumbai -400 085, India
[2]IUAC, JNU New Campus, Aruna Asaf Ali Marg, New Delhi -110 067, India

The formation of projectile-like $^{55}_{25}Mn$ ion during bombardment of a thin carbon foil by $^{51}_{23}V^{12+}$ ion beam of energies above the Coulomb barrier is inferred through the observation of unresolved $1s2p\,^3P_2^o \rightarrow 1s^2\,^1S_0$ and $1s2p\,^3P_0^o \rightarrow 1s^2\,^1S_0$ transitions of He-like Mn at 6.14 keV. From the decay of this line the measured radiative lifetime of the upper state is found to be 78.7±11.6 ps which is close to the theoretical lifetime of the $1s2p\,^3P_0^o$ state (86.18 ps), but substantially lower than that of $1s2p\,^3P_2^o$ state (147.1 ps). This suggests that the $1s2p\,^3P_0^o$ state is populated more than the $1s2p\,^3P_2^o$ state when He-like Mn exits the carbon foil [1]. Such behavior is explained on the basis of radiative resonant energy transfer process in beam-foil excitation observed recently [2].

REFERENCES

[1] Adya. P. Mishra, T. Nandi, B.N. Jagatap, J Quant Spectrosc Radiat Transfer, 118 (2013) 74.
[2] Nandi T, et al. J Quant Spectrosc Radiat Transfer 113(2012) 783.

5.4.4 Resonances in the population of circular Rydberg states formed in the beam-foil excitations

Adya P. Mishra,[1] T. Nandi,[2] and B. N. Jagatap[1]

[1]Atomic and Molecular Physics Division, BARC, Trombay, Mumbai -400 085, India
[2]IUAC, JNU New Campus, Aruna Asaf Ali Marg, New Delhi -110 067, India

By directing fast moving 164 MeV $^{56}_{26}Fe^{12+}$ ion beam on 90 g/cm^2 thick carbon foil we have studied the decay of *2p* state of H-like Fe in the time range 2.4×10^4–9.1×10^5 τ_{2p}, where τ_{2p} is the lifetime of the *2p* state (≈3.3 fs). At such large times four resonances have been observed in the decay curve of the beam-foil-excited 2p state. This unusual behavior is explained due to cascades from circular Rydberg states, which modify the time dependence of the photon intensity, *I(t),* of the *2p*-1*s* transition from an exponential to hump-like structures for $t>>\tau_{2p}$. It is seen that only selective circular Rydberg states are populated when fast H-like Fe ions emerge from the back surface of a thin solid foil [1]. The relative population of CRS is determined. At least two levels contribute to a resonance-structure.

REFERENCE

[1] Adya. P. Mishra, T. Nandi, B.N. Jagatap, J Quant Spectrosc Radiat Transfer, 120 (2013) 114.

5.5 ACCELERATOR MASS SPECTROMETRY RESEARCH

5.5.1 Stripping of a molecular beam to a higher charge state by means of two successive stripper foils in the Tandem accelerator"

Pankaj Kumar[1, 2], G. Korschinek[1], S. Chopra[2], T. Faestermann[1], P. Ludwig[1], G. Rugel[1], D.Seiler[1], A. Wallner[1]*, S. Ojha[2], S. Gargari[2], R. Joshi[2] and D. Kanjilal[2]

[1]Physik Department der Technischen Universität München, Garching, Germany
[2]Inter-University Accelerator Center (IUAC), New Delhi, India
*Now at Physics Division, Australian Nuclear Science and Technology Organization (ANSTO), PMB 1, Menai, NSW 2234, Australia

Many times molecular ions are extracted from the ion source especially when the ion source yield is too low for atomic ions or to reduce the isobaric background in case of AMS. In these cases the achieved energy is reduced as it is shared by other constituents of the molecule during the first leg of acceleration. We studied the charge state distribution of Sr, Ca and Mn (injected as SrF_3^-, CaF_3^- and MnF_3^- respectively) using single and double stripper foils at various terminal voltages with IUAC and Munich accelerator. This was a collaborative project between IUAC and Technical university Munich funded by DST-Govt of India and DAAD Germany.

We found that a double stripper system with a marginal gap between the stripper-foils produces higher charge states and higher ion yields for the constituents of multiple molecules. That is because of the low distance and therefore interference between the ions in a single stripper foil, which is overcome by employing a second stripper foil. Thus the capability of Tandem accelerators for molecular beams can be improved in terms of higher energy with higher yield by the use of a double stripper foil system made of two foils having some separation between them. This small separation (~0.5mm) between two foils can be easily achieved by spot welding two stripper foil holders. The details about the experimental set and results can be found in Ref1.

REFERENCE

[1] Pankaj Kumar et.al, Nuclear Instruments and Methods in Physics Research B 269 (2011), 1986-1991

5.5.2 Application of ^{10}Be to estimate the rate of glacial retreat in Ladakh region of Himalaya

Soumya Prakash Dhal[1], Pankaj Kumar[2], S. Balakrishnan[1], R.K. Ganjoo[3] and S. Chopra[2]

[1]Department of Earth Sciences, Pondicherry University, Puducherry-605014
[2]AMS Group, Inter University Accelerator Centre, New Delhi -110067
[3]Department of Geology, University of Jammu, Jammu and Kashmir.

Glaciers are nice indicator of climate variation and major contributor to global sea level rise. [1] Due to the continuous retreat of the glacial mass in the high mountain region as a result of temperature increase, a large quantity of water is supplied to the sea which leads to sea level rising. MoEF reports that Glaciers in the Himalayas have been exhibiting a continuous secular retreat with an average annual retreat of the glaciers around 5 m till upto late 50s of the 20th century which increased many folds in some glaciers in the Central and the Eastern Himalayas during the decade of mid seventies to late eighties and touched a value of as high 25m-30m in recent time. [2] WWF Nepal program, 2005 report that, "glaciers in the Himalayas are receding faster than in any other part of the world". [3] The maximal regional thinning rates in the Jammu–Kashmir region were reported by Andreas Kaab et. al (2012) which is 0.66±0.09 meters per year. The glacial retreat phenomena are studied manually either by direct observation or by satellite images in the past 200 years. But utilizing cosmogenic nuclides like ^{10}Be and ^{26}Al, the information about glacial retreat in the past few million years can be studied. Here a preliminary attempt has been made to examine the suitability and validity of ^{10}Be for the above work.

Methodology: Quartzite samples were from Choskar area with geo co-ordinate varies from 34° 22' 4.2" N to 34° 22' 5.6" N and 76°22'48.0"E to 76°22'48.5"E with different elevations. Three samples were crushed and 80-120 mesh fractions were taken for experiment. At 1.2 amp current with reverse slope quartz grains were isolated. Grains were leached with 2% HF to remove the surface inclusion if present. Concentrated HF was used to digest the samples followed by fuming with conc. HNO3 to remove the fluoride complex. The samples were passed through anion column and Be was collected in 45 ml of 1.2 N HCl by passing through cation column. The solutions were dried and precipitated as Be(OH)3 using NH4OH at 7.8 pH. The Be(OH)2 was converted to BeO by heating at 900°C for 8 hr. BeO powder with Nb powder in 1:1 ratio was loaded in cathode of AMS for analysis. Chemical separation and ^{9}Be analysis by ICP-AES were done in the Department of Earth Sciences, Pondicherry University and ^{10}Be was measured using AMS at IUAC, New Delhi.

Results: ^{9}Be result from ICP-AES and ^{10}Be/^{9}Be ratio from AMS were used to calculate ^{10}Be concentration. Assuming no erosion and constant production rate the exposure ages of different samples was calculated. Table given below shows the result.

Table

Sample	Latitude	Longitude	Weight (g)	Conc. (10Be/g)	Exposure Age (Year)
Choskar-1	34° 22' 4.2" N	76°22'48.0"E	15.00301	1.18E+06	(2.27±0.57)* 10^4
Choskar-2	34° 22' 4.5" N	76°22'48.3"E	15.00358	8.07E+06	(1.62±0.32)* 10^5
Choskar-4	34° 22' 5.6" N	76°22'48.5"E	12.7586	9.21E+06	(1.84±0.35)* 10^5

From the above result it is confirmed that ^{10}Be proxy is suitable for the study of glacial retreat in this region. More detailed studies on determining ^{10}Be and ^{26}Al exposure ages to estimate rates of glacial retreat in North-Western Himalayas is being planned.

REFERENCES

[1] "Contrasting patterns of early twenty-first-century glacier mass change in the Himalayas", Andreas Kaab et. al., 23 august 2012, vol 488, nature, 495-498.

[2] "Himalayan Glaciers, A state-of- art review of glacial studies, glacial retreat and climate change", V. K Raina, Published by Ministry of Environment and Forest, Govt. of India.

[3] "An Overview of Glaciers, Glacier Retreat, and Subsequent Impacts in Nepal, India and China" WWF Nepal program, 2005.

5.5.3 An environmental magnetic study & elemental composition of a marine sediment core from the central western Bay of Bengal: implications for paleo-oceanographic studies

P.V.L.narayana[1], Pankaj Kumar[2], Archna Bohra[2], Rajveer Sharma[2], S.Chopra[2], I.N.Rao[3] and A.D.P.Rao[1]

[1] Department of Nuclear Physics, Andhra University, Visakhapatnam, Andhra Pradesh-530 003
[2] Inter-University Accelerator Centre, Aruna Asaf Ali Marg, 110067, New Delhi.
[3] Marine Chemistry Division, School of Chemistry, Andhra University, Visakhapatnam, Andhra Pradesh-530 003

A 4.12 m long marine sediment gravity core was collected during 157 cruise of ORV Sagar Kanya (October 2000) from the marginal coastal waters of central western Bay of Bengal. The core was sub sampled (2 cm), half part of the each sub sampled, undisturbed whole length of the core samples were dried and used for environmental magnetic properties such as magnetic susceptibility. Remaining parts were also dried; grinded and sieved through 230 sieve size were used for different chemical analysis. The whole length of the grained core samples was used to study major and minor elements by using PIXE technique, organic carbon (OC), $CaCo_3$, was estimated by using standard methods. The age of the core and the rate of sedimentation were estimated from $^{10}Be/ ^{9}Be$ ratio using AMS facility of IUAC, New Delhi. The elemental concentrations were increased from bottom to towards the surface layer.

Initially we have selected seven sediment subsamples from the sediment core, one blank sample to monitor background. The procedure of chemical processing of sediments is taken from reference [1]. These processed samples were analyzed for $^{10}Be/^{9}Be$ ratio using AMS facility of IUAC, New Delhi. Data analysis is under progress.

REFERENCE

[1] Pankaj Kumar et al., 2011. J. Radioanal Nucl Chem (2011), Vol. 290, Issue 1, pp 179-182